ARGONNE NATIONAL LABORATORY

9700 South Cass Avenue, Argonne, Illinois 60439

ANL/ATHRP-47

Implementation of the High-Order Schemes QUICK and LECUSSO in the COMMIX-1C Program

by K. Sakai, J. G. Sun, and W. T. Sha

Energy Technology Division

Analytical Thermal-Hydraulics Section

August1995

Work sponsored by The Multiphase Flow Research Institute

DISCLAIMER

Argonne National Laboratory, with facilities in the states of Illinois and Idaho, is owned by the United States government, and operated by the University of Chicago under the provisions of a contract with the Department of Energy.

Reproduced from the best available copy.

Available to DOE and DOE contractors from the
Office of Scientific and Technical Information
P.O. Box 62
Oak Ridge, TN 37831
Prices available from (423) 576-8401

Available to the public from the
National Technical Information Service
U.S. Department of Commerce
5285 Port Royal Road
Springfield, VA 22161

Figures

Tables

IMPLEMENTATION OF THE HIGH-ORDER SCHEMES QUICK AND LECUSSO

IN THE COMMIX-1C PROGRAM

1 Introduction

1.1 Need for High–Order Schemes in Space and Time

Multidimensional analysis programs based on the finite-difference method have been commonly used to simulate thermohydraulic phenomena in nuclear reactor components. Among these programs, the COMMIX–1C computer program[1] was developed at Argonne National Laboratory in the U.S., and designed to analyze steady–state/transient, single–phase, three–dimensional flows with heat transfer in a reactor component/multicomponent system.

In this program, first–order schemes with respect to both space and time are used. Namely, the first–order upwind scheme is used for all convection terms in the governing equations, and the flow-modulated skew-upwind (FMSUD) scheme is used for convective terms in the energy equation only. A fully implicit or fully explicit scheme with respect to time is used.

However, the first–order upwind scheme has failed to predict temperature oscillations caused by the up and down motions of the thermal stratification interface, and the use of high–order schemes is therefore necessary, especially when convective effects dominate in multidimensional flow and temperature fields with a steep gradient of transported quantities.[2]

Further, fluid flow fluctuations have been observed even in natural circulation tests performed in the SLAB facility at KfK in Germany.[3] These turbulent phenomena play an important role in the movement of the thermal stratification interface and its temperature distribution. When we perform the direct numerical simulations for these fluctuating fluid flows, we need at least the second–order numerical schemes in space and time to essentially eliminate the numerical diffusions of the second–order derivative in space, and to correctly evaluate the molecular viscosity effects.

Moreover, the first–order schemes in space cannot realize the higher–order phenomena such as von Karmann vortex shedding and the secondary or tertiary vortex developed at the corners in shear–driven cavity flows.

1.2 Review of High–Order Schemes in Space

Reflecting the above situations, a growing need has recently developed for highly accurate analysis of multidimensional fluid flows that involve heat transfer. However, usually high–order schemes, such as the central schemes, third–order upwind scheme,[4] and the

QUICK scheme,[5] tend to suffer from unphysical oscillations (numerical oscillations) when mesh Reynolds or Peclet numbers exceed a critical value (≈2), especially in regions of steep gradient.

To cope with the numerical oscillations, some revised schemes[6,7] and more sophisticated methods such as ENO[8] and TVD[9] are proposed. The last two schemes are mainly for analysis of compressible fluids. On the other hand, artificial techniques to suppress the local numerical oscillations, such as FRAM,[10] FCT,[11] and a modified scheme of QUICK, such as EXQUISITE,[12] are proposed. The FRAM technique uses the transient Lagrangian transport equation as a tool to locate the region with oscillations in the Euler solution, and to devise an appropriate technique to damp the oscillations. Because the Lagrangian equation does not include the convective term, its numerical solution is free from numerical oscillations.

Recently, new modern schemes free of any mesh Reynolds number restriction were proposed, which use either four-base points (LECUSSO[13]) or five-base points (LSUDS[14]). The essence of these modern schemes consists in determining adaptive upwinding weight such that the difference equations satisfy the exact solution of the convection-diffusion equation with constant coefficients. These schemes are derived in uniform mesh size grids. The LECUSSO scheme was recently extended into nonuniform mesh size grids based on the conservative form of Sakai.[15]

1.3 Review of High-Order Schemes in Time

For time integration, fully implicit schemes such as SIMPLE[16] and SIMPLER[17] are preferred to explicit schemes like SMAC,[18] because they are not subject to the Courant restriction for a time increment. In the case of steady-state calculations, the time increment has nothing to do with the numerical accuracy of final steady-state solutions obtained in the time-marching technique. Hence, the fully implicit scheme is quite preferable for steady-state calculations. However, the numerical accuracy in the case of transient calculations is closely related to the time increment. It is especially important to use higher order schemes when we use an implicit scheme in time coupled with a higher order scheme in space for transient calculations, because the leading term of the truncation error is the second-order derivative with respect to space, and its magnitude becomes larger than that coming from the first-order upwind scheme in a case that uses the larger time increment beyond the Courant condition.

Regarding the time integration schemes with second-order accuracy, the Lax-Wendroff, Adams-Bashforth, and RRK methods[19] are known for explicit integration. The RRK method is unconditionally stable and free from the Courant restriction. The Crank-Nicolson and ADI[20] methods for implicit integration are unconditionally stable and they satisfy the Lax-Richtmeyer's stability criteria. But attention should be paid to the Crank-Nicolson scheme, which could produce oscillatory solutions, if one uses a time increment larger than the Courant restrictions.[21] Because a large time increment degrades the accuracy of numerical solutions in transient calculations, it is preferable to use a small time increment as much as possible, even when we use implicit schemes that are free from the Courant restriction.

1.4 Objectives

Reflecting the above reviews of high–order schemes, the objectives in the present study are as follows:

- Reformulate the finite-volume equations to deal consistently with all governing equations with high-order schemes. The high–order scheme has not been used earlier for the continuity equation, which also includes a convection term for mass per unit volume. Conventionally, the derivations of finite-volume equations in the COMMIX–1C program have been based on transported quantities per unit mass. When we consider the high–order scheme for all governing equations, inclusive of the continuity equation, it is preferable to base the constitution the balanced equations on transported quantities per unit volume, such as the mass per unit volume ρ, the momentum per unit volume $\rho\vec{v}$, the energy per unit volume ρh, the turbulence kinetic energy per unit volume ρk, and the dissipation of turbulence kinetic energy per unit volume $\rho\varepsilon$.

- Implement the second–order scheme QUICK, which is widely used in the field of nuclear engineering, for the convection terms in all governing equations, such as mass, momentum, energy, turbulence kinetic energy, and turbulence diffusivity transport equations. As pointed out in the first objective, the high–order scheme has not been employed for the continuity equation, which is considered important for strongly coupled momentum/energy problems in natural convection and fluid flows with phase change.

- Employ the FRAM method as a damping technique against oscillations, because the QUICK scheme suffers from numerical oscillations.

- Implement the LECUSSO scheme, which shows quite stable solutions, in the convection terms of all governing equations. The two–dimensional LECUSSO scheme was already implemented by Sakai and Weinberg[22] in COMMIX–2(V), which is a highly vectorized version of KfK; however, the three–dimensional LECUSSO scheme has never been implemented.

- Implement the second-order scheme for various boundary conditions, and the shear flow condition (tangential velocity component) on the boundaries with second-order accuracy, because when we perform high–order calculations, it is necessary to increase the numerical accuracy for boundary conditions to also maintain the same accuracy as that in the interior region. For this purpose, a finer mesh grid should be used near the boundary, or generally, it is preferable to use high–order schemes on the boundaries also.

- Regarding high–order schemes in time, implement the semi-implicit treatment with an arbitrary value of the implicitness parameter α. The case when $\alpha = 0.5$ corresponds to the Crank–Nicolson scheme with second-order accuracy.

  There are a number of high–order schemes with respect to time, as we reviewed above. The concept of implicitness parameter α has been implemented in the

COMMIX-1C program; hence, it is easy to change the program by using the α to realize high-order accuracy in time.

- Examine the present improved COMMIX-1C program through basic numerical experiments with the Burger equation, shear-driven cavity flows, and experimental analyses of von Karmann vortex shedding and Strouhal numbers.

2 Numerical Diffusions and Numerical Instability

2.1 Numerical Diffusions

2.1.1 One-Dimensional Flows

As pointed out in Sec. 1, numerical diffusions can be introduced from the transient term as well as the space terms. In Ref. 23, we can clearly see this situation, which we briefly summarize below.

Let us consider a one-dimensional transient transport equation for a scalar quantity f as follows:

$$\frac{\partial f}{\partial t} + u\frac{\partial f}{\partial x} = 0, \tag{2.1}$$

where u is the transporting velocity, t is time, and x is the coordinate. For simplicity, we assume that u is constant and positive. Forward discretization in time and upwind discretization of the convective term yields

$$f_i^{n+1} = (1 - C)f_i^n + f_{i-1}^n, \tag{2.2}$$

where

$$C = u\Delta t/\Delta x \tag{2.3}$$

is the Courant number.

We consider a Taylor expansion, both in space and time, of the numerical solution f_i around point (x_i, t_n):

$$f_i^{n+1} = f_i^n + \Delta t\left(\frac{\partial f}{\partial t}\right)_i^n + \frac{1}{2}\Delta t^2\left(\frac{\partial^2 f}{\partial t^2}\right)_i^n + 0\left(\Delta t^3\right), \tag{2.4}$$

and

$$f_{i-1}^n = f_i^n - \Delta x\left(\frac{\partial f}{\partial x}\right)_i^n + \frac{1}{2}\Delta x^2\left(\frac{\partial^2 f}{\partial x^2}\right)_i^n + 0\left(\Delta x^3\right). \tag{2.5}$$

Introducing Eqs. 2.4 and 2.5 into Eq. 2.2, one derives

$$\left(\frac{\partial f}{\partial t}\right)_i^n + u\left(\frac{\partial f}{\partial x}\right)_i^n = \frac{1}{2}\left[u\Delta x\left(\frac{\partial^2 f}{\partial x^2}\right)_i^n - \Delta t\left(\frac{\partial^2 f}{\partial t^2}\right)_i^n\right] + 0\left(\Delta x^2\right) + 0\left(\Delta t^2\right). \tag{2.6}$$

The second-order time derivative in Eq. 2.6 can be transformed into a spatial derivative by using

$$\frac{\partial^2 f}{\partial t^2} = u^2 \frac{\partial^2 f}{\partial x^2}, \tag{2.7}$$

which is derived by differentiating Eq. 2.1 with respect to time and spatial coordinate, and then eliminating the $\partial^2 f/\partial x\partial t$ terms. Introducing Eq. 2.7 into Eq. 2.6, one obtains

$$\left(\frac{\partial f}{\partial t}\right)_i^n + u\left(\frac{\partial f}{\partial x}\right)_i^n = \frac{u\Delta x}{2}(1 - C)\left(\frac{\partial^2 f}{\partial x^2}\right)_i^n + 0\left(\Delta x^2\right) + 0\left(\Delta t^2\right). \tag{2.8}$$

The right-hand side (RHS) of Eq. 2.8 corresponds to the truncation error (TE). The leading term of TE acts as a false diffusion with second-order derivative in space; the false or numerical diffusion coefficient is

$$L_{exp} = \frac{u\Delta x}{2}(1 - C). \tag{2.9}$$

The first term in Eq. 2.9 comes from the numerical error of the first-order upwind scheme with respect to space. The second term, with C, in Eq. 2.9 comes from the numerical error due to the discretization with respect to time.

Similar conclusions are obtained when the convective term of Eq. 2.1 is discretized implicitly at time level n+1. For the case of an implicit scheme, the numerical diffusion coefficient is given as follows:

$$L_{imp} = \frac{u\Delta x}{2}(1 + C). \tag{2.10}$$

In the implicit case, the Courant number C can exceed 1, but Eq. 2.10 shows that this occurs at the expense of an even greater numerical diffusion. Then, the numerical diffusion due to time discretization is greater than that due to the first-order upwind scheme. This is the reason why we need high-order schemes in time, even if we use implicit schemes with respect to time.

2.1.2 Multidimensional Flows

In the case of one-dimensional flows, the numerical diffusions are introduced only in the flow direction. But, in the case of multidimensional flows with a skewed angle between the computational grids and the flow direction, a new numerical diffusion is introduced into the direction normal to the flow direction.

In a two-dimensional computational grid with the skewed angle θ between the x-coordinate axis and the flow line, we consider the convection terms with constant positive transporting velocities u and v as follows:

$$u\frac{\partial f}{\partial x} + v\frac{\partial f}{\partial y}. \tag{2.11}$$

The first-order upwind scheme for the above convection terms yields the truncation error

$$TE = \frac{1}{2}u\Delta x\frac{\partial^2 f}{\partial x^2} + \frac{1}{2}v\Delta y\frac{\partial^2 f}{\partial y^2} + O\left(\Delta x^2\right) + O\left(\Delta y^2\right). \tag{2.12}$$

If we transform the (x-y) coordinate to the new (s-n) coordinate (see Fig. 2.1), in which s and n are parallel and normal to the flow direction, respectively, we have

$$TE = \left(L_x \cos\theta + L_y \sin\theta\right)\frac{\partial^2 f}{\partial s^2} + 2\sin\theta\cos\theta\left(L_x - L_y\right)\frac{\partial^2 f}{\partial s \partial n}$$

$$+ \left(L_x \sin\theta + L_y \cos\theta\right)\frac{\partial^2 f}{\partial n^2} + O\left(\Delta s^2\right) + O\left(\Delta n^2\right), \tag{2.13}$$

where

$$L_x = u\,\Delta x/2, \tag{2.14}$$

and

$$L_y = v\,\Delta y/2. \tag{2.15}$$

The third term in the RHS of Eq. 2.13 stands for the numerical diffusion in the direction normal to the flow direction. Because convection does not exist in the n direction, this new numerical diffusion turns out to be a significant error, especially for a steep gradient of the transported quantity f in the n direction. This is another reason why we need high-order schemes or skewed upwind schemes in space in multidimensional flows.

2.2 Numerical Instability

According to the equivalence theorem of Lax, stability of numerical solutions (ϕ) is the necessary and sufficient condition for ϕ to converge to the exact solution (ϕ_{pdf}) of the partial differential equation, given a well-posed initial-value problem and a finite-difference approximation to it that satisfies the consistency conditions. The difference between ϕ and ϕ_{pdf} is numerical error (E), which is decomposed into two parts in terms of the exact solution (ϕ_t) of the finite-difference equation as follows:

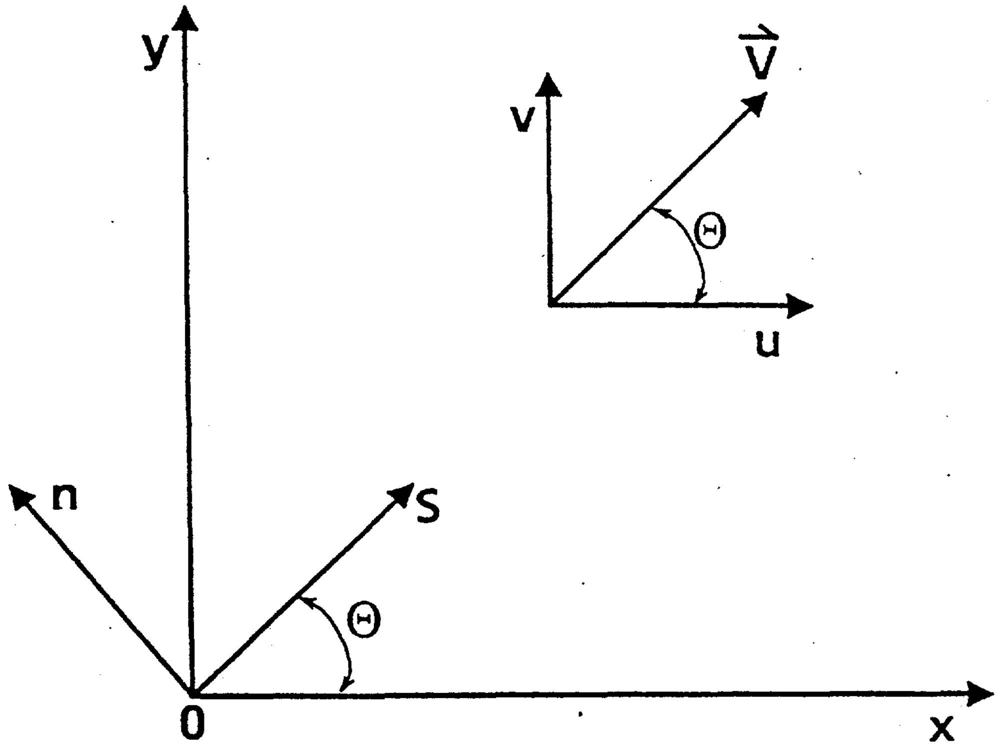

Fig. 2.1 Numerical diffusion when computational grid lines are skewed to the velocity direction

$$E \equiv \phi - \phi_{pdf}$$

$$= E_1 + E_2, \quad (2.16)$$

$$E_1 \equiv \phi - \phi_t, \quad (2.17)$$

$$E_2 \equiv \phi_t - \phi_{pdf}. \quad (2.18)$$

Here, E_1 comes mainly from accumulation of round-off errors and the errors inherent to numerical solution procedures. E_2 includes truncation errors, as well as numerical oscillations, as discussed in Sec. 1.

2.2.1 Round-Off Errors

Here, we consider a well-posed transport equation

$$\frac{\partial \phi}{\partial t} + u\frac{\partial \phi}{\partial x} = \nu\frac{\partial^2 \phi}{\partial x^2}, \quad (2.19)$$

where t is time, x is coordinate, u is transporting velocity, and ν is a diffusion parameter. Discretization of Eq. 2.19 in a single step with respect to time, in a computation grid with N mesh points, yields

$$(\Phi^{n+1}) = (A)(\Phi^n) + (B), \quad (2.20)$$

with time step number n. In Eq. 2.20, A and B are N x N and N matrixes, respectively, which are composed of time step Δt, space increment Δx, ν, $\phi_i^n (i = 1, \ldots N)$, and boundary values ϕ_0 and ϕ_{N+1} in the case of the Dirichlet condition.

For the numerical solution (Φ^{n+1}) to be stable at each time step n+1, we need

$$\|A\| \leqq 1, \tag{2.21}$$

where $\|A\|$ stands for a norm of matrix A.[24]

When we want to obtain a steady-state solution by means of the time-marching technique, for the steady-state solution (Φ^{∞}) to be stable, we get

$$\rho(A) \leqq 1, \tag{2.22}$$

where ρ means the spectrum radius of A.[25]

Periodic boundary conditions, among all boundary conditions, present the most severe restrictions for stability. In the case of a periodic boundary condition, the stability condition, Eq. 2.22, is equivalent to von Neumann analysis.[21,26] Fig. 2.2 shows the stability domain given by von Neumann stability analyses for the Forward Time-Centered Space (FTCS) scheme, the QUICK scheme, and the LECUSSO scheme.

2.2.2 Numerical Oscillations

Numerical oscillations, which are different from numerical instability due to the accumulation of round-off errors, are the indication of the performance of exact solutions of finite-difference equations. Hence, we examine the performance of the exact solution of the finite-difference equations.

Methods to perform numerical oscillation analysis are available. In the following, we review and apply these methods to the turbulence equations.

2.2.2.1 Patanker's Rules[17]

According to Patanker's rule for numerical stability, in the following difference equation,

$$a_0 \phi_0 = \Sigma a_i \phi_i + S, \tag{2.23}$$

(Rule 2): $a_i > 0$ $(i = 0, 1, \ldots)$,

and in the source term $S = S_0 + a_S \phi$,

(Rule 3): $a_S < 0$.

In the two-equation turbulence model (k-ε), the source term S_k in the turbulence kinetic energy (k) equation is

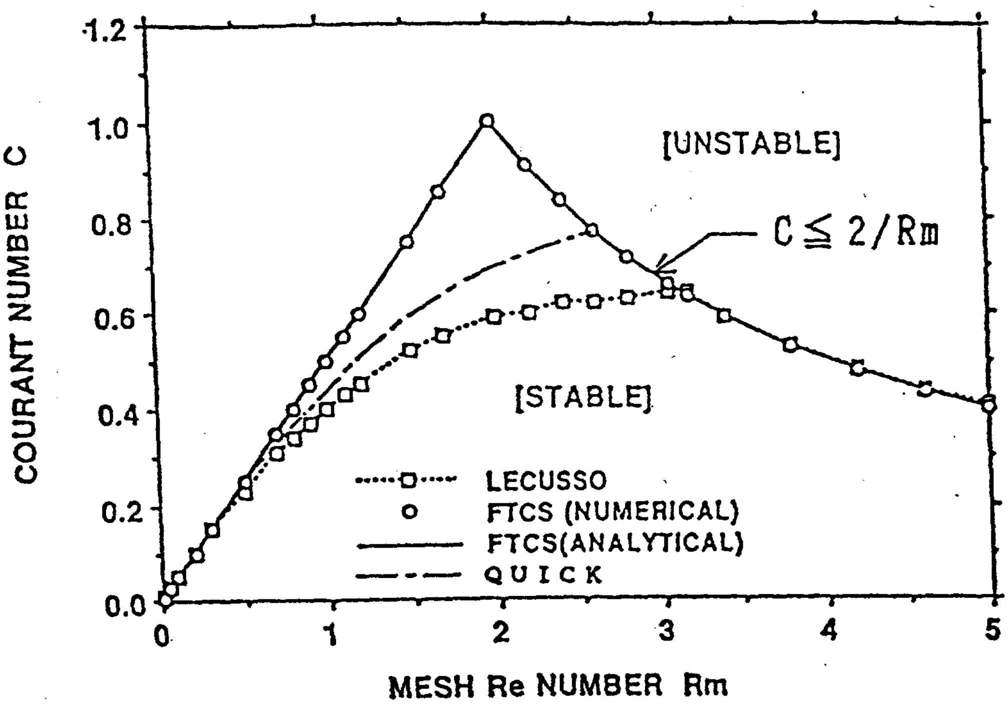

Fig. 2.2. Stability domain for explicit scheme

$$S_k = P_k + G_k - \rho\varepsilon. \tag{2.24}$$

In the vicinity of the wall, using the mixing length (L) theory, we get

$$S_k = P_k + G_k - [C_d\rho(k^n)^{1/2}/L]k^{n+1}, \tag{2.25}$$

which satisfies Rule 3. The source term S_ε of dissipation of k is

$$S_\varepsilon = C_1(P_k + C_3G_k)\varepsilon/k - C_2\varepsilon^2/k. \tag{2.26}$$

We can linealize Eq. 2.26 by two methods:

$$S_\varepsilon = [C_1(P_k + C_3G_k)/k - C_2\varepsilon^n/k]\varepsilon^{n+1}, \tag{2.27}$$

which seems to be most adequate in numerical accuracy, but does not always satisfy Rule 3; and

$$S_\varepsilon = C_1(P_k + C_3G_k)\varepsilon^n/k - (C_2\varepsilon^n/k)\varepsilon^{n+1}, \tag{2.28}$$

which satisfies Rule 3. Hence, from the viewpoint of numerical stability, the second method, Eq. 2.28, is adequate.

The high-order schemes such as QUICK never satisfy Rule 2, but they give nonoscillating solutions for the mesh with Reynolds number <≈2. Therefore, Patanker's rule 2 is too restrictive. Hence, we should go to the next method.

2.2.2.2 Characteristic Polynomial Analysis

Discretization of the convection term in Eq. 2.19 without a transient term by using four base points, and the diffusion term by a centered-space scheme for $u > 0$, yields

$$A\phi_{i+1} - B\phi_i + C\phi_{i-1} - D\phi_{i-2} = 0. \quad (2.29)$$

The general solution of Eq. 2.29 is

$$\phi_i = a(\lambda_1)_i + b(\lambda_2)_i + c(\lambda_3)_i, \quad (2.30)$$

where λ_1, λ_2, and λ_3 are the roots of the following characteristic equation

$$A\lambda^3 - B\lambda^2 + C\lambda - D = 0. \quad (2.31)$$

Because numerical schemes are generally constructed in such a way as to realize a constant solution ($\phi = 1$), we have the following relation

$$A - B + C - D = 0. \quad (2.32)$$

Hence, the roots of Eq. 2.31 are given as follows

$$\lambda_1 = 1, \quad \lambda_2 = \frac{B - A + \Sigma^{1/2}}{2A}, \quad \lambda_3 = \frac{B - A - \Sigma^{1/2}}{2A}, \quad (2.33)$$

$$\Sigma \equiv (A - B)^2 - 4AD. \quad (2.34)$$

Even if one of the roots is negative, the solution of Eq. 2.30 oscillates. Therefore, the necessary and sufficient condition for nonoscillating steady-state solution is given as follows:

$$\Sigma \geqq 0, \quad \lambda_2 \geqq 0, \quad \lambda_3 \geqq 0 \quad (2.35)$$

In the case of the QUICK scheme, we have

$$A = 1 - 3R_m/8, \; B = 2 + 3R_m/8, \; C = 1 + 7R_m/8, \; D = R_m/8,$$

where R_m is the mesh Re number. From the condition of Eq. 2.35, we get

$$R_m \leqq 8/3. \quad (2.36)$$

In cases of the second-order central scheme, the QUICK scheme and the LECUSSO scheme with uniform-mesh-size grids, nonoscillating conditions are shown in Table 2.1. This characteristic polynomial analysis was recently extended into nonuniform-mesh-size grids and the numerical oscillation analysis on the LECUSSO scheme was performed in nonuniform-mesh-size grids.[27] It has been shown that the LECUSSO scheme can give solutions that suffer from numerical oscillations in nonuniform-mesh-size grids, although the LECUSSO scheme shows quite stable solutions as compared with the conventional high-order schemes such as QUICK and the third-order upwind scheme.

Table 2.1. Nonoscillating conditions based on characteristic polynomial analysis

Scheme	2nd–Order CS[a]	QUICK[a]	LECUSSO[a,b]
A	$1 - R_m/2$	$1 - 3R_m/8$	$1 - (0.5 - \xi)R_m$
B	2	$2 + 3R_m/8$	$2 + 3\xi R_m$
C	$1 + R_m/2$	$1 + 7R_m/8$	$1 + (0.5 + 3\xi) R_m$
D	0	$R_m/8$	ξR_m
Σ	$R_m^2/4$	$1 + R_m + 3R_m^2/4$	$1 + R_m + (1/4 + 4\xi)R_m^2$
λ_1	1	1	1
λ_2	$\frac{2 + R_m}{2 - R_m}$	$\frac{1 + 3R_m/4 + \sqrt{\Sigma}}{2(1 - 3R_m/8)}$	$\frac{1 + 0.5R_m + 2\xi R_m + \sqrt{\Sigma}}{2[1 - (0.5 - \xi)R_m]}$
λ_3	None	$\frac{1 + 3R_m/4 - \sqrt{\Sigma}}{2(1 - 3R_m/8)}$	$\frac{1 + 0.5R_m + 2\xi R_m - \sqrt{\Sigma}}{2[1 - (0.5 - \xi)R_m]}$
Nonoscillating Condition	$R_m \leqq 2$	$R_m \leqq 8/3$	Nonrestriction

a. $R_m = V\Delta x/\nu$ (mesh Reynolds number).

b. $\xi \equiv \dfrac{(R_m - 2)\exp[R_m] + R_m + 2}{2R_m(\exp[R_m] - 2 + \exp[-R_m])}$

2.2.2.3 Tomiyama's Method[28]

Tomiyama recently proposed a general theory to obtain the onset condition of the dynamic numerical oscillations in transient problems. Although this theory is rigorous and includes boundary condition effects, we need to solve eigenvalue problems for each computational grid. The nonoscillating condition depends on the node number in the computational grid and the boundary conditions. In the case of QUICK with uniform mesh grids, the nonoscillating condition of transient solutions is

$$R_m \leqq (1.5 - 2.6). \tag{2.37}$$

Comparing Eq. 2.36 with Eq. 2.37, one finds that the dynamic oscillating condition for transient solutions gives a more restrictive condition than the static oscillating condition for steady solutions.

3 General Form of Conservation Equations

All conservation equations of mass, momentum, energy, turbulence kinetic energy, and dissipation of turbulence kinetic energy possess a common form. If we denote the general dependent variable as ϕ per unit volume, the corresponding conservation equations have the following form in the Cartesian coordinate system:

In continuum domain

$$\underbrace{\frac{\partial}{\partial t}(\phi)}_{\text{Unsteady}} + \underbrace{\frac{\partial}{\partial x}(u\phi) + \frac{\partial}{\partial y}(v\phi) + \frac{\partial}{\partial z}(w\phi)}_{\text{Convection}} = \underbrace{\frac{\partial}{\partial x}\left(\Gamma_\phi \frac{\partial \phi}{\partial x}\right) + \frac{\partial}{\partial y}\left(\Gamma_\phi \frac{\partial \phi}{\partial y}\right) + \frac{\partial}{\partial z}\left(\Gamma_\phi \frac{\partial \phi}{\partial z}\right)}_{\text{Diffusion}} + \underbrace{S_\phi}_{\text{Source}} \tag{3.1a}$$

In quasicontinuum domain[29]

$$\underbrace{\frac{\partial}{\partial t}(\gamma_v \phi)}_{\text{Unsteady}} + \underbrace{\frac{\Delta(\gamma_x u\phi)}{\Delta x} + \frac{\Delta(\gamma_y v\phi)}{\Delta y} + \frac{\Delta(\gamma_z w\phi)}{\Delta z}}_{\text{Convection}}$$

$$= \underbrace{\frac{\Delta\left(\gamma_x \Gamma_\phi \frac{\partial \phi}{\partial x}\right)}{\Delta x} + \frac{\Delta\left(\gamma_y \Gamma_\phi \frac{\partial \phi}{\partial y}\right)}{\Delta y} + \frac{\Delta\left(\gamma_z \Gamma_\phi \frac{\partial \phi}{\partial z}\right)}{\Delta z}}_{\text{Diffusion}} + \underbrace{\gamma_v S_\phi}_{\text{Source}} \tag{3.1b}$$

Here, u, v, and w are the velocities in the x, y, and z directions, respectively; γ_v is the volume porosity (fraction of the volume occupied by the fluid) and γ_x, γ_y, and γ_z are the directional surface porosities (fraction of the surface area that is unobstructed to fluid flow) in the x, y, and z directions, respectively. The diffusion coefficient Γ_ϕ and the source term S_ϕ are specific to each meaning of ϕ. ϕ and the sources for all conservation equations are given in Table 3.1.

The general form (Eq. 3.1) of the conservation equations in the cylindrical coordinate system is the same as it is in the Cartesian coordinate system, when we place the centrifugal and Coriolis force terms in the source term S_ϕ. We can, therefore, apply all formulations for the Cartesian coordinates to cylindrical coordinates with the simple transformations shown in Table 3 of Ref. 1.

In the conventional COMMIX-1C program, ϕ is defined as a quantity per unit mass and $\phi = 1$ is adopted for the continuity equation. But, by reformulating ϕ as a quantity per unit volume, we can deal with all of the unified governing equations. Moreover, the convection term involves the form of

Missing MathType's Belmont font.

Table 3.1. Source terms in Cartesian coordinate system[a]

Equation (e)	Variable (ϕ) (e/m^3)	Direction	Diffusion Coefficient (Γ_ϕ)(m^2/s)	Source Term (S_ϕ)
Mass	ρ	Scalar	0	0
Momentum				
(i)	ρu	x	$\nu_\ell + \nu_t$	$\rho g_x + V_x - R_x - \left(\frac{\partial p}{\partial x}\right)$
(ii)	ρv	y	$\nu_\ell + \nu_t$	$\rho g_y + V_y - R_y - \left(\frac{\partial p}{\partial y}\right)$
(iii)	ρw	z	$\nu_\ell + \nu_t$	$\rho g_z + V_z - R_z - \left(\frac{\partial p}{\partial z}\right)$
Energy	ρh	Scalar	$\alpha_\ell + \frac{\nu_t}{\sigma_h}$	$\frac{dp}{dt} + \dot{Q}_{rb} + \dot{Q} + \Phi$
Turbulence Kinetic Energy	ρk	Scalar	$\nu_\ell + \frac{\nu_t}{\sigma_k}$	$P_k + G_k - \rho\varepsilon$
Dissipation of Turbulence Kinetic Energy	$\rho\varepsilon$	Scalar	$\nu_\ell + \frac{\nu_t}{\sigma_\varepsilon}$	$C_1(P_k + G_k)\frac{\varepsilon}{k} - C_2\rho\frac{\varepsilon^2}{k}$

[a]Symbols in the table are defined as follows:

V_x, V_y, V_z	Balance of the viscous diffusion terms
R_x, R_y, R_z	Distributed resistances due to solid structures in a momentum control volume
$\dot{Q}_{rb}$	Rate of heat liberated from solid structures per unit fluid volume
$\dot{Q}$	Rate of internal heat generation per unit fluid volume
Φ	Dissipation function
ν_ℓ	Laminar kinetic viscosity
ν_t	Turbulence kinematic viscosity $\nu_t = C_D k^2/\varepsilon$
α_ℓ	Laminar thermal diffusivity $\alpha_\ell = \lambda_\ell/(\rho C_p)$, ($\lambda_\ell$: thermal conductivity; C_p: specific heat)
σ_h, σ_k, σ_ε	Turbulent Prandtl number for h, k, and ε, respectively
P_k	Production of k due to mean shear
G_k	Production or suppression of k due to buoyancy
C_1,C_2	Constant of coefficients

4 High–Order Schemes for Convection Terms

4.1 Control Volume and Computational Grid

In COMMIX–1C, the computational cell is defined by the locations of the cell volume faces, and a grid point is placed in the geometrical center of each cell volume. Cell sizes can be nonuniform. This type of construction is shown in Fig. 4.1. The convention used in COMMIX–1C for defining neighboring cells and faces is given in Table 4.1.

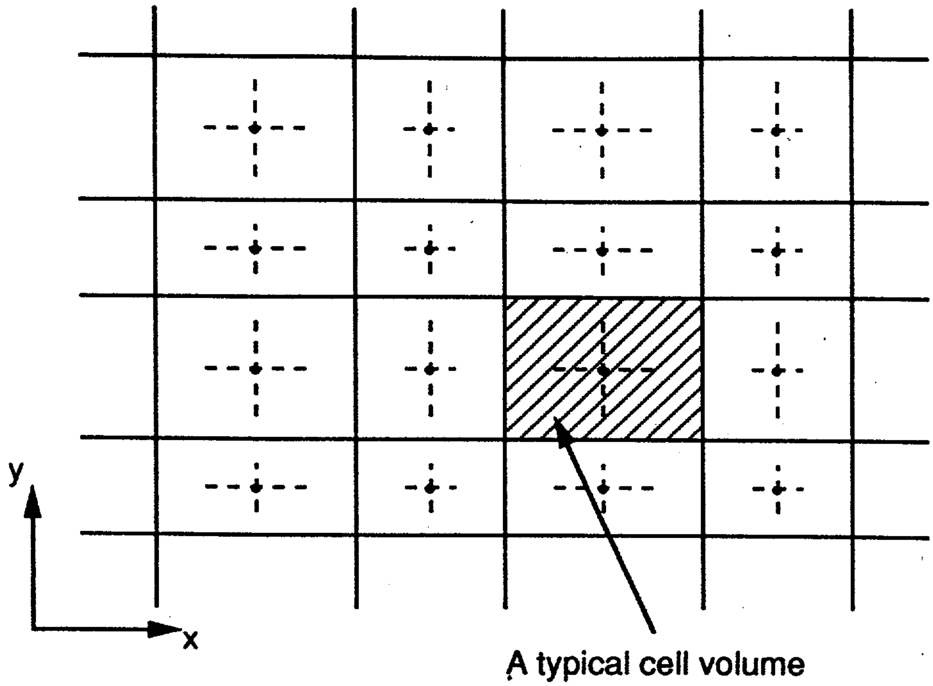

Fig. 4.1. Construction of cell volumes

Table 4.1. Convention used in COMMIX-1C to define neighboring-cell control volumes

Subscript	Cell Centers x	Cell Centers y	Cell Centers z	Cell Face Center x	Cell Face Center y	Cell Face Center z
0	i,	j,	k			
1	i−1,	j,	k	i−1/2	j,	k
2	i+1,	j,	k	i+1/2,	j,	k
3	i,	j−1,	k	i,	j−1/2,	k
4	i,	j+1,	k	i,	j+1/2	k
5	i,	j,	k−1	i,	j,	k−1/2
6	i,	j,	k+1	i,	j,	k+1/2

We use a staggered grid in the above cell system, in which all dependent field variables (pressure, temperature, density, enthalpy, turbulence kinetic energy, dissipation of turbulence kinetic energy, physical properties, etc.) are calculated at a cell center, as shown in Fig. 4.2, and all flow variables (velocity components) are calculated at the surface of a cell, as shown in Fig. 4.3. This staggered grid system plays a role in suppressing spurious oscillations of pressure. The number in a circle in Fig. 4.2 denotes the surface number used for a main control volume. The number and letter in a circle in Fig. 4.4 denote the surface number used for a momentum control volume. In the case of z-momentum control volume, surface number 1 is decomposed into two parts, 1-M and 1-P, which denote, respectively, the negative and positive half surfaces of surface No. 1.

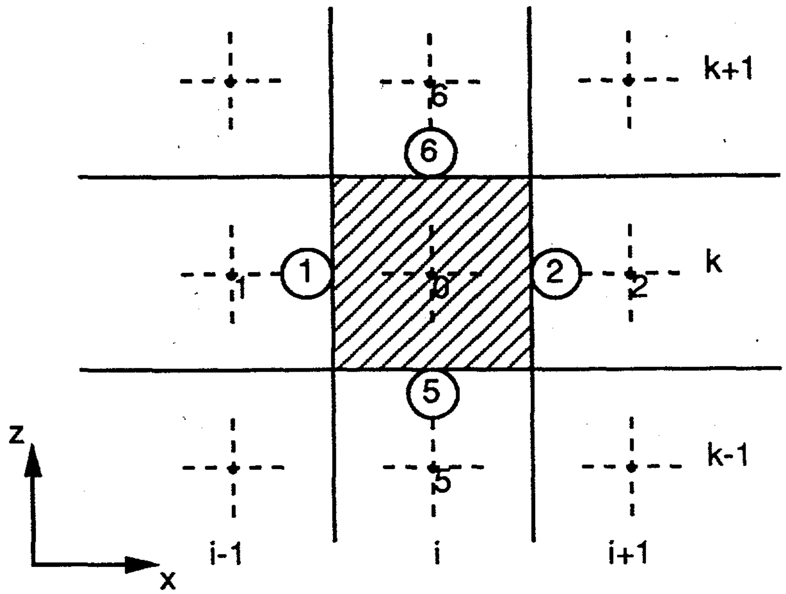

Fig. 4.2. Cell volume around point 0 in i,j,k notation. The number in a circle denotes the surface number.

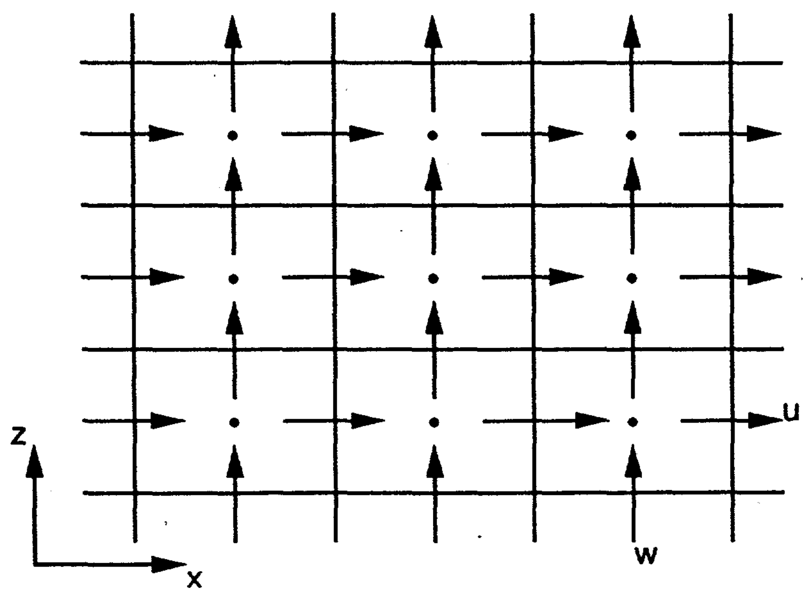

Fig. 4.3. Staggered grid

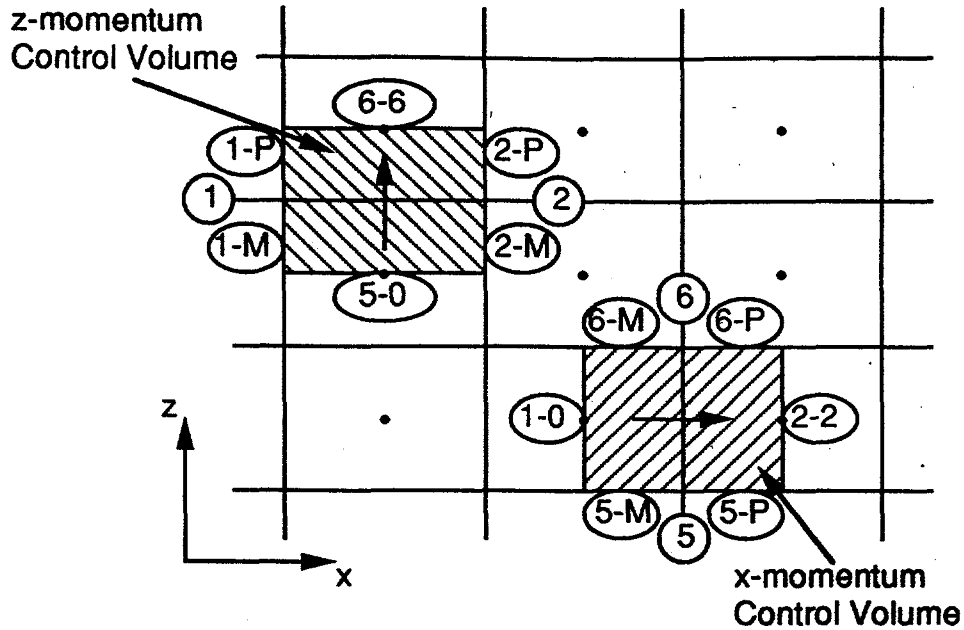

Fig. 4.4. Momentum control volumes. The numbers and letters in a circle denote the surface number

Table 4.2. Convention used in COMMIX-1C to define neighboring control volumes for z-direction momentum equations

	Momentum Control Volume Centers			Momentum Control Volume Face Centers		
Subscript	x	y	z	x	y	z
0	i,	j,	k+1/2			
1	i–1,	j,	k+1/2	i–1/2,	j,	k+1/2
2	i+1,	j,	k+1/2	i+1/2,	j,	k+1/2
3	i,	j–1,	k+1/2	i,	j–1/2,	k+1/2
4	i,	j+1,	k+1/2	i,	j+1/2	k+1/2
5	i,	j,	k–1/2	i,	j,	k
6	i,	j,	k+3/2	i,	j,	k+1

A direct consequence of the staggered grid is that the control volumes to be used for the conservation of momentum must also be staggered. The control volumes shown in Figs. 4.1 and 4.2 will now be referred to as the main control volumes. The control volumes for momentum will be staggered in the direction of the momentum so that the faces normal to that direction pass through the grid points (see Fig. 4.4). Thus, the pressures at these grid points can be used directly for calculating the pressure force on the momentum control volume. Table 4.2 shows the convention used for the subscripts of the z-direction momentum control volume, and Fig. 4.4 shows the momentum control volumes for the x and z directions.

4.2 QUICK Scheme in Nonuniform Mesh Grids

Here, we derive the QUICK scheme in a computational grid with nonuniform mesh size for equations written in the conservative form. We approximate the convection term in the governing equations for positive transporting velocity u as follows:

$$\left.\frac{d(u\phi)}{dx}\right|_i = \frac{u_{i+1/2}\hat{\phi}_{i+1/2} - u_{i-1/2}\hat{\phi}_{i-1/2}}{\Delta x_i} \tag{4.1}$$

in a computational grid with mesh increment Δx_i, as shown in Fig. 4.5. In Eq. 4.1, the transported quantities $\hat{\phi}_{i+1/2}$ and $\hat{\phi}_{i-1/2}$ on the surfaces of control volume i are approximated by the following quadratic upstream interpolation for $u_{i+1/2} > 0$ and $u_{i-1/2} > 0$:

$$\hat{\phi}_{i+1/2} = \alpha^+_{i+1/2}\phi_{i-1} + \beta^+_{i+1/2}\phi_i + \gamma^+_{i+1/2}\phi_{i+1} \tag{4.2a}$$

and

$$\hat{\phi}_{i-1/2} = \alpha^+_{i-1/2}\phi_{i-2} + \beta^+_{i-1/2}\phi_{i-1} + \gamma^+_{i-1/2}\phi_i, \tag{4.2b}$$

where superscript + denotes positive transporting velocity.

In the following, we derive the expressions of α^+, β^+, and γ^+ in Eq. 4.2a for nonuniform mesh size. We have a second-order interpolation formula such that

$$\hat{\phi}(x) = \frac{(x - x_i)(x - x_{i+1})}{(x_{i-1} - x_i)(x_{i-1} - x_{i+1})}\phi_{i-1} + \frac{(x - x_{i-1})(x - x_{i+1})}{(x_i - x_{i-1})(x_i - x_{i+1})}\phi_i$$
$$+ \frac{(x - x_{i-1})(x - x_i)}{(x_{i+1} - x_{i-1})(x_{i+1} - x_i)}\phi_{i+1}. \tag{4.3}$$

At $x = x_{i+1/2} = x_i + \Delta x_i/2$, we have

$$\begin{aligned}
x - x_i &= x_i + \Delta x_i/2 - x_i = \Delta x_i/2, \\
x - x_{i+1} &= x_i + \Delta x_i/2 - x_{i+1} = -(\Delta x_i + \Delta x_{i+1})/2 + \Delta x_i/2 = -\Delta x_{i+1}/2, \\
x - x_{i-1} &= \Delta x_i + \Delta x_{i-1}/2 = (2\Delta x_i + \Delta x_{i-1})/2, \\
x_{i-1} - x_i &= -(\Delta x_{i-1} + \Delta x_i)/2, \\
x_{i-1} - x_{i+1} &= -(\Delta x_{i-1} + 2\Delta x_i + \Delta x_{i+1})/2, \\
x_i - x_{i+1} &= -(\Delta x_i + \Delta x_{i+1})/2.
\end{aligned}$$

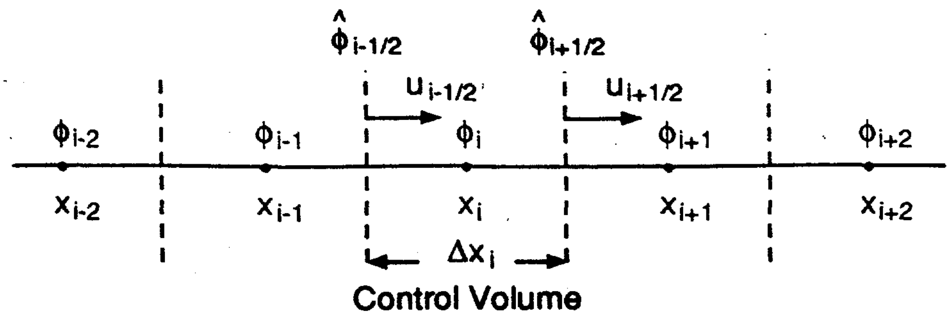

Fig. 4.5. One–dimensional computational grid

Hence, we get

$$\alpha^{+}_{i+1/2} = -\frac{\Delta x_i \; \Delta x_{i+1}}{(\Delta x_{i-1} + \Delta x_i)(\Delta x_{i-1} + 2\Delta x_i + \Delta x_{i+1})}, \tag{4.4a}$$

$$\beta^{+}_{i+1/2} = \frac{(2\Delta x_i + \Delta x_{i-1})\Delta x_{i+1}}{(\Delta x_{i-1} + \Delta x_i)(\Delta x_i + \Delta x_{i+1})}, \tag{4.4b}$$

and

$$\gamma^{+}_{i+1/2} = \frac{(2\Delta x_i + \Delta x_{i-1})\Delta x_i}{(\Delta x_{i-1} + 2\Delta x_i + \Delta x_{i+1})(\Delta x_i + \Delta x_{i+1})}. \tag{4.4c}$$

For $\Delta x_i = \Delta x_{i+1} = \Delta x_{i-1}$, we get

$$\hat{\phi}_{i+1/2} = -\frac{1}{8}\phi_{i-1} + \frac{6}{8}\phi_i + \frac{3}{8}\phi_{i+1}.$$

When $u_{i+1/2} < 0$, $\hat{\phi}_{i+1/2}$ is interpolated as follows

$$\hat{\phi}_{i+1/2} = \alpha^{-}_{i+1/2}\phi_i + \beta^{-}_{i+1/2}\phi_{i+1} + \gamma^{-}_{i+1/2}\phi_{i+2}. \tag{4.5}$$

We have interpolation formula

$$\hat{\phi}(x) = \frac{(x - x_{i+1})(x - x_{i+2})}{(x_i - x_{i+1})(x_i - x_{i+2})}\phi_i + \frac{(x - x_i)(x - x_{i+2})}{(x_{i+1} - x_i)(x_{i+1} - x_{i+2})}\phi_{i+1}$$
$$+ \frac{(x - x_i)(x - x_{i+1})}{(x_{i+2} - x_i)(x_{i+2} - x_{i+1})}\phi_{1+2}. \tag{4.6}$$

At $x = x_{i+1/2}$, we have

$$x_i - x_{i+1} = -(\Delta x_{i+1} + \Delta x_{i+2})/2,$$

$$x - x_{i+2} = -(2\Delta x_{i+1} + \Delta x_{i+2})/2,$$

$$x_i - x_{i+2} = -(\Delta x_i + 2\Delta x_{i+1} + \Delta x_{i+2})/2,$$

and

$$x_{i+1} - x_{i+2} = -(\Delta x_{i+1} + \Delta x_{i+2})/2.$$

Hence, we get

$$\alpha^-_{i+1/2} = \frac{\Delta x_{i+1}(2\Delta x_{i+1} + \Delta x_{i+2})}{(\Delta x_i + \Delta x_{i+1})(\Delta x_i + 2\Delta x_{i+1} + \Delta x_{i+2})}, \tag{4.7a}$$

$$\beta^-_{i+1/2} = \frac{\Delta x_i(2\Delta x_{i+1} + \Delta x_{i+2})}{(\Delta x_i + \Delta x_{i+1})(\Delta x_{i+1} + \Delta x_{i+2})}, \tag{4.7b}$$

and

$$\gamma^-_{i+1/2} = -\frac{\Delta x_i \, \Delta x_{i+1}}{(\Delta x_i + 2\Delta x_{i+1} + \Delta x_{i+2})(\Delta x_{i+1} + \Delta x_{i+2})}. \tag{4.7c}$$

For $\Delta x_i = \Delta x_{i+1} = \Delta x_{i+2}$,

$$\hat{\phi}_{i+1/2} = \frac{3}{8}\phi_i + \frac{6}{8}\phi_{i+1} - \frac{1}{8}\phi_{i+2}.$$

4.3 LECUSSO Scheme in Nonuniform Mesh Grids

Here, we extend the LECUSSO scheme to nonuniform-mesh-size grids based on the conservative form. Following the methodology used in Ref. 13, we consider the following one–dimensional steady convection/diffusion equation in the conservative form

$$\frac{d(u\phi)}{dx} = \nu\frac{d^2\phi}{dx^2}, \tag{4.8}$$

where u is the fluid velocity; ν is a diffusion parameter, such as kinematic viscosity or thermal diffusivity; x is the spatial coordinate; and ϕ is the transported quantity. We approximate the convection term for $u > 0$ as follows:

$$\left.\frac{d(u\phi)}{dx}\right|_i = \frac{\left(u_{i+1/2}\hat{\phi}_{i+1/2} - u_{i-1/2}\hat{\phi}_{i-1/2}\right)}{\Delta x_i}, \tag{4.9}$$

in a nonuniform-mesh-size grid with mesh increment Δx_i, as shown in Fig. 4.5, and ϕ_i and u_i defined at x_i.

Similar to the idea in the QUICK scheme, the transported quantities ϕ on the surfaces of control volume i are approximated by the following expressions for $u_{i+1/2} > 0$ and $u_{i-1/2} > 0$

$$\hat{\phi}_{i+1/2} = \alpha^+_{i+1/2}\phi_{i-1} + \beta^+_{i+1/2}\phi_i + \gamma^+_{i+1/2}\phi_{i+1}, \tag{4.10a}$$

and

$$\hat{\phi}_{i-1/2} = \alpha^+_{i-1/2}\phi_{i-2} + \beta^+_{i-1/2}\phi_{i-1} + \gamma^+_{i-1/2}\phi_i. \tag{4.10b}$$

Here, based on the basic idea of the LECUSSO scheme, we impose the condition that Eqs. 4.10a and 4.10b satisfy an analytical solution of Eq. 4.8 with constant u. Namely, with the requirement that Eq. 4.10a exactly realize $\phi = 1$, $\phi = x$, and $\phi = a \cdot \exp(R_{i+1/2}x) + b$, where a and b are determined by boundary conditions, but here may be arbitrary, and $R_{i+1/2} \equiv u_{i+1/2}/v_{i+1/2}$, we obtain

$$\alpha^+_{i+1/2} + \beta^+_{i+1/2} + \gamma^+_{i+1/2} = 1 \tag{4.11a}$$

$$-\alpha^+_{i+1/2}\left(\Delta x_i + \Delta x_{i-1}\right) + \gamma^+_{i+1/2}\left(\Delta x_i + \Delta x_{i+1}\right) = \Delta x_i, \tag{4.11b}$$

and

$$\alpha^+_{i+1/2}\exp\left[-R_{i+1/2}(\Delta x_i + \Delta x_{i-1})/2\right] + \beta^+_{i+1/2}$$

$$+ \gamma^+_{i+1/2}\exp\left[R_{i+1/2}(\Delta x_i + \Delta x_{i+1})/2\right] = \exp\left(R_{i+1/2}\Delta x_i/2\right). \tag{4.11c}$$

From the above algebraic equations, we derive the solution as follows:

$$\alpha^+_{i+1/2} = W^{-1}\{-\Delta x_i \exp[R_{i+1/2}(\Delta x_i + \Delta x_{i+1})/2] + (\Delta x_i + \Delta x_{i+1})\exp(R_{i+1/2}\Delta x_i/2) - \Delta x_{i+1}\}, \tag{4.12a}$$

$$\beta^+_{i+1/2} = W^{-1}\{\Delta x_{i+1}\exp[-R_{i+1/2}(\Delta x_i + \Delta x_{i-1})/2] - (\Delta x_{i+1} + 2\Delta x_i + \Delta x_{i-1})\exp(R_{i+1/2}\Delta x_i/2)$$

$$+ (2\Delta x_i + \Delta x_{i-1})\exp[R_{i+1/2}(\Delta x_i + \Delta x_{i+1})/2]\}, \tag{4.12b}$$

and

$$\gamma^+_{i+1/2} = W^{-1}\{(\Delta x_i + \Delta x_{i-1})\exp(R_{i+1/2}\Delta x_i/2)$$

$$+ \Delta x_i \exp[-R_{i+1/2}(\Delta x_i + \Delta x_{i-1})/2] - 2\Delta x_i - \Delta x_{i-1}\}, \tag{4.12c}$$

where

$$W = (\Delta x_i + \Delta x_{i-1})\exp[R_{i+1/2}(\Delta x_i + \Delta x_{i+1})/2]$$
$$+ (\Delta x_i + \Delta x_{i+1})\exp[-R_{i+1/2}(\Delta x_i + \Delta x_{i-1})/2]$$
$$- 2\Delta x_i - \Delta x_{i-1} - \Delta x_{i+1}, \tag{4.13}$$

and the mesh Reynolds number is defined as $R_m = R_{i+1/2}\Delta x_i$. In the same manner as that in the case of uniform mesh sizes, the coefficients $\alpha^+_{i+1/2}$, $\beta^+_{i+1/2}$, and $\gamma^+_{i+1/2}$ are expressed in terms of local variables, such as space mesh increments and mesh Reynolds number.

The coefficients for $\hat{\phi}_{i-1/2}$ can be obtained by changing the suffix i in Eq. 4.12 with the suffix i–1, when $u_{i-1/2}$ is positive.

In the case of $u_{i+1/2} < 0$, $\hat{\phi}_{i+1/2}$ is approximated as follows:

$$\hat{\phi}_{i+1/2} = \alpha^-_{i+1/2}\phi_i + \beta^-_{i+1/2}\phi_{i+1} + \gamma^-_{i+1/2}\phi_{i+2}. \tag{4.14}$$

With the requirement that $\hat{\phi}_{i+1/2}$ exactly realize $\phi = 1$, $\phi = x$, and $\phi = \exp(R_{i+1/2}x)$, we obtain

$$\alpha^-_{i+1/2} + \beta^-_{i+1/2} + \gamma^-_{i+1/2} = 1, \tag{4.15a}$$

$$\beta^-_{i+1/2}(\Delta x_i + \Delta x_{i+1}) + \gamma^-_{i+1/2}(\Delta x_i + 2\Delta x_{i+1} + \Delta x_{i+2}) = \Delta x_i, \tag{4.15b}$$

$$\alpha^-_{i+1/2} + \beta^-_{i+1/2}\exp\left[R_{i+1/2}(\Delta x_i + \Delta x_{i+1})/2\right] + \gamma^-_{i+1/2}\exp\left[R_{i+1/2}(\Delta x_i + 2\Delta x_{i+1} + \Delta x_{i+2})/2\right]$$
$$= \exp(R_{i+1/2}\Delta x_i/2). \tag{4.15c}$$

From these linear equations, we derive the solution as follows:

$$\alpha^-_{i+1/2} = \frac{\left\{\begin{aligned}&-(2\Delta x_{i+1} + \Delta x_{i+2})\exp\left[R_{i+1/2}(\Delta x_i + \Delta x_{i+1})/2\right]\\ &+(\Delta x_{i+1} + \Delta x_{i+2})\exp\left(R_{i+1/2}\Delta x_i/2\right)\\ &+\Delta x_{i+1}\exp\left[R_{i+1/2}(\Delta x_i + 2\Delta x_{i+1} + \Delta x_{i+2})/2\right]\end{aligned}\right\}}{W}, \tag{4.16a}$$

$$\beta^-_{i+1/2} = \frac{\left\{\begin{aligned}&\Delta x_i\exp\left[R_{i+1/2}(\Delta x_i + 2\Delta x_{i+1} + \Delta x_{i+2})/2\right]\\ &-(\Delta x_i + 2\Delta x_{i+1} + \Delta x_{i+2})\exp\left(R_{i+1/2}\Delta x_i/2\right)\\ &+2\Delta x_{i+1} + \Delta x_{i+2}\end{aligned}\right\}}{W}, \tag{4.16b}$$

and

$$\gamma^-_{i+1/2} = \frac{(\Delta x_i + \Delta x_{i+1})\exp\left(R_{i+1/2}\Delta x_i/2\right) - \Delta x_i\exp\left[R_{i+1/2}(\Delta x_i + \Delta x_{i+1})/2\right] - \Delta x_{i+1}}{W}, \tag{4.16c}$$

where

$$W = (\Delta x_i + \Delta x_{i+1})\exp\left[R_{i+1/2}(\Delta x_i + 2\Delta x_{i+1} + \Delta x_{i+2})/2\right] + \Delta x_{i+1} + \Delta x_{i+2}$$

$$- (\Delta x_i + 2\Delta x_{i+1} + \Delta x_{i+2})\exp\left[R_{i+1/2}(\Delta x_i + \Delta x_{i+1})/2\right]. \tag{4.17}$$

We have another way to derive the conservative form of the equation directly from its nonconservative form, which was derived already in Ref. 22, by making use of the relations between the coefficients in both forms. We call this form the *straightforward scheme*, which is different from the above scheme which is based on *QUICK*. Both of the schemes approach the second-order upwind scheme when the transporting velocity goes to infinity. However, when the transporting velocity goes to zero, the scheme based on the *QUICK scheme* approaches the QUICK formulation, while the *straightforward scheme* approaches another second-order upwind formulation. In the case of uniform-mesh-size grids, the truncation error of the *QUICK scheme* is

$$TE = \frac{\Delta x^2}{24}\frac{\partial^3\phi}{\partial x^3} + 0\left(\Delta x^3\right), \tag{4.18a}$$

whereas the truncation error of the *straightforward scheme* is given by

$$TE = \frac{\Delta x^2}{12}\frac{\partial^3\phi}{\partial x^3} + 0\left(\Delta x^3\right). \tag{4.18b}$$

Because the TE of the scheme based on the *QUICK scheme* is smaller than that of the *straightforward scheme*, hereafter we adopt the *QUICK scheme* as a conservative LECUSSO scheme.

4.4 Optimized Flow-Modulated Skew-Upwind Scheme

As we discussed in Sec. 2, the pure upwind scheme causes increased numerical diffusions in the direction normal to the flow direction for fluid flows inclined to computational grid lines. A skew-upwind scheme is one of the methods to effectively reduce those numerical diffusions.

In COMMIX-1C, the flow-modulated skew-upwind (FMSUD) scheme, which is a modified version of the mass-flow-weighted skew-upwind scheme by Hassan et al,[30] is implemented. Derivation of the mass-flow-weighted skew-upwind scheme is heuristic and involves ad hoc assumptions. Although derivation of the FMSUD scheme is mathematically more systematic, it still involves some ambiguity. Namely, determination of difference coefficients for corner cells in the FMSUD scheme is based on Patanker's stability conditions to avoid numerical oscillations. However, Patanker's conditions are too restrictive for numerical stability, as we discussed in Sec. 2. Therefore, we can optimize the difference coefficients of the FMSUD scheme from the viewpoint of truncation errors. In addition, the mathematical formulation of the FMSUD scheme has not been derived consistently. We try to derive an optimized FMSUD scheme from the viewpoint of reducing numerical truncation errors.

We consider the convection term in two-dimensional uniform flow field with $u > 0$ and $v > 0$, as shown in Fig. 4.6. The convection term in the two-dimensional partial differential equation (PDE) is

$$\text{(PDE)} : \operatorname{div}(\rho\vec{v}h) = \frac{\partial}{\partial x}(\rho u h) + \frac{\partial}{\partial y}(\rho v h). \tag{4.19}$$

To derive its finite difference form (FDE), we have, in a frame of the first-order skew-upwind scheme with $u > 0$ and $v > 0$,

$$\hat{h}_1 = \alpha_1 h_1 + \beta_1 h_{13} \qquad \hat{h}_2 = \alpha_2 h_0 + \beta_2 h_3$$

$$\hat{h}_3 = \alpha_3 h_3 + \beta_3 h_{13} \qquad \hat{h}_4 = \alpha_4 h_0 + \beta_4 h_1$$

$$\begin{aligned}\text{(FDE)}: \frac{1}{\Delta V}\int \operatorname{div}(\rho\vec{v}h)dV &= \frac{1}{\Delta x\Delta y\Delta z}\left(m_x\hat{h}_2 - m_x\hat{h}_1 + m_y\hat{h}_4 - m_y\hat{h}_3\right) \\ &= \frac{1}{\Delta x\Delta y\Delta z}\left(a_0 h_0 - a_1 h_1 - a_3 h_3 - a_{13} h_{13}\right),\end{aligned} \tag{4.20}$$

where $m_x = \rho u\Delta y\Delta z$, $m_y = \rho v\Delta x\Delta z$, $\Delta V = \Delta x\Delta y\Delta z$, $a_0 = m_x\alpha_2 + m_y\alpha_4$, $a_1 = m_x\alpha_1 - m_y\beta_4$, $a_3 = -m_x\beta_2 + m_y\alpha_3$, $a_{13} = m_x\beta_1 + m_y\beta_3$.

The truncation error between the (FDE) and (PDE) is

$$\text{(TE)}\Delta V \equiv [\text{(FDE)} - \text{(PDE)}]\Delta V$$

$$= a_0 h_0 - a_1 h_1 - a_3 h_3 - a_{13} h_{13} - m_x\Delta x\frac{\partial h}{\partial x} - m_y\Delta y\frac{\partial h}{\partial y}. \tag{4.21}$$

Taylor expansions for h_1, h_3, and h_{13} with respect to the point (x_0, y_0) are

$$h_1 = h_0 + \frac{\partial h}{\partial x}(-\Delta x) + \frac{1}{2}\frac{\partial^2 h}{\partial x^2}(-\Delta x)^2 + 0\left(\Delta x^3\right), \tag{4.22}$$

$$h_3 = h_0 + \frac{\partial h}{\partial y}(-\Delta y) + \frac{1}{2}\frac{\partial^2 h}{\partial y^2}(-\Delta y)^2 + 0\left(\Delta y^3\right), \tag{4.23}$$

$$\begin{aligned}h_{13} = h_0 &+ \frac{\partial h}{\partial x}(-\Delta x) + \frac{\partial h}{\partial y}(-\Delta y) + \frac{1}{2}\frac{\partial^2 h}{\partial x^2}(-\Delta x)^2 \\ &+ \frac{1}{2}\frac{\partial^2 h}{\partial y^2}(-\Delta y)^2 + \frac{\partial h}{\partial x\partial y}(-\Delta x)(-\Delta y) + 0\left(\Delta x^3\right) + 0\left(\Delta y^3\right) \\ &+ 0\left(\Delta x^2\Delta y\right) + 0\left(\Delta x\Delta y^2\right),\end{aligned} \tag{4.24}$$

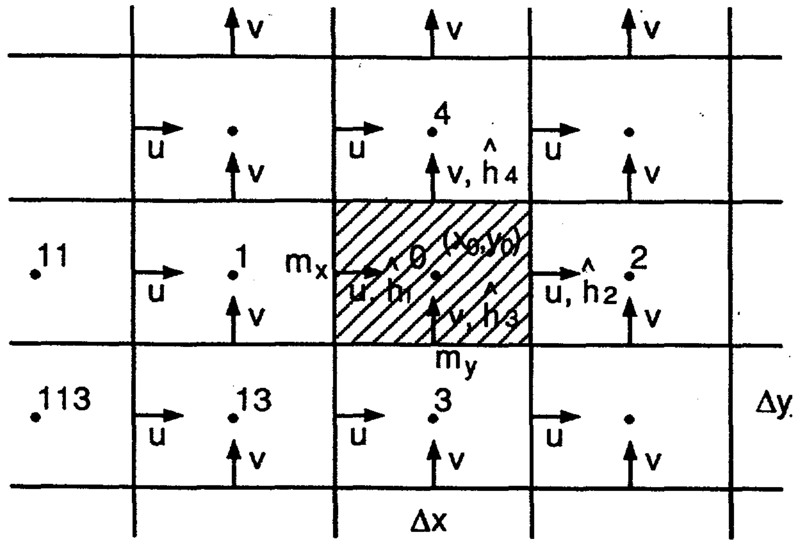

Fig. 4.6. Two-dimensional computational grid

where all the differentiations are evaluated at point (x_o, y_o). Substitution of Eqs. 4.22–4.24 into Eq. 4.21 yields

$$(TE)\Delta V = (a_0 - a_1 - a_3 - a_{13})h_0 + (a_1 + a_{13})\Delta x\left(\frac{\partial h}{\partial x}\right) + (a_3 + a_{13})\Delta y\left(\frac{\partial h}{\partial y}\right)$$

$$- \left[\frac{1}{2}(a_1 + a_{13})\Delta x^2\left(\frac{\partial^2 h}{\partial x^2}\right) + \frac{1}{2}(a_3 + a_{13})\Delta y^2\left(\frac{\partial^2 h}{\partial y^2}\right) + a_{13}\Delta x\Delta y\left(\frac{\partial^2 h}{\partial x\partial y}\right)\right]$$

$$+ 0\left(\Delta x^3\right) + 0\left(\Delta y^3\right) + 0\left(\Delta x^2\Delta y\right) + 0\left(\Delta x\Delta y^2\right) - m_x\Delta x\left(\frac{\partial h}{\partial x}\right) - m_y\Delta y\left(\frac{\partial h}{\partial y}\right). \quad (4.25)$$

To reduce (TE) as much as possible, we get for

$$\text{(0th–order):} \quad a_0 - a_1 - a_3 - a_{13} = 0, \qquad (4.26)$$

$$\text{(1st–order):} \quad \begin{cases} a_1 + a_{13} = m_x, \\ a_3 + a_{13} = m_y. \end{cases} \qquad (4.27)$$

Here, we require that a_1 and a_3 are positive, i.e., $a_1 \geq 0$ and $a_3 \geq 0$. Therefore, Eq. 4.27 gives $a_{13} \leq m_x$ and $a_{13} \leq m_y$. In the case of the FMSUD scheme, $a_{13} = \min(m_x, m_y)$, i.e., $a_{13} \leq \min(m_x, m_y)$. In the following, a_{13} is determined by minimizing the second–order truncation error.

The second–order truncation error is then characterized by

$$A \equiv \frac{1}{2}\left[m_x \Delta x^2 \frac{\partial^2 h}{\partial x^2} + 2a_{13}\Delta x \Delta y \frac{\partial^2 h}{\partial x \partial y} + m_y \Delta y^2 \frac{\partial^2 h}{\partial y^2}\right]. \tag{4.28}$$

It is impossible to reduce A to 0 with only one variable a_{13} to be determined as shown in Eq. 4.28. To minimize A by a_{13}, we make a coordinate transformation from (x, y) to (s, n), as shown in Fig. 4.7,

$$\begin{pmatrix} s \\ n \end{pmatrix} = \begin{pmatrix} \cos\theta & \sin\theta \\ -\sin\theta & \cos\theta \end{pmatrix}\begin{pmatrix} x \\ y \end{pmatrix} \quad \text{or} \quad \begin{pmatrix} x \\ y \end{pmatrix} = \begin{pmatrix} \cos\theta & -\sin\theta \\ \sin\theta & \cos\theta \end{pmatrix}\begin{pmatrix} s \\ n \end{pmatrix} \tag{4.29}$$

We have

$$\begin{pmatrix} \partial h/\partial s \\ \partial h/\partial n \end{pmatrix} = \begin{pmatrix} \cos\theta & \sin\theta \\ -\sin\theta & \cos\theta \end{pmatrix}\begin{pmatrix} \partial h/\partial x \\ \partial h/\partial y \end{pmatrix}, \tag{4.30}$$

and

$$\frac{\partial^2 h}{\partial s^2} = \cos^2\theta \frac{\partial^2 h}{\partial x^2} + 2\sin\theta\cos\theta \frac{\partial^2 h}{\partial x \partial y} + \sin^2\theta \frac{\partial^2 h}{\partial y^2}. \tag{4.31}$$

Here, we define

$$U \equiv \sqrt{u^2 + v^2}, \qquad \Delta\tau \equiv \sqrt{\Delta x^2 + \Delta y^2}.$$

Then, $\cos\theta = u/U$ and $\sin\theta = v/U$. Multiplying $\frac{\rho U \Delta\tau}{2}\Delta V$ to Eq. 4.31 yields,

$$\left(\frac{\rho U \Delta\tau}{2}\right)\Delta V \frac{\partial^2 h}{\partial s^2} = \frac{1}{2}\left(\frac{\cos\theta}{\cos\phi} m_x \Delta x^2 \frac{\partial^2 h}{\partial x^2} + 2\rho U \Delta\tau \cos\theta \sin\theta \Delta x \Delta y \Delta z \frac{\partial^2 h}{\partial x \partial y} + \frac{\sin\theta}{\sin\phi} m_y \Delta y^2 \frac{\partial^2 h}{\partial y^2}\right), \tag{4.32}$$

where $\cos\phi = \Delta x/\Delta\tau$ and $\sin\phi = \Delta y/\Delta\tau$. Equation 4.32 gives the numerical diffusion in the flow direction s.

Because A is the total numerical diffusion, and Eq. 4.32 gives the numerical diffusion in the flow direction, it follows that the terms $\left(1-\frac{\cos\theta}{\cos\phi}\right) m_x \Delta x^2 \frac{\partial^2 h}{\partial x^2}$ and $\left(1-\frac{\sin\theta}{\sin\phi}\right) m_y \Delta y^2 \frac{\partial^2 h}{\partial y^2}$ represent the numerical diffusion in the n–direction. A comparison of Eq. 4.32 with Eq. 4.28 yields

$$a_{13} = \rho U \Delta\tau \cos\theta \sin\theta \Delta z = \left(\frac{\rho uv}{U}\right)\Delta\tau \Delta z. \tag{4.33}$$

Therefore, a_{13} represents a mass flow rate. There are two special cases for a_{13}:

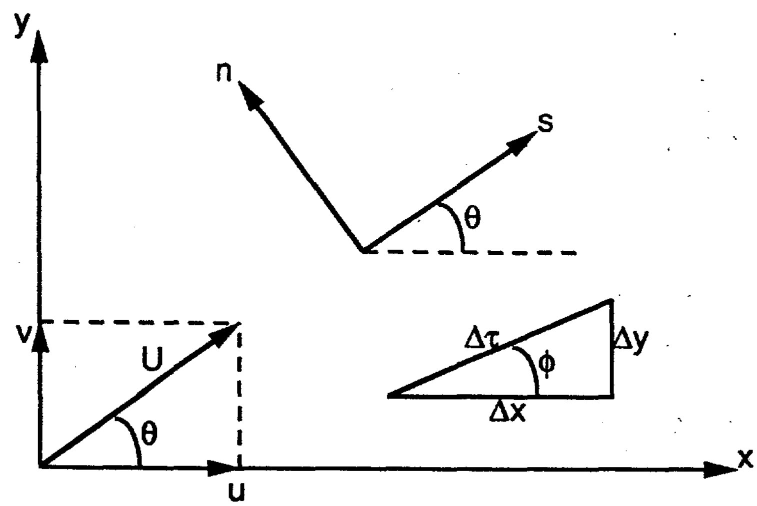

Fig. 4.7. Relationship between coordinates (x, y) and (s, n)

$\theta = 0$ or $\theta = \pi/2$, $a_{13} = 0$ (pure upwind),

and

$\theta = \pi/4$, $a_{13} = \rho u[(\Delta x^2 + \Delta y^2)/2]^{1/2}\Delta z$ (maximum).

When $\Delta x = \Delta y$, $a_{13} = \rho u \Delta x \Delta z = m_x = m_y$, which corresponds to the FMSUD scheme.

5 Finite–Difference Formulation with High–Order Schemes in Space and Time

Although the finite–volume formulation is applied to a grid in both the Cartesian and cylindrical coordinate systems, only a Cartesian coordinate grid system is used here to demonstrate the formulation of the finite–volume equations. Similarly, we have used only the z–momentum equation to illustrate the formulation of the momentum equation. Finite–volume formulations for the x and y momentum equations can be derived by a similar procedure.

The finite–volume equations are derived by integrating the governing equation (Eq. 3.1) over a control volume. We integrate each term separately. All terms, except the convection term, are the same as those in the original COMMIX–1C.

5.1 General Form For Convection Terms

5.1.1 Field Variables in Main Control Volume

Integration of the convection terms in the governing equations Eq. 3.1 over the main control volume in the staggered–grid system gives

$$\int \mathrm{div}(\bar{v}\,\phi)\, dV = \int (\bar{v} \bullet \bar{n})\,\phi\, dA, \tag{5.1}$$

where A denotes the surface area of the control volume and $\bar{n}$ the unit vector normal to the control surface. In the Cartesian coordinate system, the RHS of Eq. 5.1 is expressed as

$$\int(\bar{v} \bullet \bar{n})\phi dA = f_2 \langle\phi\rangle_2 - f_1 \langle\phi\rangle_1 + f_4 \langle\phi\rangle_4 - f_3 \langle\phi\rangle_3 + f_6 \langle\phi\rangle_6 - f_5 \langle\phi\rangle_5 \,. \tag{5.2}$$

Here, f(transporting velocity x flow area) is the volumetric flow rate across the surface of the volume, and subscripts 1–6 denote the west, east, bottom, top, south, and north surfaces, respectively (see Fig. 5.1). For example,

$$f_2 = (v_x A_x)_2 \tag{5.3}$$

is the volumetric flow rate at the east surface. $<\phi>_2$ is the value of ϕ associated with surface 2, which is convected by the volumetric flow rate f_2. The second–order upwind schemes of QUICK and LECUSSO provide

$$\begin{aligned}\langle\phi\rangle_2 = [0, f_2] &\left(\alpha^+_{i+1/2}\, \phi_{i-1} + \beta^+_{i+1/2}\, \phi_i + \gamma^+_{i+1/2}\, \phi_{i+1}\right) \\ &- [0, -f_2] \left(\alpha^-_{i+1/2}\, \phi_i + \beta^-_{i+1/2}\, \phi_{i+1} + \gamma^-_{i+1/2}\, \phi_{i+2}\right) .\end{aligned} \tag{5.4}$$

The operator [A,B] is defined as the maximum of the two real numbers A and B, i.e.,

$$\begin{aligned}[A, B] &= A \text{ if } A > B \\ &= B \text{ if } B > A.\end{aligned} \tag{5.5}$$

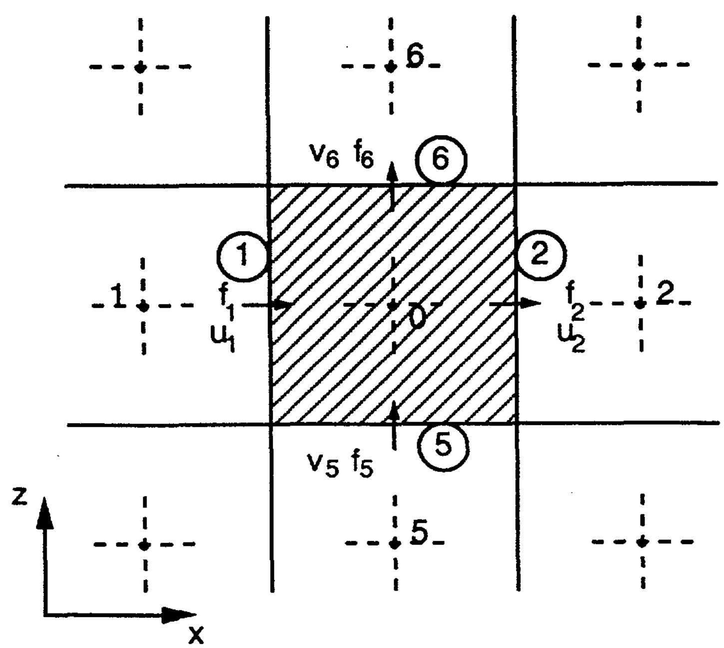

Fig. 5.1. Convective volume fluxes for main control volume

In Eq. 5.4, superscripts + and – denote positive and negative transporting velocities, respectively. $\alpha_{i+1/2}$, $\beta_{i+1/2}$, and $\gamma_{i+1/2}$ are given by Eq. 4.4 for the QUICK scheme or Eq. 4.12 for the LECUSSO scheme. Further, in Eq. 5.4 we use abbreviations in the x-axis, such as

$$\alpha_{i+1/2} = \alpha_{i+1/2,j,k} \tag{5.6a}$$

$$\beta_{i+1/2} = \beta_{i+1/2,j,k} \tag{5.6b}$$

$$\gamma_{i+1/2} = \gamma_{i+1/2,j,k} \tag{5.6c}$$

$$\phi_i = \phi_{i,j,k}. \tag{5.6d}$$

Hereafter, we also use the abbreviation corresponding to Eq. 5.6 in the y- and z-directions unless otherwise stated.

In accordance with the above convention, we rewrite Eq. 5.2 as

$$\begin{aligned}
\int \operatorname{div}(\vec{v}\phi)\,dV = {} & [0,f_2]\left(\alpha^+_{i+1/2}\ \phi_{i-1} + \beta^+_{i+1/2}\ \phi_i + \gamma^+_{i+1/2}\ \phi_{i+1}\right) \\
& - [0,-f_2]\left(\alpha^-_{i+1/2}\ \phi_i + \beta^-_{i+1/2}\ \phi_{i+1} + \gamma^-_{i+1/2}\ \phi_{i+2}\right) \\
& - [0,f_1]\left(\alpha^+_{i-1/2}\ \phi_{i-2} + \beta^+_{i-1/2}\ \phi_{i-1} + \gamma^+_{i-1/2}\ \phi_i\right) \\
& + [0,-f_1]\left(\alpha^-_{i-1/2}\ \phi_{i-1} + \beta^-_{i-1/2}\ \phi_i + \gamma^-_{i-1/2}\ \phi_{i+1}\right) \\
& + [0,f_4]\left(\alpha^+_{j+1/2}\ \phi_{j-1} + \beta^+_{j+1/2}\ \phi_j + \gamma^+_{j+1/2}\ \phi_{j+1}\right) \\
& - [0,-f_4]\left(\alpha^-_{j+1/2}\ \phi_j + \beta^-_{j+1/2}\ \phi_{j+1} + \gamma^-_{j+1/2}\ \phi_{j+2}\right) \\
& - [0,f_3]\left(\alpha^+_{j-1/2}\ \phi_{j-2} + \beta^+_{j-1/2}\ \phi_{j-1} + \gamma^+_{j-1/2}\ \phi_j\right) \\
& + [0,-f_3]\left(\alpha^-_{j-1/2}\ \phi_{j-1} + \beta^-_{j-1/2}\ \phi_j + \gamma^-_{j-1/2}\ \phi_{j+1}\right) \\
& + [0,f_6]\left(\alpha^+_{k+1/2}\ \phi_{k-1} + \beta^+_{k+1/2}\ \phi_k + \gamma^+_{k+1/2}\ \phi_{k+1}\right) \\
& - [0,-f_6]\left(\alpha^-_{k+1/2}\ \phi_k + \beta^-_{k+1/2}\ \phi_{k+1} + \gamma^-_{k+1/2}\ \phi_{k+2}\right) \\
& - [0,f_5]\left(\alpha^+_{k-1/2}\ \phi_{k-2} + \beta^+_{k-1/2}\ \phi_{k-1} + \gamma^+_{k-1/2}\ \phi_k\right) \\
& + [0,-f_5]\left(\alpha^-_{k-1/2}\ \phi_{k-1} + \beta^-_{k-1/2}\ \phi_k + \gamma^-_{k-1/2}\ \phi_{k+1}\right).
\end{aligned} \tag{5.7}$$

All six convective volume fluxes f_1, f_2, ... f_6 for the main control volume are listed in Table 5.1.

Table 5.1. Convective volume fluxes for main control volume

$f_1 = (A_x u)_{i-1/2}$
$f_2 = (A_x u)_{i+1/2}$
$f_3 = (A_y v)_{j-1/2}$
$f_4 = (A_y v)_{j+1/2}$
$f_5 = (A_z w)_{k-1/2}$
$f_6 = (A_z w)_{k+1/2}$

5.1.2. Flow Variables in Momentum Control Volume

Figure 5.2 shows the control volume for the z–component of momentum. Integration the z–component of the convection term in the momentum equation over the momentum control volume, as shown in Fig. 5.2, yields

$$\begin{aligned}\int \mathrm{div}(\bar{v}\phi)\ dV = \{&<u\ A_x\ \phi>_{2-M} + <u\ A_x\ \phi>_{2-P} - <u\ A_x\ \phi>_{1-M} \\ &- <u\ A_x\ \phi>_{1-P} + <v\ A_y\ \phi>_{4-M} + <v\ A_y\ \phi>_{4-P} \\ &- <v\ A_y\ \phi>_{3-M} - <v\ A_y\ \phi>_{3-P}\}/2 + <w\ A_z\ \phi>_{6-6} \\ &- <w\ A_z\ \phi>_{5-0},\end{aligned} \tag{5.8}$$

with $\phi = \rho w$. Suffixes 2–M and 2–P indicate the lower and upper surfaces of the east surface, i.e., surface No. 2, respectively, as shown in Fig. 4.4 or Fig. 5.2. Suffixes 1–M and 1–P indicate the lower and upper surfaces of the west surface, i.e., surface No. 1, respectively. Suffixes 4–M, 4–P, and 3–M and 3–P correspond to the above definitions of surfaces No. 4 and 3 respectively.

Here we define

$$(z - x)\ \text{term} = \{<u\ A_x\ \phi>_{2-M} + <u\ A_x\ \phi>_{2-P} - <u\ A_x\ \phi>_{1-M} - <u\ A_x\ \phi>_{1-P}\}/2. \tag{5.9a}$$

$$(z - y)\ \text{term} = \{<v\ A_y\ \phi>_{4-M} + <v\ A_y\ \phi>_{4-P} - <v\ A_y\ \phi>_{3-M} - <v\ A_y\ \phi>_{3-P}\}/2. \tag{5.9b}$$

$$(z - z)\ \text{term} = <w\ A_z\ \phi>_{6-6} - <w\ A_z\ \phi>_{5-0}. \tag{5.9c}$$

We calculate each term of Eq. 5.9 by using an interpolation or averaging technique.

5.1.2.1 (z – z) Term

We decompose $<w\ A_z\ \phi>$ into two parts as follows:

$$<w\ A_z\ \phi>_{6-6} = <w\ A_z>_{6-6}\ <\phi>_{6-6}. \tag{5.10}$$

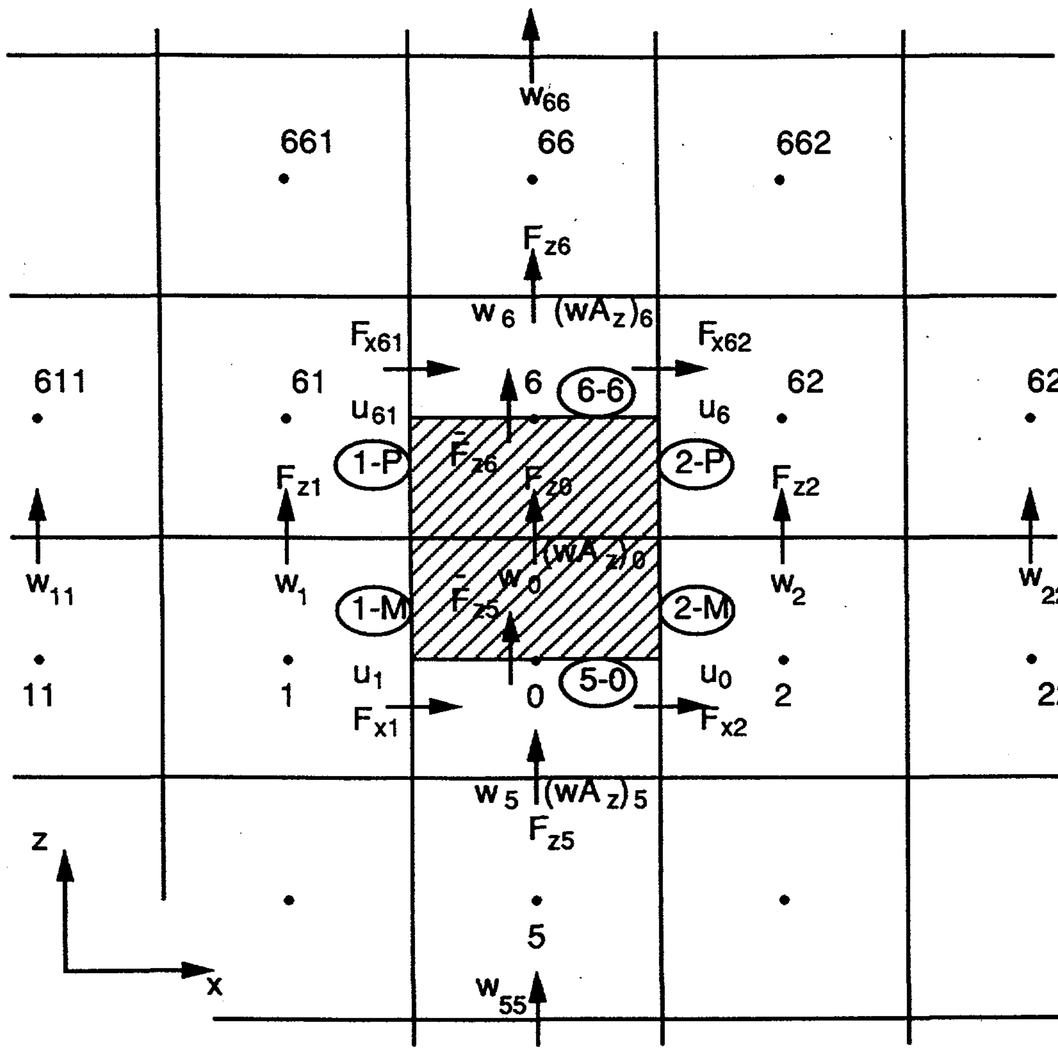

Fig. 5.2. Convective fluxes and average velocties for z–momentum control volume. The numbers in circles indicate surface numbers

Interpolation of the volume flow <w A_z>. In COMMIX–1C, the location at which the flow area A_z is defined coincides with the location for the velocity w. We interpolate the volumetric flow rate <w A_z> at surfaces No. 6–6 by using $\alpha^{\pm}_{k+1/2}$, $\beta^{\pm}_{k+1/2}$, and $\gamma^{\pm}_{k+1/2}$. Namely, for $<w\ A_z>_{6-6} > 0$:

$$<w\ A_z>_{6-6} \ = \alpha^{+}_{k+1/2}(w\ A_z)_5 + \beta^{+}_{k+1/2}(w\ A_z)_0 + \gamma^{+}_{k+1/2}(w\ A_z)_6; \tag{5.11a}$$

and for $<w\ A_z>_{6-6} < 0$:

$$<w\ A_z>_{6-6} \ = \alpha^{-}_{k+1/2}(w\ A_z)_0 + \beta^{-}_{k+1/2}(w\ A_z)_6 + \gamma^{-}_{k+1/2}(w\ A_z)_{66} \tag{5.11b}$$

We use the linear interpolation as an initial guess as follows:

$$<w\ A_z>_{6-6} = [(w\ A_z)_6 + (w\ A_z)_0]/2. \tag{5.12}$$

With respect to the sign of $<w\ A_z>_{6-6}$ obtained from Eq. 5.12, we perform appropriate calculations of $<w\ A_z>_{6-6}$ from Eq. 5.11.

Interpolation of the momentum $\phi = \rho w$. The locations defined for density in a staggered-mesh system are different from those for velocities. However, the surface centers of the z-momentum control volume coincides with the location defined for the density of cells No. 6 and 0. Therefore, we need only to interpolate w at the surface centers 6-6 and 5-0 based on the QUICK or LECUSSO scheme, multiply ρ_6 or ρ_0, and obtain $\phi = (\rho w)_{6-6}$ and $\phi = (\rho w)_{5-0}$.

Namely, for $<w\ A_z>_{6-6} > 0$,

$$< w >_{6-6} = \alpha^{+}_{k+1/2} w_5 + \beta^{+}_{k+1/2} w_0 + \gamma^{+}_{k+1/2} w_6 \tag{5.13a}$$

and for $<w\ A_z>_{6-6} < 0$,

$$< w >_{6-6} = \alpha^{-}_{k+1/2} w_0 + \beta^{-}_{k+1/2} w_6 + \gamma^{-}_{k+1/2} w_{66}. \tag{5.13b}$$

Then we get

$$<\phi>_{6-6} = \rho_6 <w>_{6-6}. \tag{5.14}$$

Finally, we obtain

$$(z - z)\ \text{term} = <w\ A_z>_{6-6}\ \rho_6 <w>_{6-6} - <w\ A_z>_{5-0}\ \rho_0 <w>_{5-0} \tag{5.15a}$$

$$= (f_z)_{6-6}\ \rho_6 <w>_{6-6} - (f_z)_{5-0}\ \rho_0 <w>_{5-0} \tag{5.15b}$$

$$= (F_z)_{6-6} <w>_{6-6} - (F_z)_{5-0} <w>_{5-0} \tag{5.15c}$$

$$\begin{aligned} &= [0,F_z]_{6-6}\left(\alpha^{+}_{k+1/2} w_5 + \beta^{+}_{k+1/2} w_0 + \gamma^{+}_{k+1/2} w_6\right) \\ &\quad - [0,-F_z]_{6-6}\left(\alpha^{-}_{k+1/2} w_0 + \beta^{-}_{k+1/2} w_6 + \gamma^{-}_{k+1/2} w_{66}\right) \\ &\quad - [0,F_x]_{5-0}\left(\alpha^{+}_{k-1/2} w_{55} + \beta^{+}_{k-1/2} w_5 + \gamma^{+}_{k-1/2} w_0\right) \\ &\quad + [0,-F_z]_{5-0}\left(\alpha^{-}_{k-1/2} w_5 + \beta^{-}_{k-1/2} w_0 + \gamma^{-}_{k-1/2} w_6\right), \end{aligned} \tag{5.15d}$$

where

$$(F_z)_{6-6} = \rho_6\ (f_z)_{6-6} = \rho_6 <w\ A_z>_{6-6} = \overline{F}_{z6}, \tag{5.16a}$$

$$(F_z)_{5-0} = \rho_0\ (f_z)_{5-0} = \rho_0 <w\ A_z>_{5-0} = \overline{F}_{z5}, \tag{5.16b}$$

which correspond to the mass flow rate.

5.1.2.2 (z − x) Term

$\langle u\, A_x\, \phi \rangle_{1-M} = \langle u\, A_x\, \rho\, w \rangle_{1-M}$ on surface No. 1–M. Because the density is not defined on surface No. 1–M, we calculate approximately by decomposing $\langle u\, A_x\, \rho\, w \rangle$ into three terms as follows:

$$\langle u\, A_x\, \rho\, w \rangle_{1-M} = \langle u\, A_x \rangle_{1-M} \langle \rho \rangle_{1-M} \langle w \rangle_{1-M}. \tag{5.17}$$

The first term:

The first term on the RHS of Eq. 5.17 can be calculated exactly on surface No. 1–M. Namely,

$$\langle u\, A_x \rangle_{1-M} = u_l (A_x)_1 \tag{5.18a}$$

$$= f_{x1}. \tag{5.18b}$$

The second term:

An interpolation method is needed for the calculation of $\langle \rho \rangle_{1-M}$. We can use the QUICK or LECUSSO interpolation,

$$\langle \rho \rangle_{1-M} = \alpha^{+,M}_{i-1/2}\, \rho_{11} + \beta^{+,M}_{i-1/2}\, \rho_1 + \gamma^{+,M}_{i-1/2}\, \rho_0 \qquad (\text{for } u_l > 0) \tag{5.19a}$$

$$= \alpha^{-,M}_{i-1/2}\, \rho_1 + \beta^{-,M}_{i-1/2}\, \rho_0 + \gamma^{-,M}_{i-1/2}\, \rho_2 \qquad (\text{for } u_l < 0); \tag{5.19b}$$

the linear interpolation,

$$\langle \rho \rangle_{1-M} = (\rho_1\, \Delta x_1 + \rho_0\, \Delta x_0)/(\Delta x_1 + \Delta x_0); \tag{5.20}$$

or the first-order upwind interpolation,

$$\langle \rho \rangle_{1-M} = \rho_1 \qquad (u_l > 0) \tag{5.21a}$$

$$= \rho_0. \qquad (u_l < 0). \tag{5,21b}$$

The conventional COMMIX-1C uses the first-order upwind method. Although the QUICK or LECUSSO interpolation with high-order accuracy is recommended, we now use the linear interpolation. Because COMMIX-1C is a single-phase code, linear interpolation is adequate. For a two-phase flow system, high-order interpolation is strongly recommended.

The third term:

For the third term $\langle w \rangle_{1-M}$, we use the QUICK or LECUSSO interpolation

$$\langle w \rangle_{1-M} = \alpha^{+,M}_{i-1/2}\, w_{11} + \beta^{+,M}_{i-1/2}\, w_1 + \gamma^{+,M}_{i-1/2}\, w_0 \qquad (\text{for } u_l > 0) \tag{5.22a}$$

$$= \alpha^{-,M}_{i-1/2}\ w_1 + \beta^{-,M}_{i-1/2}\ w_0 + \gamma^{-,M}_{i-1/2}\ w_2 \qquad \text{(for } u_1 < 0\text{)}. \tag{5.22b}$$

Finally, we get

$$<u\ A_x\ \rho w>_{1-M} = F_{x1}\ <w>_{1-M}, \tag{5.23}$$

where

$$F_{x1} = <u\ A_x>_{1-M}\ <\rho>_{1-M} \tag{5.24a}$$

$$= u_1\ A_{x1}\ <\rho>_{1-M}. \tag{5.24b}$$

$<u\ A_x\ \phi>_{1-P} = <u\ A_x\ \rho\ w>_{1-P}$ on surface No. 1-P. In the same manner as that for $<u\ A_x\ \phi>_{1-M}$, we get

$$<u\ A_x\ \rho w>_{1-P} = F_{x61}\ <w>_{1-P}, \tag{5.25}$$

where

$$F_{x61} = <u\ A_x>_{1-P}\ <\rho>_{1-P} \tag{5.26a}$$

$$= u_{61}\ A_{x61}\ <\rho>_{1-P}. \tag{5.26b}$$

$$<\rho>_{1-P} = (\rho_{61}\ \Delta x_1 + \rho_6\ \Delta x_0)/(\Delta x_1 + \Delta x_0), \tag{5.27}$$

$$< w >_{1-P} = \alpha^{+,P}_{i-1/2}\ w_{11} + \beta^{+,P}_{i-1/2}\ w_1 + \gamma^{+,P}_{i-1/2}\ w_0 \qquad \text{(for } u_{61} > 0\text{)}, \tag{5.28a}$$

$$= \alpha^{-,P}_{i-1/2}\ w_1 + \beta^{-,P}_{i-1/2}\ w_0 + \gamma^{-,P}_{i-1/2}\ w_2 \qquad \text{(for } u_{61} < 0\text{)}. \tag{5.28b}$$

$<u\ A_x\ \phi>_{2-M} = <u\ A_x\ \rho\ w>_{2-M}$ on surface No. 2-M. In the same manner as that for $<u\ A_x\ \phi>_{1-M}$, we get

$$<u\ A_x\ \rho w>_{2-M} = F_{x2}\ <w>_{2-M} \tag{5.29}$$

where

$$F_{x2} = <u\ A_x>_{2-M}\ <\rho>_{2-M} \tag{5.30a}$$

$$= u_0\ A_{x0}\ <\rho>_{2-M}. \tag{5.30b}$$

$$<\rho>_{2-M} = (\rho_0\ \Delta x_0 + \rho_2\ \Delta x_2)/(\Delta x_0 + \Delta x_2), \tag{5.31}$$

$$< w >_{2-M} = \alpha^{+,M}_{i+1/2}\ w_1 + \beta^{+,M}_{i+1/2}\ w_0 + \gamma^{+,M}_{i+1/2}\ w_2 \qquad \text{(for } u_0 > 0\text{)}, \tag{5.32a}$$

$$= \alpha^{-,M}_{i+1/2}\ w_0 + \beta^{-,M}_{i+1/2}\ w_2 + \gamma^{-,M}_{i+1/2}\ w_{22} \qquad \text{(for } u_0 < 0\text{)}. \tag{5.32b}$$

$<u\ A_x\ \phi>_{2-P} = <u\ A_x\ \rho\ w>_{2-P}$ on surface No. 2-P. In the same manner as that for $<uA_x\ \phi>_{1-P}$, we get

$$<u\ A_x\ \rho w>_{2-P} = F_{x62}\ <w>_{2-P} \tag{5.33}$$

where

$$F_{x62} = <u\ A_x>_{2-P}\ <\rho>_{2-P} \tag{5.34a}$$

$$= u_{62}\ A_{x62}\ <\rho>_{2-P}. \tag{5.34b}$$

$$<\rho>_{2-P} = (\rho_6\ \Delta x_0 + \rho_{62}\ \Delta x_2)/(\Delta x_0 + \Delta x_2), \tag{5.35}$$

$$< w >_{2-P} = \alpha^{+,P}_{i+1/2}\ w_1 + \beta^{+,P}_{i+1/2}\ w_0 + \gamma^{+,P}_{i+1/2}\ w_2 \qquad (\text{for } u_6 > 0), \tag{5.36a}$$

$$= \alpha^{-,P}_{i+1/2}\ w_0 + \beta^{-,P}_{i+1/2}\ w_2 + \gamma^{-,P}_{i+1/2}\ w_{22} \qquad (\text{for } u_6 < 0). \tag{5.36b}$$

Finally, we obtain

$$\begin{aligned}
(z - x)\ \text{term} = \Big\{ & [0,F_{x2}]\left(\alpha^{+,M}_{i+1/2}\ w_1 + \beta^{+,M}_{i+1/2}\ w_0 + \gamma^{+,M}_{i+1/2}\ w_2\right) \\
& - [0,-F_{x2}]\left(\alpha^{-,M}_{i+1/2}\ w_0 + \beta^{-,M}_{i+1/2}\ w_2 + \gamma^{-,M}_{i+1/2}\ w_{22}\right) \\
& + [0,F_{x62}]\left(\alpha^{+,P}_{i+1/2}\ w_1 + \beta^{+,P}_{i+1/2}\ w_0 + \gamma^{+,P}_{i+1/2}\ w_2\right) \\
& - [0,-F_{x62}]\left(\alpha^{-,P}_{i+1/2}\ w_0 + \beta^{-,P}_{i+1/2}\ w_2 + \gamma^{-,P}_{i+1/2}\ w_{22}\right) \\
& - [0,F_{x1}]\left(\alpha^{+,M}_{i-1/2}\ w_{11} + \beta^{+,M}_{i-1/2}\ w_1 + \gamma^{+,M}_{i-1/2}\ w_0\right) \\
& + [0,-F_{x1}]\left(\alpha^{-,M}_{i-1/2}\ w_1 + \beta^{-,M}_{i-1/2}\ w_0 + \gamma^{-,M}_{i-1/2}\ w_2\right) \\
& - [0,F_{x61}]\left(\alpha^{+,P}_{i-1/2}\ w_{11} + \beta^{+,P}_{i-1/2}\ w_1 + \gamma^{+,P}_{i-1/2}\ w_0\right) \\
& + [0,-F_{x61}]\left(\alpha^{-,P}_{i-1/2}\ w_1 + \beta^{-,P}_{i-1/2}\ w_0 + \gamma^{-,P}_{i-1/2}\ w_2\right)\Big\} \Big/ 2.
\end{aligned} \tag{5.37}$$

In the same manner as for the (z – x) term, we get the (z – y) term.

Finally, we get the finite difference form for the convection terms of the z-component of momentum as follows:

$$\int \mathrm{div}(\vec{v}\phi)dV = \Big\{ [0,F_{x2}]\left(\alpha^{+,M}_{i+1/2}\ w_1 + \beta^{+,M}_{i+1/2}\ w_0 + \gamma^{+,M}_{i+1/2}\ w_2\right)$$

$$
\begin{aligned}
&- [0,-F_{x2}]\left(\alpha^{-,M}_{i+1/2}\ w_0 + \beta^{-,M}_{i+1/2}\ w_2 + \gamma^{-,M}_{i+1/2}\ w_{22}\right) \\
&+ [0,F_{x62}]\left(\alpha^{+,P}_{i+1/2}\ w_1 + \beta^{+,P}_{i+1/2}\ w_0 + \gamma^{+,P}_{i+1/2}\ w_2\right) \\
&- [0,-F_{x62}]\left(\alpha^{-,P}_{i+1/2}\ w_0 + \beta^{-,P}_{i+1/2}\ w_2 + \gamma^{-,P}_{i+1/2}\ w_{22}\right) \\
&- [0,F_{x1}]\left(\alpha^{+,M}_{i-1/2}\ w_{11} + \beta^{+,M}_{i-1/2}\ w_1 + \gamma^{+,M}_{i-1/2}\ w_0\right) \\
&+ [0,-F_{x1}]\left(\alpha^{-,M}_{i-1/2}\ w_1 + \beta^{-,M}_{i-1/2}\ w_0 + \gamma^{-,M}_{i-1/2}\ w_2\right) \\
&- [0,F_{x61}]\left(\alpha^{+,P}_{i-1/2}\ w_{11} + \beta^{+,P}_{i-1/2}\ w_1 + \gamma^{+,P}_{i-1/2}\ w_0\right) \\
&+ [0,-F_{x61}]\left(\alpha^{-,P}_{i-1/2}\ w_1 + \beta^{-,P}_{i-1/2}\ w_0 + \gamma^{-,P}_{i-1/2}\ w_2\right)\Big\}\Big/2 \\
&+ \Big\{ [0,F_{y4}]\left(\alpha^{+,M}_{j+1/2}\ w_3 + \beta^{+,M}_{j+1/2}\ w_0 + \gamma^{+,M}_{j+1/2}\ w_4\right) \\
&- [0,-F_{y4}]\left(\alpha^{-,M}_{j+1/2}\ w_0 + \beta^{-,M}_{j+1/2}\ w_4 + \gamma^{-,M}_{j+1/2}\ w_{44}\right) \\
&+ [0,F_{y64}]\left(\alpha^{+,P}_{j+1/2}\ w_3 + \beta^{+,P}_{j+1/2}\ w_0 + \gamma^{+,P}_{j+1/2}\ w_4\right) \\
&- [0,-F_{y64}]\left(\alpha^{-,P}_{j+1/2}\ w_0 + \beta^{-,P}_{j+1/2}\ w_4 + \gamma^{-,P}_{j+1/2}\ w_{44}\right) \\
&- [0,F_{y3}]\left(\alpha^{+,M}_{j-1/2}\ w_{33} + \beta^{+,M}_{j-1/2}\ w_3 + \gamma^{+,M}_{j-1/2}\ w_0\right) \\
&+ [0,-F_{y3}]\left(\alpha^{-,M}_{j-1/2}\ w_3 + \beta^{-,M}_{j-1/2}\ w_0 + \gamma^{-,M}_{j-1/2}\ w_4\right) \\
&- [0,F_{y63}]\left(\alpha^{+,P}_{j-1/2}\ w_{33} + \beta^{+,P}_{j-1/2}\ w_3 + \gamma^{+,P}_{j-1/2}\ w_0\right) \\
&+ [0,-F_{y63}]\left(\alpha^{-,P}_{j-1/2}\ w_3 + \beta^{-,P}_{j-1/2}\ w_0 + \gamma^{-,P}_{j-1/2}\ w_4\right)\Big\}\Big/2 \\
&+ [0,F_z]_{6-6}\left(\alpha^{+}_{k+1/2}\ w_5 + \beta^{+}_{k+1/2}\ w_0 + \gamma^{+}_{k+1/2}\ w_6\right) \\
&- [0,-F_z]_{6-6}\left(\alpha^{-}_{k+1/2}\ w_0 + \beta^{-}_{k+1/2}\ w_6 + \gamma^{-}_{k+1/2}\ w_{66}\right) \\
&- [0,F_z]_{5-0}\left(\alpha^{+}_{k-1/2}\ w_{55} + \beta^{+}_{k-1/2}\ w_5 + \gamma^{+}_{k-1/2}\ w_0\right) \\
&+ [0,-F_z]_{5-0}\left(\alpha^{-}_{k-1/2}\ w_5 + \beta^{-}_{k-1/2}\ w_0 + \gamma^{-}_{k-1/2}\ w_6\right). \qquad (5.38)
\end{aligned}
$$

5.2 General Form for Diffusion Terms

The integration of diffusion terms is the same as in the original COMMIX-1C, as follows.

5.2.1 Field Variables in Main Control Volume

$$\int \left[\frac{\Delta\left(\gamma_x \Gamma_\phi \frac{\partial\phi}{\partial x}\right)}{\Delta x} + \frac{\Delta\left(\gamma_y \Gamma_\phi \frac{\partial\phi}{\partial y}\right)}{\Delta y} + \frac{\Delta\left(\gamma_z \Gamma_\phi \frac{\partial\phi}{\partial z}\right)}{\Delta z} \right] dx\,dy\,dz$$

$$= D_2(\phi_2 - \phi_0) - D_1(\phi_0 - \phi_1) + D_4(\phi_4 - \phi_0) - D_3(\phi_0 - \phi_3) + D_6(\phi_6 - \phi_0) - D_5(\phi_0 - \phi_5)$$

$$= D_1\,\phi_1 + D_2\,\phi_2 + D_3\,\phi_3 + D_4\,\phi_4 + D_5\,\phi_5 + D_6\,\phi_6$$

$$- (D_1 + D_2 + D_3 + D_4 + D_5 + D_6)\,\phi_0\,. \tag{5.39}$$

Here, D (= effective diffusivity x flow area/distance between the centers of two control volumes) is the diffusion strength across the surface of the control volume, and Γ_ϕ is the effective diffusivity for the variable ϕ.

To determine the value of D at a surface, we assume that the diffusivity Γ varies continuously from one main control volume to the next and we use the average diffusion strength, e.g.,

$$D_2 = (A_x)_{i+1/2}(\Gamma_0 + \Gamma_2)/(\Delta x_0 + \Delta x_2). \tag{5.40}$$

The values of diffusion strength for the main control volume are listed in Table 5.2.

5.2.2 Flow Variables in z-Momentum Control Volume

The integration of the diffusion terms over the z-momentum control volume (Fig. 5.3) results in an expression similar to Eq. 5.39, i.e.,

$$\int \left[\frac{\Delta\left(\gamma_x \Gamma_\phi \frac{\partial\phi}{\partial x}\right)}{\Delta x} + \frac{\Delta\left(\gamma_y \Gamma_\phi \frac{\partial\phi}{\partial y}\right)}{\Delta y} + \frac{\Delta\left(\gamma_z \Gamma_\phi \frac{\partial\phi}{\partial z}\right)}{\Delta z} \right] dx\,dy\,dz$$

$$= \overline{D}_1\phi_1 + \overline{D}_2\phi_2 + \overline{D}_3\phi_3 + \overline{D}_4\phi_4 + \overline{D}_5\phi_5 + \overline{D}_6\phi_6$$

$$- \left(\overline{D}_1 + \overline{D}_2 + \overline{D}_3 + \overline{D}_4 + \overline{D}_5 + \overline{D}_6\right)\phi_0\,. \tag{5.41}$$

The only difference is that we now use the momentum control volume diffusion strength $\overline{D}$ instead of the main control volume diffusion strength D, e.g.,

Table 5.2. Diffusion strengths for main control volume

$D_1 = (A_x)_{i-1/2}(\Gamma_0 + \Gamma_1)/(\Delta x_0 + \Delta x_1)$
$D_2 = (A_x)_{i+1/2}(\Gamma_0 + \Gamma_2)/(\Delta x_0 + \Delta x_2)$
$D_3 = (A_y)_{j-1/2}(\Gamma_0 + \Gamma_3)/(\Delta y_0 + \Delta y_3)$
$D_4 = (A_y)_{j+1/2}(\Gamma_0 + \Gamma_4)/(\Delta y_0 + \Delta y_4)$
$D_5 = (A_z)_{k-1/2}(\Gamma_0 + \Gamma_5)/(\Delta z_0 + \Delta z_5)$
$D_6 = (A_z)_{k+1/2}(\Gamma_0 + \Gamma_6)/(\Delta z_0 + \Delta z_6)$

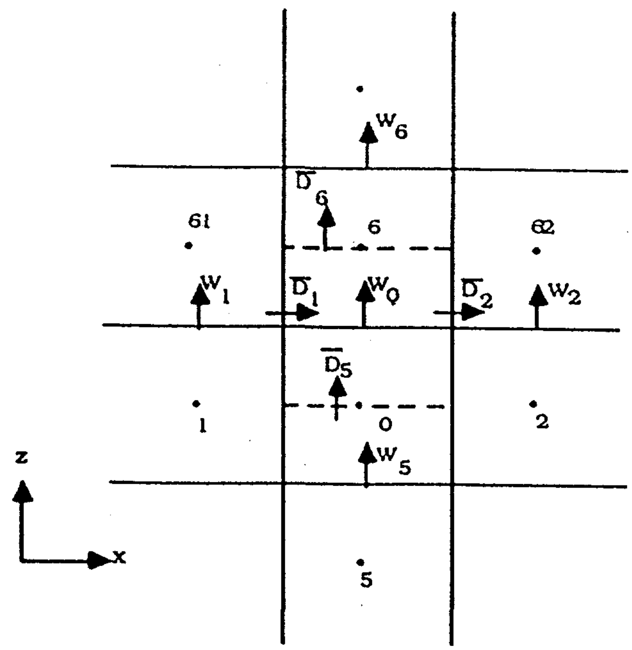

Fig. 5.3. Diffusion fluxes for z-momentum control volume

$$\overline{D}_6 = \frac{1}{2}\left[(A_z)_k + (A_z)_{k+1}\right]\left(\frac{\Gamma}{\Delta z}\right)_6 . \tag{5.42}$$

The values of the diffusion strengths $\overline{D}$ for the z-momentum control volume are listed in Table 5.3.

5.3 General Finite-Volume Equation with Unsteady Term

5.3.1 Field Variables in Main Control Volume

Integrating the general form of the conservation equation, Eq. 3.1, over the phase volume dt dV ($dV = \gamma_v$ dx dy dz) in a main control volume, based on the concept of implicitness parameter α, and dividing by dt gives

Table 5.3. Diffusion strengths for z-momentum control volume

$$\overline{D}_1 = \frac{1}{4}\left[(A_x)_{i-1/2,k} + (A_x)_{i-1/2,k+1}\right]\left[\frac{(\Gamma_0 + \Gamma_1)}{(\Delta x_0 + \Delta x_1)} + \frac{(\Gamma_6 + \Gamma_{61})}{(\Delta x_6 + \Delta x_{61})}\right]$$

$$\overline{D}_2 = \frac{1}{4}\left[(A_x)_{i+1/2,k} + (A_x)_{i+1/2,k+1}\right]\left[\frac{(\Gamma_0 + \Gamma_2)}{(\Delta x_0 + \Delta x_2)} + \frac{(\Gamma_6 + \Gamma_{62})}{(\Delta x_6 + \Delta x_{62})}\right]$$

$$\overline{D}_3 = \frac{1}{4}\left[\left(A_y\right)_{j-1/2,k} + \left(A_y\right)_{j-1/2,k+1}\right]\left[\frac{(\Gamma_0 + \Gamma_3)}{(\Delta y_0 + \Delta y_3)} + \frac{(\Gamma_6 + \Gamma_{63})}{(\Delta y_6 + \Delta y_{63})}\right]$$

$$\overline{D}_4 = \frac{1}{4}\left[\left(A_y\right)_{j+1/2,k} + \left(A_y\right)_{j+1/2,k+1}\right]\left[\frac{(\Gamma_0 + \Gamma_4)}{(\Delta y_0 + \Delta y_4)} + \frac{(\Gamma_6 + \Gamma_{64})}{(\Delta y_6 + \Delta y_{64})}\right]$$

$$\overline{D}_5 = \frac{1}{2}\left[(A_z)_k + (A_z)_{k-1}\right]\left(\frac{\Gamma}{\Delta z}\right)_0$$

$$\overline{D}_6 = \frac{1}{2}\left[(A_z)_k + (A_z)_{k+1}\right]\left(\frac{\Gamma}{\Delta z}\right)_6$$

$$\left(\frac{\phi_0^{n+1} - \phi_0^n}{\Delta t}\right)V_0 + \alpha(\text{Eq. } 5.7)^{n+1} + \beta(\text{Eq. } 5.7)^n$$

$$= \alpha(\text{Eq. } 5.39)^{n+1} + \beta(\text{Eq. } 5.39)^n + S_c V_0 + S_p\left(\alpha\phi_0^{n+1} + \beta\phi_0^n\right)V_0, \qquad (5.43)$$

where S_c and S_p are the source term coefficients associated with linearization of the source term. In Eq. 5.43, $\beta = 1 - \alpha$, and superscript n denotes the time step number. Hereafter, we omit superscript n+1.

By substituting Eqs. 5.7 and 5.39 into Eq. 5.43, and rearranging we obtain

$$a_0\phi_0 = \alpha\sum_{\ell=1}^{6} a_\ell\phi_\ell + b_0 + c_0. \qquad (5.44)$$

Here,

$$a_0 = \frac{V_0}{\Delta t} + \alpha a_{00},$$

$$a_{00} = \beta_{i-1/2}^-[-f_1,0] + \beta_{i+1/2}^+[f_2,0] + \beta_{j-1/2}^-[-f_3,0] + \beta_{j+1/2}^+[f_4,0]$$

$$+ \beta_{k-1/2}^-[-f_5,0] + \beta_{k+1/2}^+[f_6,0] + D_1 + D_2 + D_3 + D_4 + D_5 + D_6 - S_{p\phi}V_0,$$

$$a_1 = \beta^+_{i-1/2}[f_1,0] + D_1 \qquad a_2 = \beta^-_{i+1/2}[-f_2,0] + D_2$$

$$a_3 = \beta^+_{j-1/2}[f_3,0] + D_3 \qquad a_4 = \beta^-_{j+1/2}[-f_4,0] + D_4$$

$$a_5 = \beta^+_{k-1/2}[f_5,0] + D_5 \qquad a_6 = \beta^-_{k+1/2}[-f_6,0] + D_6$$

$$b_0 = b_{10} + b_{20} + b_{30}$$

$$b_{10} = \beta \sum_{\ell=1}^{6} a_\ell^n \, \phi_\ell^n$$

$$b_{20} = -\beta \, a_{00}^n \, \phi_0^n$$

$$b_{30} = \frac{\rho_0^n \, \phi_0^n \, V_0}{\Delta t} + S_{c\phi} V_0$$

$$c_0 = \alpha c_{00} + \beta c_{00}^n .$$

$$\begin{aligned} c_{00} = {} & [f_1,0]\left(\alpha^+_{i-1/2}\ \phi_{11} + \gamma^+_{i-1/2}\ \phi_0\right) - [-f_1,0]\left(\alpha^-_{i-1/2}\ \phi_1 + \gamma^-_{i-1/2}\ \phi_2\right) \\ & - [f_2,0]\left(\alpha^+_{i+1/2}\ \phi_1 + \gamma^+_{i+1/2}\ \phi_2\right) + [-f_2,0]\left(\alpha^-_{i+1/2}\ \phi_0 + \gamma^-_{i+1/2}\ \phi_{22}\right) \\ & + [f_3,0]\left(\alpha^+_{j-1/2}\ \phi_{33} + \gamma^+_{j-1/2}\ \phi_0\right) - [-f_3,0]\left(\alpha^-_{j-1/2}\ \phi_3 + \gamma^-_{j-1/2}\ \phi_4\right) \\ & - [f_4,0]\left(\alpha^+_{j+1/2}\ \phi_3 + \gamma^+_{j+1/2}\ \phi_4\right) + [-f_4,0]\left(\alpha^-_{j+1/2}\ \phi_0 + \gamma^-_{j+1/2}\ \phi_{44}\right) \\ & + [f_5,0]\left(\alpha^+_{k-1/2}\ \phi_{55} + \gamma^+_{k-1/2}\ \phi_0\right) - [-f_5,0]\left(\alpha^-_{k-1/2}\ \phi_5 + \gamma^-_{k-1/2}\ \phi_6\right) \\ & - [f_6,0]\left(\alpha^+_{k+1/2}\ \phi_5 + \gamma^+_{k+1/2}\ \phi_6\right) + [-f_6,0]\left(\alpha^-_{k+1/2}\ \phi_0 + \gamma^-_{k+1/2}\ \phi_{66}\right). \end{aligned}$$

Equation 5.44 is solved by using any one of the matrix solvers in the COMMIX-IC – direct solver YSMP, and iterative solvers SOR or PCG.

In deriving Eq. 5.44, only the six quantities w_ℓ (ℓ = 1, 2, .., 6) that are treated implicitly in the original COMMIX-1C with first-order upwind scheme, are treated implicitly; the remaining quantities are moved to the source term c_0. Namely, only the nearest neighbor nodes (ℓ = 1, 2, .., 6) are treated implicitly, thus reducing the five-point formula to a three-point implicit one. This makes the conventional algorithm treatable with a solution package that is already available for three-point formulas. However, as a result, even if we use α (implicitness parameter) = 1, this treatment is not fully implicit. If we want the fully implicit method, we can use an iterative procedure to solve Eq. 5.44 by using it ≥ 2.* This situation also relates to the Courant condition. It is known that the fully-implicit method is unconditionally stable with respect to time increments. However, the solution procedure for Eq. 5.44 suffers from conditionally stable conditions because of the partly explicit treatment. In actual calculations, this may not be a severe problem, because a larger time increment than the Courant condition is allowable for $\alpha = 1$. But we should pay attention to this. If we perform the numerical stability analysis, such as the von Newmann analysis, we could obtain the exact criteria regarding time increments for the above current solution procedure.

5.3.2 Flow Variables in z-Momentum Control Volume

Similar to the derivation of Eq. 5.43, the z-momentum equation in the z-momentum control volume is

$$\left(\frac{\phi_0 - \phi_0^n}{\Delta t}\right)\overline{V}_0 + \alpha(\text{Eq. } 5.38) + \beta(\text{Eq. } 5.38)^n$$

$$= \alpha(\text{Eq. } 5.41) + \beta(\text{Eq. } 5.41)^n + S_c\,\overline{V}_0 + S_p\left(\alpha\phi_0 + \beta\phi_0^n\right)\overline{V}_0, \qquad (5.45)$$

with $\phi = \rho w$.

By substituting Eqs. 5.38 and 5.41 into Eq. 5.45, and rearranging we obtain

$$a_0 w_0 = \alpha\sum_{\ell=1}^{6} a_\ell w_\ell + b_0 + c_0 - \alpha d^w(P_6 - P_0) - \beta d^w\left(P_6^n - P_0^n\right). \qquad (5.46)$$

Here,

$$a_0 = \frac{\overline{\rho}_0\overline{V}_0}{\Delta t} + \alpha a_{00},$$

$$a_{00} = \Big\{\beta^{-,M}_{i-1/2}[-F_{x1},0] + \beta^{+,M}_{i+1/2}[F_{x2},0] + \beta^{-,M}_{j-1/2}[-F_{y3},0] + \beta^{+,M}_{j+1/2}[F_{y4},0]$$

$$+ \beta^{-,P}_{i-1/2}[-F_{x61},0] + \beta^{+,P}_{i+1/2}[F_{x62},0] + \beta^{-,P}_{j-1/2}[-F_{y63},0] + \beta^{+,P}_{j+1/2}[F_{y64},0]\Big\}/2$$

$$+ \beta^{-}_{k-1/2}[-\overline{F}_{z5},0] + \beta^{+}_{k+1/2}[\overline{F}_{z6},0] + \overline{D}_1 + \overline{D}_2 + \overline{D}_3 + \overline{D}_4 + \overline{D}_5 + \overline{D}_6 - S_{p\phi}\overline{V}_{0,},$$

$$a_1 = \frac{1}{2}\left\{\beta^{+,M}_{i-1/2}[F_{x1},0] + \beta^{+,P}_{i-1/2}[F_{x61},0]\right\} + \overline{D}_1,$$

---

* Iteration number for the momentum calculation and energy calculation in the same time step.

$$a_2 = \frac{1}{2}\left\{\beta^{-,M}_{i+1/2}\left[-F_{x2},0\right] + \beta^{-,P}_{i+1/2}\left[-F_{x62},0\right]\right\} + \overline{D}_2,$$

$$a_3 = \frac{1}{2}\left\{\beta^{+,M}_{j-1/2}\left[F_{y3},0\right] + \beta^{+,P}_{j-1/2}\left[F_{y63},0\right]\right\} + \overline{D}_3,$$

$$a_4 = \frac{1}{2}\left\{\beta^{-,M}_{j+1/2}\left[-F_{y4},0\right] + \beta^{-,P}_{j+1/2}\left[-F_{y64},0\right]\right\} + \overline{D}_4,$$

$$a_5 = \beta^{+}_{k-1/2}\left[\overline{F}_{z5},0\right] + \overline{D}_5,$$

$$a_6 = \beta^{-}_{k+1/2}\left[-\overline{F}_{z6},0\right] + \overline{D}_6,$$

$$b_0 = b_{10} + b_{20} + b_{30},$$

$$b_{10} = \beta\sum_{\ell=1}^{6} a_\ell^n\, w_\ell^n,$$

$$b_{20} = -\beta\, a_{00}^n\, w_0^n,$$

$$b_{30} = \frac{\overline{\rho}_0^n\, w_0^n\, \overline{V}_0}{\Delta t} + S_{c\phi}\,\overline{V}_0,$$

$$c_0 = \alpha c_{00} + \beta c_{00}^n,$$

and

$$\begin{aligned}
c_{00} = \frac{1}{2}\Big\{&\left[F_{x1},0\right]\left(\alpha^{+,M}_{i-1/2}\ w_{11} + \gamma^{+,M}_{i-1/2}\ w_0\right) - \left[-F_{x1},0\right]\left(\alpha^{-,M}_{i-1/2}\ w_1 + \gamma^{-,M}_{i-1/2}\ w_2\right)\\
&+ \left[F_{x61},0\right]\left(\alpha^{+,P}_{i-1/2}\ w_{11} + \gamma^{+,P}_{i-1/2}\ w_0\right) - \left[-F_{x61},0\right]\left(\alpha^{-,P}_{i-1/2}\ w_1 + \gamma^{-,P}_{i-1/2}\ w_2\right)\\
&- \left[F_{x2},0\right]\left(\alpha^{+,M}_{i+1/2}\ w_1 + \gamma^{+,M}_{i+1/2}\ w_2\right) + \left[-F_{x2},0\right]\left(\alpha^{-,M}_{i+1/2}\ w_0 + \gamma^{-,M}_{i+1/2}\ w_{22}\right)\\
&- \left[F_{x62},0\right]\left(\alpha^{+,P}_{i+1/2}\ w_1 + \gamma^{+,P}_{i+1/2}\ w_2\right) + \left[-F_{x62},0\right]\left(\alpha^{-,P}_{i+1/2}\ w_0 + \gamma^{-,P}_{i+1/2}\ w_{22}\right)\\
&+ \left[F_{y3},0\right]\left(\alpha^{+,M}_{j-1/2}\ w_{33} + \gamma^{+,M}_{j-1/2}\ w_0\right) - \left[F_{y3},0\right]\left(\alpha^{-,M}_{j-1/2}\ w_3 + \gamma^{-,M}_{j-1/2}\ w_4\right)\\
&+ \left[F_{y63},0\right]\left(\alpha^{+,P}_{j-1/2}\ w_{33} + \gamma^{+,P}_{j-1/2}\ w_0\right) - \left[F_{y63},0\right]\left(\alpha^{-,P}_{j-1/2}\ w_3 + \gamma^{-,P}_{j-1/2}\ w_4\right)\\
&- \left[F_{y4},0\right]\left(\alpha^{+,M}_{j+1/2}\ w_3 + \gamma^{+,M}_{j+1/2}\ w_4\right) + \left[-F_{y4},0\right]\left(\alpha^{-,M}_{j+1/2}\ w_0 + \gamma^{-,M}_{j+1/2}\ w_{44}\right)
\end{aligned}$$

$$- \left[F_{y64},0\right]\left(\alpha^{+,P}_{j+1/2}\ w_3 + \gamma^{+,P}_{j+1/2}\ w_4\right) + \left[-F_{y64},0\right]\left(\alpha^{-,P}_{j+1/2}\ w_0 + \gamma^{-,P}_{j+1/2}\ w_{44}\right)\Big\}$$

$$+ \left[\overline{F}_{z5},0\right]\left(\alpha^{+}_{k-1/2}\ w_{55} + \gamma^{+}_{k-1/2}\ w_0\right) - \left[-\overline{F}_{z5},0\right]\left(\alpha^{-}_{k-1/2}\ w_5 + \gamma^{-}_{k-1/2}\ w_6\right)$$

$$- \left[\overline{F}_{z6},0\right]\left(\alpha^{+}_{k+1/2}\ w_5 + \gamma^{+}_{k+1/2}\ w_6\right) + \left[-\overline{F}_{z6},0\right]\left(\alpha^{-}_{k+1/2}\ w_0 + \gamma^{-}_{k+1/2}\ w_{66}\right),$$

$$d^w = \frac{2\overline{V}_0}{\Delta z_0 + \Delta z_6}.$$

6 New Pressure Equation

The pressure appearing in momentum Eq. 5.46 is unknown and must be determined from the mass-conservation equation. This will be the pressure equation.

We discretize the mass continuity equation with high-order difference schemes. Hence, the pressure equation is different from that in the original COMMIX-1C. We derive the new pressure equation as follows.

By integrating Eq. 3.1, with substitution of $\phi = \rho$, diffusion coefficient $\Gamma_\phi = 0$, and source $S = 0$, over a main control volume and Δt based on the concept of implicitness parameter α, we obtain the finite volume equation for mass continuity as follows:

$$\left(\frac{\rho_0 - \rho_0^n}{\Delta t}\right)V_0 + \alpha\left[A_2 u_2 <\rho>_2 - A_1 u_1 <\rho>_1 + A_4 v_4 <\rho>_4 - A_3 v_3 <\rho>_3\right.$$

$$\left.+ A_6 w_6 <\rho>_6 - A_5 w_5 <\rho>_5\right] + \beta\left[A_2 u_2 <\rho>_2 - A_1 u_1 <\rho>_1 + A_4 v_4 <\rho>_4\right.$$

$$\left.- A_3 v_3 <\rho>_3 + A_6 w_6 <\rho>_6 - A_5 w_5 <\rho>_5\right]^n = 0. \tag{6.1}$$

Here, for a quasicontinuum formulation, $V_0 = \gamma_v \Delta x \Delta y \Delta z$ is the fluid volume of the main control volume, A_i is the unobstructed flow area of surface i, and $<\rho>_\ell$ the high-order upwind density of surface No. ℓ of the control volume under consideration. The subscripts, 1, ... 6 refer to the surface numbers of the main control volume, as shown in Fig. 5.1.

To convert the indirect specification of pressure in continuity Eq. 6.1 to an explicit form, we rewrite momentum Eq. 5.46 by using the following relations:

$$- \alpha d^w(P_6 - P_0) - \beta d^w\left(P_6^n - P_0^n\right)$$

$$= - \alpha d^w(P_6 - P_0) - (1 - \alpha)d^w\left(P_6^n - P_0^n\right)$$

$$= - \alpha d^w\left[\left(P_6 - P_6^n\right) - \left(P_0 - P_0^n\right)\right] - d^w\left(P_6^n - P_0^n\right)$$

$$= -\alpha d^w\left(\delta P_6 - \delta P_0\right) - d^w\left(P_6^n - P_0^n\right), \tag{6.2}$$

where $\delta P_6 = P_6 - P_6^n$ and $\delta P_0 = P_0 - P_0^n$. By substituting Eq. 6.2 into Eq. 5.46, we obtain

$$w_0 = \frac{1}{a_0}\left\{\alpha\left[\sum_{\ell=1}^{6} a_\ell w_\ell + c_{00}\right] + \beta\left[\sum_{\ell=1}^{6} a_\ell^n w_\ell^n - a_{00}^n w_0^n + c_{00}^n\right]\right.$$

$$\left. + \frac{\rho_0^n \overline{V}_0}{\Delta t} w_0^n + S_{c\phi}\overline{V}_0 - d^w\left(P_6^n - P_0^n\right)\right\} - a d^w(\delta P_6 - \delta P_0) \tag{6.3a}$$

$$= \hat{w}_0 - \alpha d^w(\delta P_6 - \delta P_0), \tag{6.3b}$$

where

$$d^w = \frac{2\overline{V}_0}{a_0(\Delta z_0 + \Delta z_6)}, \tag{6.4}$$

and

$$\hat{w}_0 = \frac{1}{a_0}\left[\alpha\left(\sum_{\ell=1}^{6} a_\ell w_\ell + c_{00}\right) + \beta\left(\sum_{\ell=1}^{6} a_\ell w_\ell^n - a_{00}^n w_0^n + c_{00}^n\right)\right.$$

$$\left. + \frac{\rho_0^n \overline{V}_0}{\Delta t} w_0^n + S_{c\phi}\overline{V}_0 - d^w\left(P_6^n - P_0^n\right)\right]. \tag{6.5}$$

The reason that δP (instead of P) is used in Eq. 6.3 is to speed up the convergence. This is particularly helpful when the change in pressure is small compared to the absolute pressure of the system and has been implemented early in the original COMMIX-1C.

By comparing the index conventions in the mass control volume, Fig. 5.1, and the z-momentum control volume, Fig. 5.2, it is seen that w_0 in Fig. 5.2 is w_6 in Fig. 5.1. Hence, with similar definitions of $\hat{u}$, $\hat{v}$, $\hat{w}$, d, and $\overline{V}$, the velocities appearing in Eq. 6.1 can be expressed as

$$u_1 = \hat{u}_1 - d_1^u(\delta P_0 - \delta P_1),$$

$$u_2 = \hat{u}_2 - d_2^u(\delta P_2 - \delta P_0),$$

$$v_3 = \hat{v}_3 - d_3^v(\delta P_0 - \delta P_3),$$

$$v_4 = \hat{v}_4 - d_4^v(\delta P_4 - \delta P_0),$$

$$w_5 = \hat{w}_5 - d_5^w(\delta P_0 - \delta P_5),$$

and

$$w_6 = \hat{w}_6 - d_6^w(\delta P_6 - \delta P_0), \tag{6.6}$$

where

$$d_1^u = \frac{2\overline{V}_1^u}{a_0^u(\Delta x_0 + \Delta x_1)},$$

$$d_2^u = \frac{2\overline{V}_2^u}{a_0^u(\Delta x_0 + \Delta x_2)},$$

$$d_3^v = \frac{2\overline{V}_3^v}{a_0^v(\Delta y_0 + \Delta y_3)},$$

$$d_4^v = \frac{2\overline{V}_4^v}{a_0^v(\Delta y_0 + \Delta y_4)},$$

$$d_5^w = \frac{2\overline{V}_5^w}{a_0^w(\Delta z_0 + \Delta z_5)},$$

and

$$d_6^w = \frac{2\overline{V}_6^w}{a_0^w(\Delta z_0 + \Delta z_6)}. \tag{6.7}$$

The characteristic volumes are defined as

$$\overline{V}_1^u = (\Delta x_0 + \Delta x_1)\Big/\left(\frac{\Delta x_0}{V_0} + \frac{\Delta x_1}{V_1}\right),$$

$$\overline{V}_2^u = (\Delta x_0 + \Delta x_2)\Big/\left(\frac{\Delta x_0}{V_0} + \frac{\Delta x_2}{V_2}\right),$$

$$\overline{V}_3^v = (\Delta y_0 + \Delta y_3)\Big/\left(\frac{\Delta y_0}{V_0} + \frac{\Delta y_3}{V_3}\right),$$

$$\overline{V}_4^v = (\Delta y_0 + \Delta y_4)\Big/\left(\frac{\Delta y_0}{V_0} + \frac{\Delta y_4}{V_4}\right),$$

$$\overline{V}_5^w = (\Delta z_0 + \Delta z_5) \Big/ \left(\frac{\Delta z_0}{V_0} + \frac{\Delta z_5}{V_5} \right),$$

and

$$\overline{V}_6^w = (\Delta z_0 + \Delta z_6) \Big/ \left(\frac{\Delta z_0}{V_0} + \frac{\Delta z_6}{V_6} \right). \tag{6.8}$$

The high-order upwind density $<\rho>_\ell$ is calculated in a similar way to Eq. 5.4, i.e., as follows:

$$<\rho>_1 = \frac{[0,v_1]}{|v_1|}\left(\alpha^+_{i-1/2}\rho_{11} + \beta^+_{i-1/2}\rho_1 + \gamma^+_{i-1/2}\rho_0\right)$$

$$- \frac{[0,-v_1]}{|v_1|}\left(\alpha^-_{i-1/2}\rho_1 + \beta^-_{i-1/2}\rho_0 + \gamma^-_{i-1/2}\rho_2\right),$$

$$<\rho>_2 = \frac{[0,v_2]}{|v_2|}\left(\alpha^+_{i+1/2}\rho_1 + \beta^+_{i+1/2}\rho_0 + \gamma^+_{i+1/2}\rho_2\right)$$

$$- \frac{[0,-v_2]}{|v_2|}\left(\alpha^-_{i+1/2}\rho_0 + \beta^-_{i+1/2}\rho_2 + \gamma^-_{i+1/2}\rho_{22}\right),$$

$$<\rho>_3 = \frac{[0,v_3]}{|v_3|}\left(\alpha^+_{j-1/2}\rho_{33} + \beta^+_{j-1/2}\rho_3 + \gamma^+_{j-1/2}\rho_0\right)$$

$$- \frac{[0,-v_3]}{|v_3|}\left(\alpha^-_{j-1/2}\rho_3 + \beta^-_{j-1/2}\rho_0 + \gamma^-_{j-1/2}\rho_4\right),$$

$$<\rho>_4 = \frac{[0,v_4]}{|v_4|}\left(\alpha^+_{j+1/2}\rho_3 + \beta^+_{j+1/2}\rho_0 + \gamma^+_{j+1/2}\rho_4\right)$$

$$- \frac{[0,-v_4]}{|v_4|}\left(\alpha^-_{j+1/2}\rho_0 + \beta^-_{j+1/2}\rho_4 + \gamma^-_{j+1/2}\rho_{44}\right),$$

$$<\rho>_5 = \frac{[0,w_5]}{|w_5|}\left(\alpha^+_{k-1/2}\rho_{55} + \beta^+_{k-1/2}\rho_5 + \gamma^+_{k-1/2}\rho_0\right)$$

$$- \frac{[0,-w_5]}{|w_5|}\left(\alpha^-_{k-1/2}\rho_5 + \beta^-_{k-1/2}\rho_0 + \gamma^-_{k-1/2}\rho_6\right),$$

and

$$<\rho>_6 = \frac{[0,w_6]}{|w_6|}\left(\alpha^+_{k+1/2}\rho_5 + \beta^+_{k+1/2}\rho_0 + \gamma^+_{k+1/2}\rho_6\right)$$

$$- \frac{[0,-w_6]}{|w_6|}\left(\alpha_{\bar{k}+1/2}\rho_0 + \beta_{\bar{k}+1/2}\rho_6 + \gamma_{\bar{k}+1/2}\rho_{66}\right). \tag{6.9}$$

Substitution of Eq. 6.6 into Eq. 6.1 yields

$$\alpha a_0^P \delta P - \alpha \sum_{\ell=1}^{6} a_\ell^P \delta P_\ell - b_0^P = 0. \tag{6.10}$$

Here,

$$a_1^P = A_1 <\rho>_1 d_1^u,$$

$$a_2^P = A_2 <\rho>_2 d_2^u,$$

$$a_3^P = A_3 <\rho>_3 d_3^v,$$

$$a_4^P = A_4 <\rho>_4 d_4^v,$$

$$a_5^P = A_5 <\rho>_5 d_5^w,$$

$$a_6^P = A_6 <\rho>_6 d_6^w,$$

$$a_0^P = a_1^P + a_2^P + a_3^P + a_4^P + a_5^P + a_6^P,$$

and

$$\begin{aligned} b_0^P = & -\left(\frac{\rho_0 - \rho_0^n}{\Delta t}\right)V_0 + \alpha[A_1 <\rho>_1 \hat{u}_1 - A_2 <\rho>_2 \hat{u}_2 + A_3 <\rho>_3 \hat{v}_3 - A_4 <\rho>_4 \hat{u}_4 \\ & + A_5 <\rho>_5 \hat{w}_5 - A_6 <\rho>_6 \hat{w}_6] + \beta[A_1 <\rho>_1 u_1 - A_2 <\rho>_2 u_2 + A_3 <\rho>_3 v_3 \\ & - A_4 <\rho>_4 v_4 + A_5 <\rho>_5 w_5 - A_6 <\rho>_6 w_6]^n. \end{aligned}$$

Equation 6.10 is the required pressure equation. It is solved by using any one of the matrix solvers – a direct solver YSMP and iterative solvers SOR and PCG.

7 Damping Technique for Numerical Oscillations – FRAM

Like other high-order numerical schemes, the QUICK and LECUSSO schemes may suffer from spurious numerical oscillations of the dependent variables at regions of large gradients. Because of the oscillations, the solution of the variables may contain values outside of the range of physically meaningful values. Therefore, the unphysical oscillations must be eliminated so that accurate and dependable solutions may be obtained. In this section, a new FRAM scheme is developed for use with the QUICK or LECUSSO schemes.

The FRAM scheme was originally developed by Chapman[10] and has been implemented in other codes.[31]

The FRAM scheme is based on the solution of the Lagrangian transport equation. This equation can be written in the following form:

$$\rho \frac{D\phi}{Dt} = s_\phi, \tag{7.1}$$

which is the nonconservative form (i.e., transport equation of ϕ – continuity equation) of Eq. 3.1. In Eq. 7.1, $D\phi/Dt$ contains the unsteady and convective terms, and s_ϕ contains the diffusive and source terms in Eq. 3.1. The solution of Eq. 7.1 is denoted as ϕ^L in contrast to the QUICK or LECUSSO solution ϕ of the corresponding Eulerian equation. Because Lagrangian Eq. 7.1 does not contain a convective term, its solution is free from spurious numerical oscillations. Therefore, ϕ^L can be used to construct a bound of physical values for ϕ. Let us denote ϕ_0 as the value of ϕ at Cell 0, and ϕ^L_{min} and ϕ^L_{min} as the minimum and maximum values of ϕ^L at Cell 0 and its surrounding cells (Cells 1, 2, ... 6), then an index δ for Cell 0 is defined as

$$\delta_0 = \begin{cases} 0; \text{ if } \phi^L_{min} < \phi_0 < \phi^L_{max} \\ 1; \text{ otherwise.} \end{cases} \tag{7.2}$$

From Eq. 7.2, when $\delta_0 = 1$, the solution ϕ_0 is not physically meaningful. An appropriate modification of the convective fluxes for Cell 0 then becomes necessary. For the surface between Cell 0 and 1, for instance, we define

$$\delta_{0-1} = \max(\delta_0, \delta_1). \tag{7.3}$$

Then, the flux between Cell 0 and 1 is calculated from

$$F_{0-1} = (1-\delta_{0-1})F^Q_{0-1} + \delta_{0-1} F^u_{0-1}, \tag{7.4}$$

where F^Q_{0-1} is the flux evaluated from the QUICK or LECUSSO scheme and F^u_{0-1} is the flux evaluated from the first–order upwind scheme. We use the first–order upwind scheme because it does not produce spurious oscillations. Based on the newly calculated convective fluxes on all control surfaces of Cell 0, the coefficients of the original Eulerian transport equation are re–evaluated and the final solution is obtained.

The procedure described above is based on the concept of the original FRAM scheme. It was found that, in some cases, it is difficult to obtain converged solutions.[12] The reason is because δ jumps between 0 and 1 when $\phi_0 \approx \phi^L_{min}$ or $\phi_0 \approx \phi^L_{max}$, as seen in Eq. 7.2. In the new FRAM scheme, Eq. 7.2 is modified and the index δ is smoothed as

$$\delta_0 = \begin{cases} 1 - \dfrac{\phi_0 - \phi^L_{min}}{a\left(\phi^L_{max} - \phi^L_{min}\right)}; & \text{if } \phi^L_{min} < \phi_0 < (1-a)\phi^L_{min} + a\phi^L_{max} \\ 0; & \text{if } (1-a)\phi^L_{min} + a\phi^L_{max} \le \phi_0 \le a\phi^L_{min} + (1-a)\phi^L_{max} \\ \dfrac{\phi_0 - a\phi^L_{min} - (1-a)\phi^L_{max}}{a\left(\phi^L_{max} - \phi^L_{min}\right)}; & \text{if } a\phi^L_{min} + (1-a)\phi^L_{max} < \phi_0 < \phi^L_{max} \\ 1; & \text{otherwise} \end{cases} \tag{7.5}$$

where a is an arbitrary constant in the range of 0.5 and 0. When a = 0, Eq. 7.5 degenerates into Eq. 7.2. In the implementation, the default value for a is 0.15.

8 High–Order Boundary Conditions for Velocities

8.1 Classification of Cell Combinations

Before we discuss the mathematical treatment for boundary conditions with high–order schemes, we classify all possible cell combinations relating a central cell (index m_0) with its neighbor cells, either physical or dummy (boundary) cells. Here, we consider the cell combinations in the x–direction. It is sufficient to consider the cell combinations among cells m_{11}, m_1, m_0, m_2, and m_{22}, for the second–order schemes. The total number of independent cell combinations is up to 9, and each combination is shown below. Negative or zero cell numbers stand for boundary cells, and positive cell numbers for fluid cells.

Case 1 $m_{11}>0$, $m_1>0$, $m_2>0$, $m_{22}>0$

m_{11}	m_1	m_0	m_2	m_{22}

Case 2 $m_{11}>0$, $m_1>0$, $m_2>0$, $m_{22}<0$

m_{11}	m_1	m_0	m_2	m_{22}

Case 3 $m_{11}>0$, $m_1>0$, $m_2<0$

m_{11}	m_1	m_0	m_2	

Case 4 $m_{11}<0$, $m_1>0$, $m_2>0$, $m_{22}>0$

m_{11}	m_1	m_0	m_2	m_{22}

Case 5 $m_{11}<0$, $m_1>0$, $m_2>0$, $m_{22}<0$

m_{11}	m_1	m_0	m_2	m_{22}

Case 6 $m_{11}<0$, $m_1>0$, $m_2<0$

m_{11}	m_1	m_0	m_2	

Case 7 $m_1<0$, $m_2>0$, $m_{22}>0$

	m_1	m_0	m_2	m_{22}

Case 8 $m_1<0$, $m_2>0$, $m_{22}<0$

	m_1	m_0	m_2	m_{22}

Case 9 $m_1<0$, $m_2<0$

	m_1	m_0	m_2	

8.2 Convection Terms Near a Moving Boundary

Here, we consider cases $m_{11}<0$, $m_1>0$ of the above nine cases.

We consider the (z − x) term in the z–component of momentum as shown in Fig. 8.1. We evaluate $<w>_1$, which is the velocity of z–component w on surface 1 (1–P and 1–M) at $x=x^*$. When the transporting velocities u_1 and u_{61} are negative, the boundary has nothing to do with the calculation of $<w>_1$. When the transporting velocities u_1 or u_{61} are positive, we evaluate $<w>_1$ by an interpolation technique with w_b (the velocity of moving boundary in the z–direction), w_1, and w_0. We have the following interpolation formula with second–order accuracy:

$$f(x) = \frac{(x - x_1)(x - x_2)}{(x_0 - x_1)(x_0 - x_2)} f(x_0) + \frac{(x - x_0)(x - x_2)}{(x_1 - x_0)(x_1 - x_2)} f(x_1) + \frac{(x - x_0)(x - x_1)}{(x_2 - x_0)(x_2 - x_1)} f(x_2), \tag{8.1}$$

where the locations of x_0, x_1, and x_2 are shown in Fig. 8.1. From the above interpolation formula, we obtain, for $u_1 > 0$,

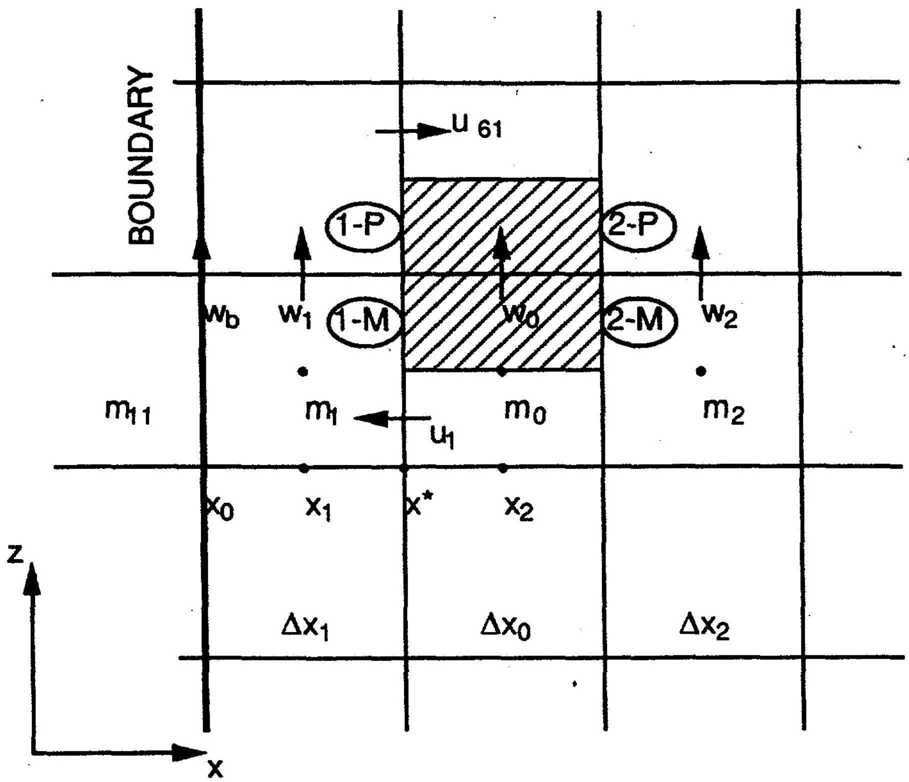

Fig. 8.1. Boundary cells for ($m_{11} < 0$, $m_1 > 0$)

$$< w >_{1-M} = \frac{(x^* - x_1)(x^* - x_2)}{(x_0 - x_1)(x_0 - x_2)} w_b + \frac{(x^* - x_0)(x^* - x_2)}{(x_1 - x_0)(x_1 - x_2)} w_1 + \frac{(x^* - x_0)(x^* - x_1)}{(x_2 - x_0)(x_2 - x_1)} w_2. \tag{8.2}$$

We have

$$x^* - x_1 = \Delta x_1/2,$$
$$x^* - x_2 = -\Delta x_0/2,$$
$$x^* - x_0 = \Delta x_1,$$
$$x_0 - x_1 = -\Delta x_1/2,$$
$$x_0 - x_2 = -(\Delta x_1 + \Delta x_0/2),$$

and

$$x_1 - x_2 = -(\Delta x_1 + \Delta x_0)/2.$$

Then we get

$$< w >_{1-M} = -\frac{\Delta x_0}{\Delta x_0 + 2\Delta x_1} w_b + \frac{2\Delta x_0}{\Delta x_0 + \Delta x_1} w_1 + \frac{2\Delta x_1^2}{(\Delta x_0 + 2\Delta x_1)(\Delta x_0 + \Delta x_1)} w_0. \tag{8.3}$$

From Eq. 8.3 we obtain

$$\alpha^{+,M}_{i-1/2} = -\frac{\Delta x_0}{\Delta x_0 + 2\Delta x_1},$$

$$\beta^{+,M}_{i-1/2} = \frac{2\Delta x_0}{\Delta x_0 + \Delta x_1},$$

and

$$\gamma^{+,M}_{i-1/2} = \frac{2\Delta x_1^2}{(\Delta x_0 + 2\Delta x_1)(\Delta x_0 + \Delta x_1)}. \tag{8.4}$$

In the same manner as the above case, for $u_{61} > 0$, we obtain

$$\alpha^{+,P}_{i-1/2} = \alpha^{+,M}_{i-1/2},$$

$$\beta^{+,P}_{i-1/2} = \beta^{+,M}_{i-1/2},$$

and

$$\gamma^{+,P}_{i-1/2} = \gamma^{+,M}_{i-1/2}. \tag{8.5}$$

For a solid boundary at west, w_b is zero in Eq. 8.3.

8.3 Diffusion Terms (Shear Forces) on a Moving Boundary

We consider the x–component shear forces when the boundary moves with a velocity u_b in the x–direction (see Fig. 8.2). The diffusion term $(DF)_x$ in the x–momentum equation can be expressed in the vector form as

$$(DF)_x = \nabla(\Gamma\nabla u). \tag{8.6}$$

Integration of Eq. 8.6 over the x–momentum control volume as shown in Fig. 8.2 yields

$$\begin{aligned}\int (DF)_x d\bar{V} &= \sum_{\ell=1}^{6} (\Gamma_\ell \nabla u_\ell \bullet \bar{n}_\ell) A_\ell \\ &= \Gamma_2 \frac{\partial u}{\partial x}\bigg|_2 A_2 - \Gamma_1 \frac{\partial u}{\partial x}\bigg|_1 A_1 + \Gamma_4 \frac{\partial u}{\partial y}\bigg|_4 A_4 \\ &\quad - \Gamma_3 \frac{\partial u}{\partial y}\bigg|_3 A_3 + \Gamma_6 \frac{\partial u}{\partial z}\bigg|_6 A_6 - \Gamma_5 \frac{\partial u}{\partial z}\bigg|_5 A_5,\end{aligned} \tag{8.7}$$

where suffix ℓ indicates the surface number and A_ℓ denotes the surface area of surface ℓ.

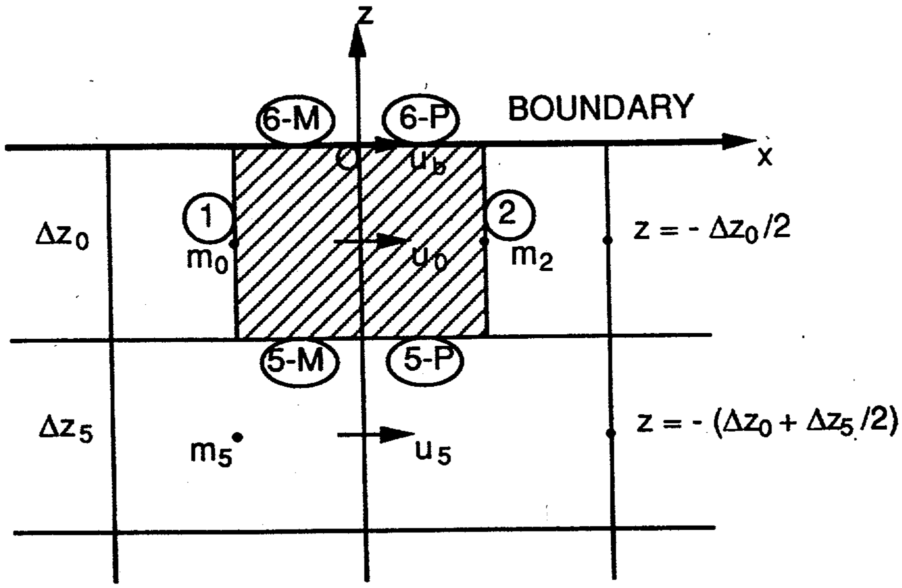

Fig. 8.2. Shear flow boundary

The shear force associated with the moving boundary u_b is related to the fifth term in Eq. 8.7. To be consistent with the second-order schemes used for internal cells, we must evaluate $\partial u/\partial z|_6$ with second-order accuracy.

Expansion of $u(z_0 + \Delta z)$ in a Taylor series with respect to $z = z_0$ yields

$$u(z_0 + \Delta z) = u(z_0) + \left.\frac{\partial u}{\partial z}\right|_{z_0} \Delta z + \frac{1}{2}\left.\frac{\partial^2 u}{\partial z^2}\right|_{z_0} (\Delta z)^2 + 0\left(\Delta z^3\right). \tag{8.8}$$

From Eq. 8.8, we get, at $z_0 = 0$,

$$u(-\Delta z_0/2) = u_0 = u_b + \left.\frac{\partial u}{\partial z}\right|_6 \left(-\frac{\Delta z_0}{2}\right) + \frac{1}{2}\left.\frac{\partial^2 u}{\partial z^2}\right|_6 \left(-\frac{\Delta z_0}{2}\right)^2 + 0\left(\Delta z_0^3\right) \tag{8.9}$$

and

$$u(-\Delta z_0 - \Delta z_5/2) = u_5 = u_b + \left.\frac{\partial u}{\partial z}\right|_6 \left(-\Delta z_0 - \frac{\Delta z_5}{2}\right)$$

$$+ \frac{1}{2}\left.\frac{\partial^2 u}{\partial z^2}\right|_6 \left(-\Delta z_0 - \frac{\Delta z_0}{2}\right)^2 + 0(\Delta z + \Delta z_5)^3. \tag{8.10}$$

From Eqs. 8.9 and 8.10, we obtain $\partial u/\partial z|_6$, with second-order accuracy,

$$\left.\frac{\partial u}{\partial z}\right|_6 = \alpha_b u_b + \beta_b u_0 + \gamma_b u_5, \tag{8.11}$$

where

$$\alpha_b = \frac{2(3\Delta z_0 + \Delta z_5)}{\Delta z_0(2\Delta z_0 + \Delta z_5)},$$

$$\beta_b = -\frac{2(2\Delta z_0 + \Delta z_5)}{\Delta z_0(2\Delta z_0 + \Delta z_5)},$$

and

$$\gamma_b = \frac{2\Delta z_0}{(2\Delta z_0 + \Delta z_5)(\Delta z_0 + \Delta z_5)}.$$

9 Solution Procedures

COMMIX-1C performs thermal-hydraulic calculations by marching in time with an implicitness parameter α with respect to time discretizaton.

For transient problems, the values of the dependent variables at a given time step, say n, are known and the values of the dependent variables at time step n+1 are calculated. By repeating the procedure, we determine thermohydraulic conditions for the desired time span. For this transient calculation, α = 0.5 (Crank-Niclolson scheme) is preferable because the numerical accuracy is second-order with respect to time increment Δt. However, the Crank-Nicolson scheme shows unconditionally stable solutions, providing that it satisfies Lax-Richtmyer's stability criterion. In general, it is preferable to use a time increment comparable with or less than the Courant condition for increasing the numerical accuracy and avoiding overshoots of the solutions.

For steady-state calculations, the same procedure is followed. We start with an initial guess and continue the marching-in-time process until the differential values of all the dependent variables are lower than some specified criteria. Because the time increment has nothing to do with the final steady solution, it is preferable to use α = 1.0 (fully implicit scheme). The size of the timestep for the implicit steady-state calculation can be many times as large as the Courant time-step criterion.

In COMMIX-1C, two options have been provided for the time-step size:

- User-specified time-step size, and

- Automatic time-step size.

In the automatic time-step option, the time-step size is evaluated on the basis of the Courant condition

$$\Delta t = C_1 \Delta t_c, \tag{9.1}$$

where C_1 is a user-prescribed coefficient and Δt_c is the time-step size evaluated from the Courant condition. The Courant time-step size is defined as the minimum time required for fluid to be convected through a cell. In COMMIX, each computational cell is examined with respect to all three component directions to calculate the Courant time-step size.

COMMIX-1C contains two distinct solution sequences: the fully implicit and the semi-implicit. Both are combined into one formulation through an implicit parameter α. The solution procedure becomes semi-implicit when $\alpha = 0$ and fully implicit when $\alpha = 1$. Therefore, in principle, we can say that the formulation covers a full range from semi-implicit ($\alpha = 0$) to fully implicit ($\alpha = 1$).

The solution procedure is outlined as follows:

(a) Substitute the updated velocities given by the finite-volume equations for momentum into the finite-volume equations for mass continuity to obtain the finite-volume pressure Eq. 6.10.

(b) Solve the resultant pressure Eq. 6.10 to determine the flow field, Eq. 6.6 (pressure and velocities).

(c) Solve the turbulence transport equations for kinetic energy and its dissipation, and determine turbulence viscosity and turbulence thermal diffusivity.

(d) Solve the finite-volume equation for energy, Eq. 5.44, and determine the thermal field (enthalpy, temperature) and material properties.

(e) Repeat steps (a) - (d) until all the convengence criteria are met.

The overall flow chart of the program is shown in Fig. 9.1.

10 Test Calculations

In this chapter, we perform some numerical experiments and compare the predictions with analytical solutions or experimental results. These numerical experiments were performed in a frame of the currently improved COMMIX-1C, except for the Burgers equation. The numerical experiment with the Burgers equation was carried out by making use of a small program independent of the COMMIX-1C.

10.1 One-Dimensional Nonlinear Burgers Equation

10.1.1 Computational Conditions

This experiment is concerned with a problem of whether wave front propagation is obeying the one-dimensional nonlinear Burgers equation:

$$\frac{\partial v}{\partial t} + v\frac{\partial v}{\partial x} = \nu\frac{\partial^2 v}{\partial x^2}, \tag{10.1}$$

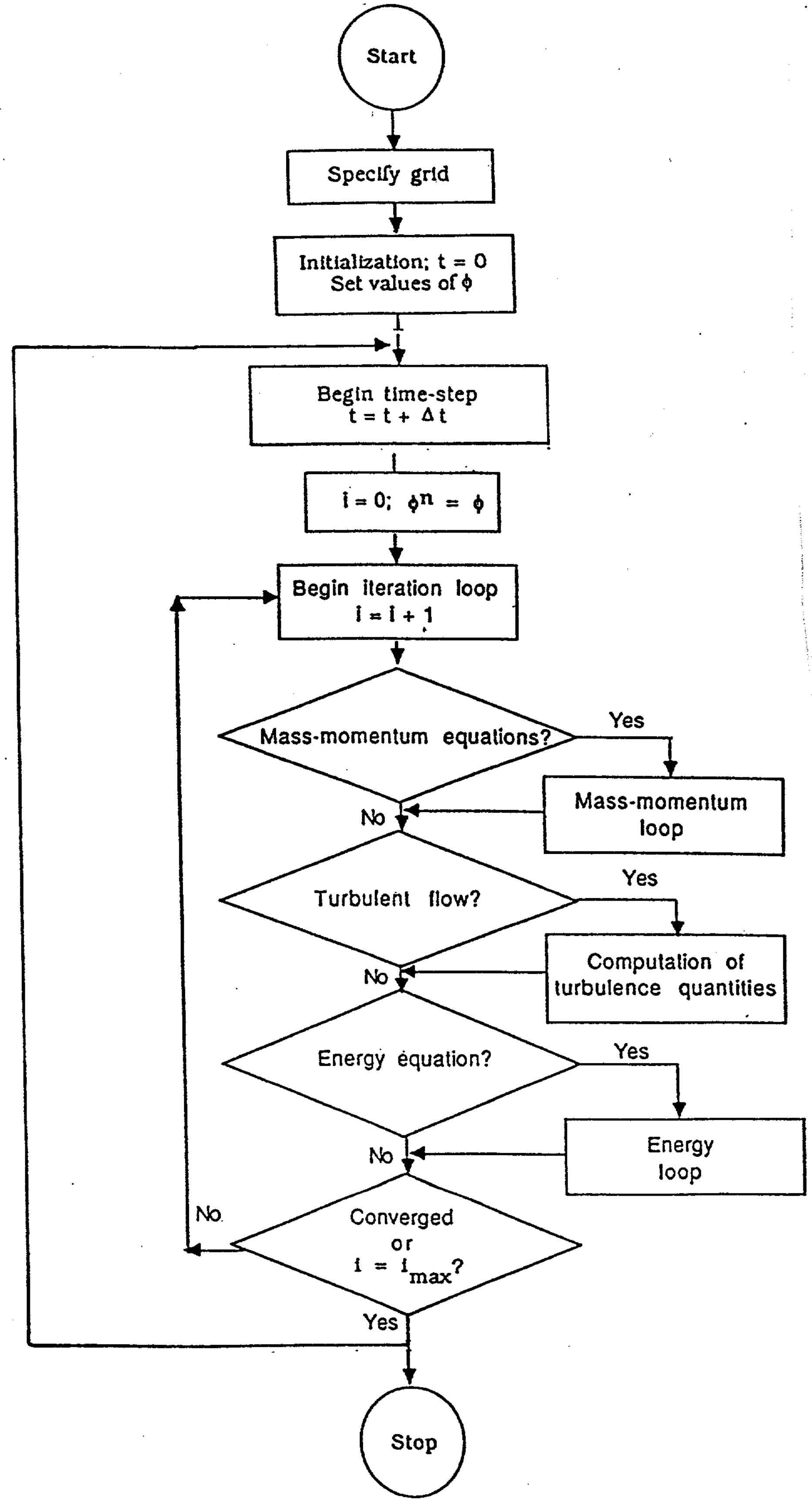

Fig. 9.1. COMMIX-1C flow chart

with the initial condition

$$v(x,0)=\begin{cases} V_0 & (x \le 0), \\ 0 & (x > 0). \end{cases} \tag{10.2}$$

Namely, a wave front is initially (t = 0) located at the origin (x = 0); this wave front is then transported, obeying Eq. 10.1. The analytical solution is

$$v(x,t) = V_0\left\{1 + \exp\left[\frac{V_0}{2\nu}\left(x-\frac{V_0 t}{2}\right)\right] \frac{1 - \mathrm{erf}\left(-x/2\sqrt{\nu t}\right)}{1 - \mathrm{erf}\left[(x - V_0 t)/2\sqrt{\nu t}\right]}\right\}^{-1}, \tag{10.3}$$

where erf represents an error function. Because this solution can describe a steep velocity gradient field, it is preferable to use Eq. 10.3 to assess whether numerical solutions suffer from unphysical oscillations. All variables are made nondimensional by using constant Δt, mesh increment Δx, and initial velocity V_0. The Courant number, $C = V_0\Delta t/\Delta x$, is 0.1. The mesh Reynolds number is defined as $R_m = V_0\Delta x/\nu$. All calculations are compared with the analytical solution at time $t = 500\Delta t$. The Crank–Nicolson scheme was used for time discretization.

Discretization of Eq. 10.1, based on the Crank–Nicolson scheme, yields

$$\frac{v^{n+1} - v^n}{\Delta t} + \alpha(CV)^{n+1} + \beta(CV)^n = \alpha(DF)^{n+1} + \beta(DF)^n. \tag{10.4}$$

Here,

α = implicitness parameter (= 0.5),

(CV) = convection term

$$= \frac{1}{2\Delta x_i}\Big[v_{i+1/2}\left(\alpha^{+}_{i+1/2}\, v_{i-1} + \beta^{+}_{i+1/2}\, v_i + \gamma^{+}_{i+1/2}\, v_{i+1}\right)$$

$$- v_{i-1/2}\left(\alpha^{+}_{i-1/2}\, v_{i-2} + \beta^{+}_{i-1/2}\, v_{i-1} + \gamma^{+}_{i-1/2}\, v_i\right)\Big], \tag{10.5}$$

(DF) = diffusion term

$$= \frac{2}{\Delta x_{i+1}(\Delta x_i + \Delta x_{i+1})}\,\phi_{i+1} - \frac{2}{\Delta x_i \Delta x_{i+1}}\,\phi_i + \frac{2}{\Delta x_i(\Delta x_i + \Delta x_{i+1})}\,\phi_{i-1}. \tag{10.6}$$

The factor 2 in the denominator of Eq. 10.5 is the result of the transformation of the convection term in Eq. 10.1 from the nonconservative form to the conservative form, namely,

$$v\frac{\partial v}{\partial x} = \frac{1}{2}\frac{\partial}{\partial x}\left(v^2\right) \rightarrow \frac{1}{2}\frac{\partial}{\partial x}(v\phi). \tag{10.7}$$

10.1.2 Comparison with Analytical Solution

Here we compare the analytical solution with solutions by the current LECUSSO scheme and the QUICK scheme, which is representative of the conventional high-order schemes.

At a low mesh Reynolds number (R_m < 2), both solutions by the current LECUSSO scheme and the QUICK scheme were smooth, without any numerical wiggles, and almost comparable to one another, as shown in Fig. 10.1. However, at higher mesh Reynolds number (R_m > 2), the difference between the two solutions became larger.

Figure 10.2 shows of the analytical solution and the calculations by the currently extended LECUSSO scheme and the QUCK scheme at R_m = 10. In this figure, the QUICK scheme suffers from numerical wiggles. The LECUSSO scheme never suffers from unphysical oscillations, even in this steep gradient field, and it gives a quite good solution.

Figure 10.3 shows results obtained with the conservative and nonconservative forms of the extended LECUSSO scheme at R_m = 10. In this nonlinear Burgers equation, the conservative form shows a solution quite better than the nonconservative form.

10.1.3 Comparisons among solutions with α = 1.0, 0.5, and 0.0

Figure 10.4 shows the results obtained with α = 1.0 (fully implicit), α = 0.5 (Crank–Nicolson scheme), and α = 0.0 (fully explicit) for the linear Burgers equation with the constant transporting velocity V_o (initial velocity). In this calculation, the Courant number C = 0.5 was used to clearly see the difference between the above three calculational results. If we use C = 0.1, we can hardly confirm the difference because truncation errors with respect to the time increment are negligibly small.

From Fig. 10.4, we can see that Crank–Nicholson scheme (α = 0.5) gives the best solution.

10.2 Symmetry Check Calculations

To confirm the correctness of programming, it is important and necessary to perform symmetry check calculations. Below, we show some results from symmetry check calculations, in which the LECUSSO scheme was used.

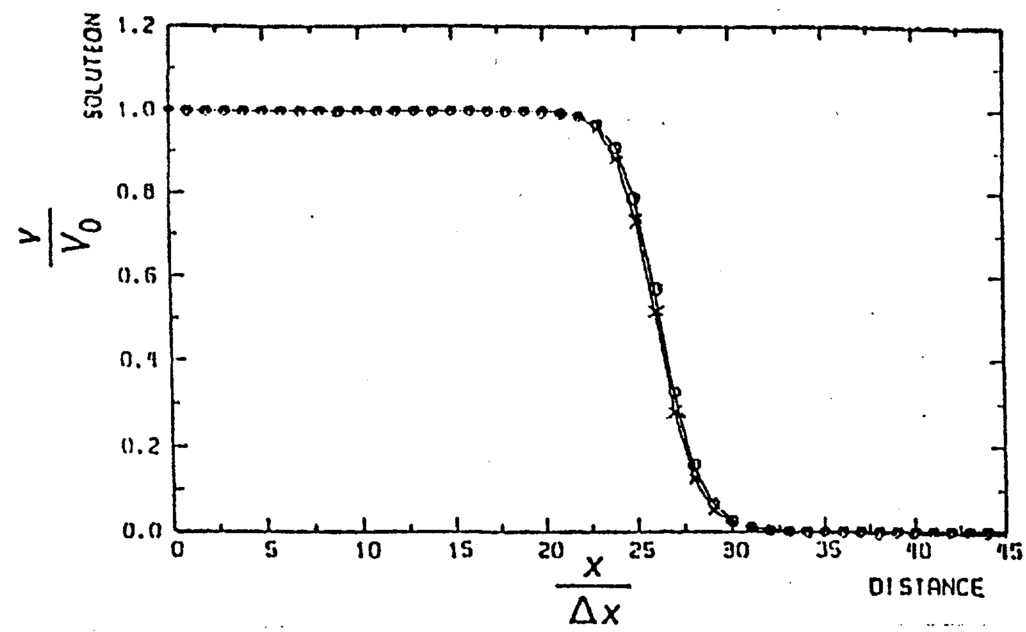

(A) QUICK

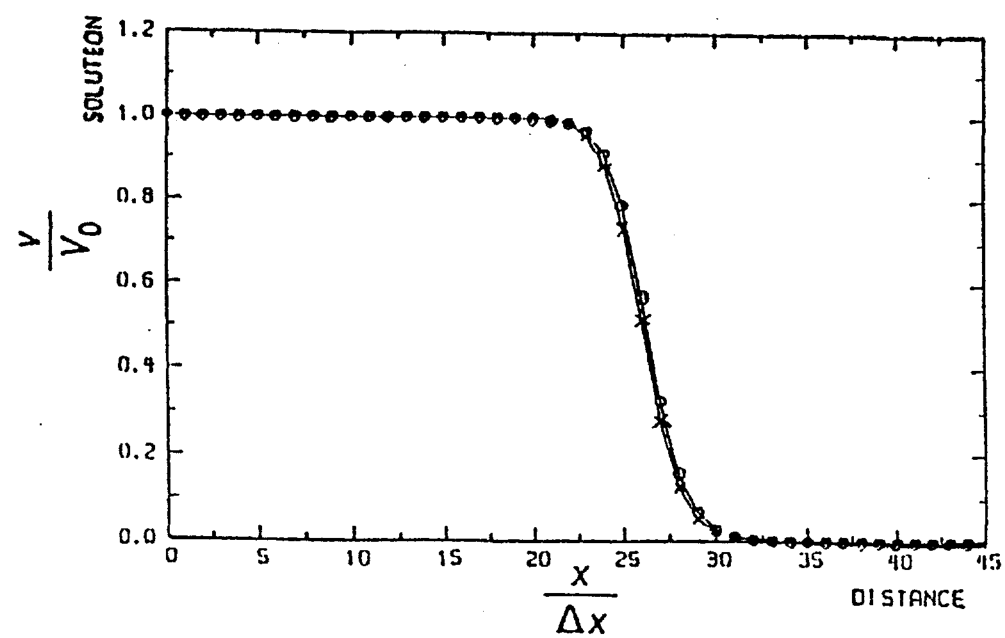

(B) LECUSSO

Fig. 10.1. Prediction of wave propagation calculated (0) by (A) QUICK and (B) LECUSSO at $R_m = 2$ and determined (x) from exact solution

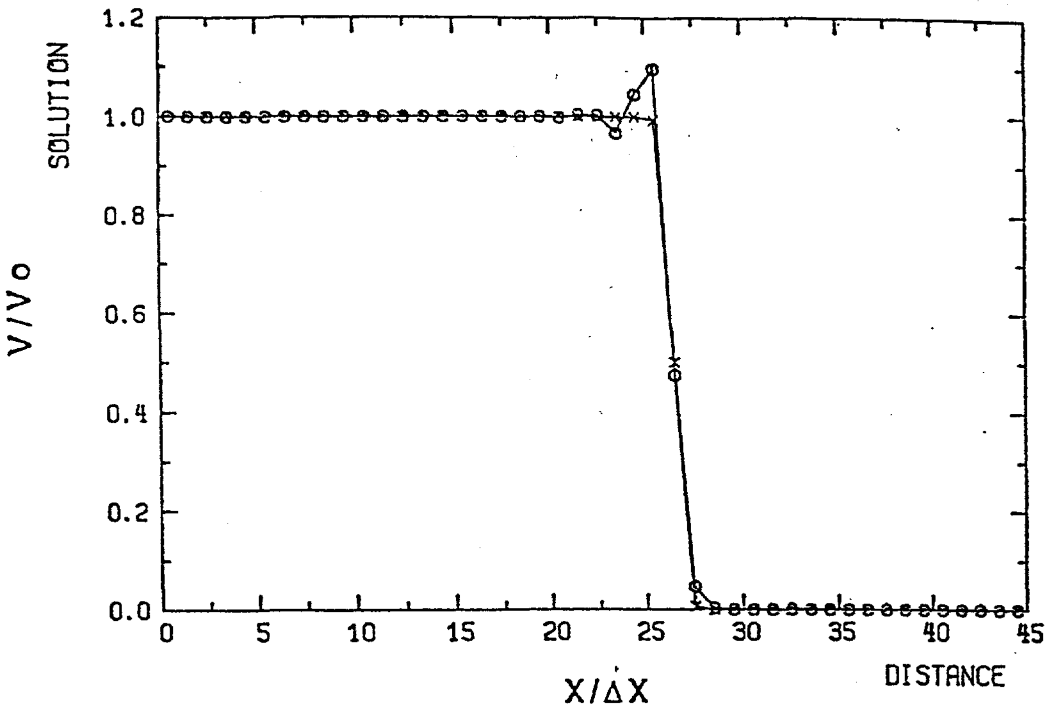

(A) QUICK

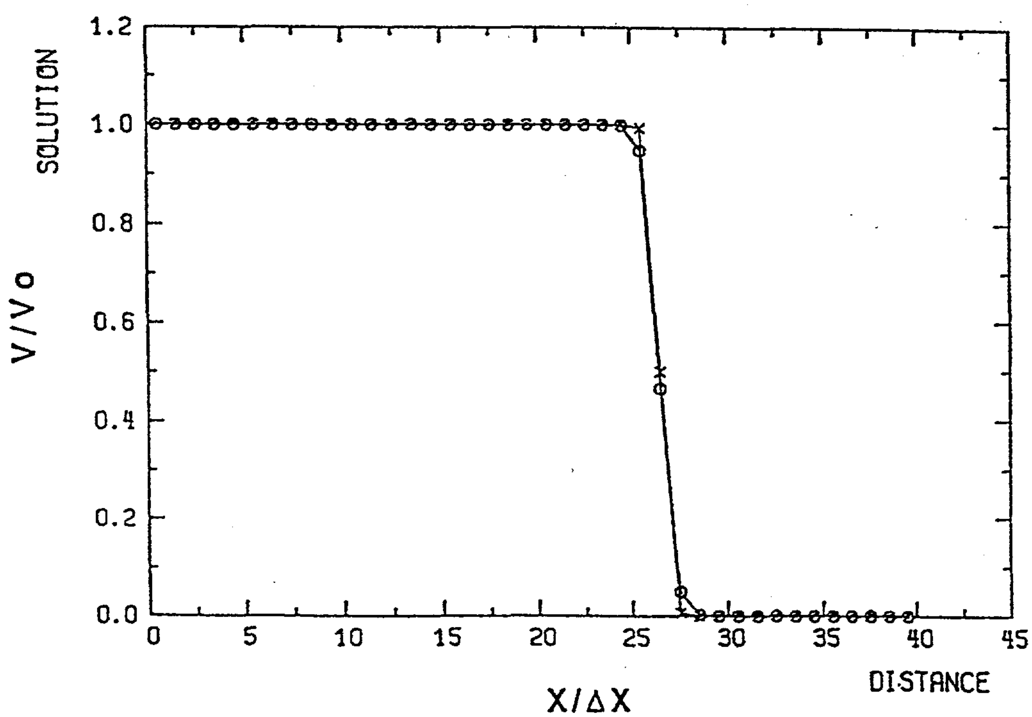

(B) LECUSSO

Fig. 10.2. Prediction of wave propagation calculated (0) by (A) QUICK and (B) LECUSSO at $R_m = 10$ and determined (x) from exact solution

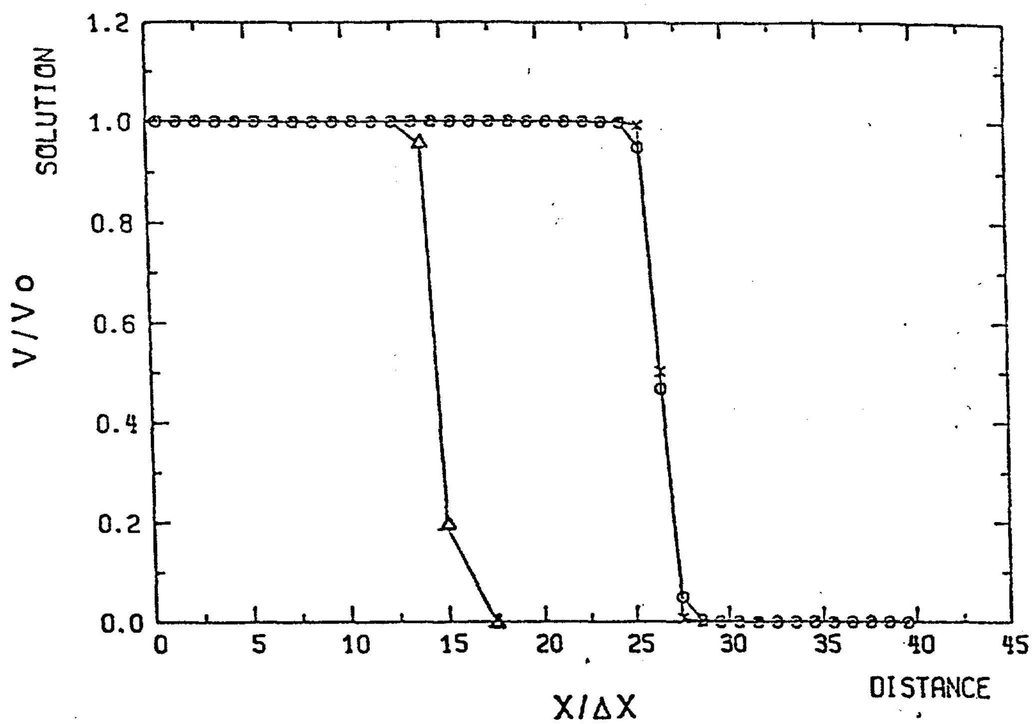

Fig. 10.3. Prediction of wave propagation calculated in conservative (0) and nonconservative (Δ) forms of LECUSSO scheme at R_m = 10 and determined (x) from exact solution

10.2.1 Forced Channel Flow

Computation conditions:

Water fluid,
Uniform inlet velocity = 0.01 (m/s),
Uniform pressure at exit,
Channel length = 8 x 0.01 (m),
Channel cross section = 6 x 0.01 (m) x 0.01 (m),
Total number of computational cells = 6 x 8 = 48.

Table 10.1 shows the input data in the x–z coordinate system. Table 10.2 shows the output for Table 10.1. Table 10.3 shows the input data in the x–y coordinate system. Table 10.4 shows the output for Table 10.3. Table 10.5 shows the input data in the z–x coordinate system. Table 10.6 shows the output for Table 10.5. Tables 10.2, 10.4, and 10.6 show the perfect symmetry property. The velocities at the cell nearest to the solid wall are maximum. This may come from an imbalance between the channel geometry and the imposed boundary conditions. We calculated another case in which the ratio of channel width to channel length was 15, and obtained a smooth distribution of velocity in both the channel width and channel length directions.

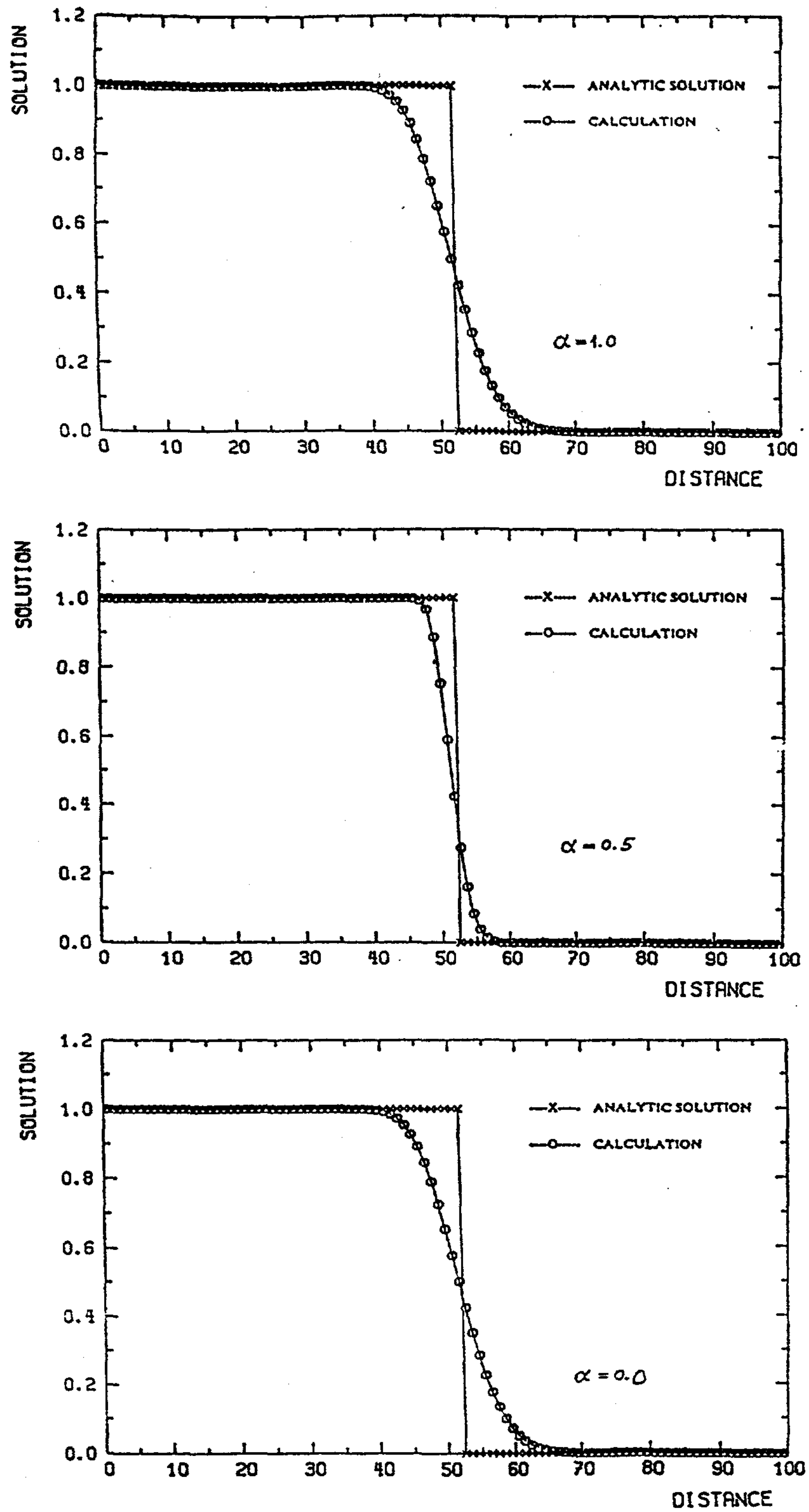

Fig. 10.4. Effect of implicitness parameter α on the accuracy of numerical solutions of the Bergers equation with constant transporting initial velocity

Table 10.1. Input data for forced flow in a square pipe (x-z coordinate)

```
--------------------------------------------------------------
     SAMPLE INPUT DATA FOR FORCED FLOW IN A SQUARE PIPE

         Uniform Outlet Pressure Boundary Condition
                       zwangx.data
--------------------------------------------------------------
 &geom
  ifres=1,
  nl1=124, nml=48, nsurf=6,
  ify=0,
  imax=8, jmax=1, kmax=6,
  isolvr=1, nnzero=1065, nspace=5570,
  xnorml= 1.0,-1.0, 0.0, 0.0, 0.0, 0.0,
  ynorml= 0.0, 0.0, 1.0,-1.0, 0.0, 0.0,
  znorml= 0.0, 0.0, 0.0, 0.0, 1.0,-1.0,
  dx=8*0.01,
  dy=0.01,
  dz=6*0.01,
  &end
reg -1.         1   1   1   1   1   6   1     inlet  +x
reg -1.         8   8   1   1   1   6   2     exit   -x
reg -1.         1   8   1   1   1   6   3     front  +y
reg -1.         1   8   1   1   1   6   4     back   -y
reg -1.         1   8   1   1   1   1   5     bottom +z
reg -1.         1   8   1   1   6   6   6     upper  -z
 &data
  alpha=1.0, eps3=1.e-6, omegav=1.0,
  iskew=0,  ifener=0, ifmom=1,
  idtime=0, dt=0.5,
  ntmax=200,  it=1,
  kpres(2)=1, pres(2)=1.0e05,
  kflow=    1,   -5,    -3,    -3,     0,     0,
  ktemp=    1,  400,     1,     1,     1,     1,
  veloc=1.e-2,  0.0,   0.0,   0.0,   0.0,   0.0,
  temp=  20.0, 20.0, 20.0, 20.0, 20.0, 20.0,
  temp0= 20.0, pres0=1.0e5,
  matype=21, mattab=21, tablot=10.0, tabhit=200.0,
  gravx=-9.8,
  ntprnt=-9999,
  nthpr= 12001, 32001, 17201,
  &end
ul   0.01       1   8   1   1   1   6
wl   0.00       1   8   1   1   1   6
tl  20.000      1   8   1   1   1   6
```

Table 10.2. *Output for zwangx.data presented in Table 10.1*

*** X-Component of Velocity (m/s) ** ul ** j Plane 1 ** Time step 88 ** Time 4.40000E+01 s **

k i-->	0	1	2	3	4	5	6	7	8
6	(1.000E-02)	9.893E-03	9.751E-03	9.589E-03	9.421E-03	9.252E-03	9.086E-03	8.925E-03	(8.925E-03)
5	(1.000E-02)	1.008E-02	1.018E-02	1.028E-02	1.038E-02	1.047E-02	1.056E-02	1.064E-02	(1.064E-02)
4	(1.000E-02)	1.003E-02	1.007E-02	1.013E-02	1.020E-02	1.028E-02	1.035E-02	1.043E-02	(1.043E-02)
3	(1.000E-02)	1.003E-02	1.007E-02	1.013E-02	1.020E-02	1.028E-02	1.035E-02	1.043E-02	(1.043E-02)
2	(1.000E-02)	1.008E-02	1.018E-02	1.028E-02	1.038E-02	1.047E-02	1.056E-02	1.064E-02	(1.064E-02)
1	(1.000E-02)	9.893E-03	9.751E-03	9.589E-03	9.421E-03	9.252E-03	9.086E-03	8.925E-03	(8.925E-03)

*** Z-Component of Velocity (m/s) ** wl ** j Plane 1 ** Time step 88 ** Time 4.40000E+01 s **

k i-->	1	2	3	4	5	6	7	8
6	(0.000E+00)	(0.000E+00)	(0.000E+00)	(0.000E+00)	(0.000E+00)	(0.000E+00)	(0.000E+00)	(0.000E+00)
5	-1.072E-04	-1.422E-04	-1.612E-04	-1.685E-04	-1.689E-04	-1.659E-04	-1.613E-04	-1.555E-04
4	-2.692E-05	-4.683E-05	-6.043E-05	-6.875E-05	-7.372E-05	-7.672E-05	-7.863E-05	-7.922E-05
3	5.377E-12	5.907E-11	1.342E-10	2.480E-10	4.170E-10	6.566E-10	9.811E-10	1.381E-09
2	2.692E-05	4.683E-05	6.043E-05	6.875E-05	7.372E-05	7.672E-05	7.863E-05	7.922E-05
1	1.072E-04	1.422E-04	1.612E-04	1.685E-04	1.689E-04	1.659E-04	1.613E-04	1.555E-04
0	(0.000E+00)	(0.000E+00)	(0.000E+00)	(0.000E+00)	(0.000E+00)	(0.000E+00)	(0.000E+00)	(0.000E+00)

Table 10.3. Input data for force flow in a square pipe (x-y coordinate)

```
-------------------------------------------------------------
     SAMPLE INPUT DATA FOR FORCED FLOW IN A SQUARE PIPE

         Uniform Outlet Pressure Boundary Condition
                       zwangy.data
-------------------------------------------------------------
 &geom
  ifres=1,
  nl1=124, nml=48, nsurf=6,
  ifz=0,
  imax=6, jmax=8, kmax=1,
  isolvr=1, nnzero=1065, nspace=5570,
  xnorml= 1.0,-1.0, 0.0, 0.0, 0.0, 0.0,
  ynorml= 0.0, 0.0, 1.0,-1.0, 0.0, 0.0,
  znorml= 0.0, 0.0, 0.0, 0.0, 1.0,-1.0,
  dx=6*0.01,
  dy=8*0.01,
  dz=0.01,
  &end
reg -1.          1   1   1   8   1   1   1     left    +x
reg -1.          6   6   1   8   1   1   2     right   -x
reg -1.          1   6   1   1   1   1   3     inlet   +y
reg -1.          1   6   8   8   1   1   4     exit    -y
reg -1.          1   6   1   8   1   1   5     front   +z
reg -1.          1   6   1   8   1   1   6     back    -z
 &data
  alpha=1.0, eps3=1.e-6, omegav=1.0,
  iskew=0,  ifener=0, ifmom=1,
  idtime=0, dt=0.5,
  ntmax=200,  it=1,
  kpres(4)=1, pres(4)=1.0e05,
  kflow=    0,     0,     1,    -5,    -3,    -3,
  ktemp=    1,     1,     1,   400,     1,     1,
  veloc=  0.0,   0.0,1.e-2,   0.0,   0.0,   0.0,
  temp=  20.0,  20.0,  20.0,  20.0,  20.0,  20.0,
  temp0= 20.0, pres0=1.0e5,
  matype=21, mattab=21, tablot=10.0, tabhit=200.0,
  gravy=-9.8,
  ntprnt=-9999,
  nthpr= 13001, 23001, 17301,
  &end
ul  0.0000       1   6   1   8   1   1
vl  1.0e-2       1   6   1   8   1   1
tl  20.000       1   6   1   8   1   1
```

Table 10.4. Output for zwangy.data presented in Table 10.3

```
*** X-Component of Velocity (m/s)                ** ul ** k Plane  1 ** Time step  88 ** Time 4.40000E+01 s **

j  i-->     0            1           2           3           4           5            6
 8      ( 0.000E+00)  1.555E-04   7.922E-05   1.381E-09  -7.922E-05  -1.555E-04  ( 0.000E+00)
 7      ( 0.000E+00)  1.613E-04   7.863E-05   9.811E-10  -7.863E-05  -1.613E-04  ( 0.000E+00)
 6      ( 0.000E+00)  1.659E-04   7.672E-05   6.566E-10  -7.672E-05  -1.659E-04  ( 0.000E+00)
 5      ( 0.000E+00)  1.689E-04   7.372E-05   4.170E-10  -7.372E-05  -1.689E-04  ( 0.000E+00)
 4      ( 0.000E+00)  1.685E-04   6.875E-05   2.480E-10  -6.875E-05  -1.685E-04  ( 0.000E+00)
 3      ( 0.000E+00)  1.612E-04   6.043E-05   1.342E-10  -6.043E-05  -1.612E-04  ( 0.000E+00)
 2      ( 0.000E+00)  1.422E-04   4.683E-05   5.907E-11  -4.683E-05  -1.422E-04  ( 0.000E+00)
 1      ( 0.000E+00)  1.072E-04   2.692E-05   5.377E-12  -2.692E-05  -1.072E-04  ( 0.000E+00)

*** y-Component of Velocity (m/s)                ** vl ** k Plane  1 ** Time step  88 ** Time 4.40000E+01 s **

j  i-->     1           2           3           4           5           6
 8      ( 8.925E-03)( 1.064E-02)( 1.043E-02)( 1.043E-02)( 1.064E-02)( 8.925E-03)
 7        8.925E-03   1.064E-02   1.043E-02   1.043E-02   1.064E-02   8.925E-03
 6        9.086E-03   1.056E-02   1.035E-02   1.035E-02   1.056E-02   9.086E-03
 5        9.252E-03   1.047E-02   1.028E-02   1.028E-02   1.047E-02   9.252E-03
 4        9.421E-03   1.038E-02   1.020E-02   1.020E-02   1.038E-02   9.421E-03
 3        9.589E-03   1.028E-02   1.013E-02   1.013E-02   1.028E-02   9.589E-03
 2        9.751E-03   1.018E-02   1.007E-02   1.007E-02   1.018E-02   9.751E-03
 1        9.893E-03   1.008E-02   1.003E-02   1.003E-02   1.008E-02   9.893E-03
 0      ( 1.000E-02)( 1.000E-02)( 1.000E-02)( 1.000E-02)( 1.000E-02)( 1.000E-02)
```

Table 10.5. Input data for forced flow in a square pipe (z-x coordinate)

```
--------------------------------------------------------------
     SAMPLE INPUT DATA FOR FORCED FLOW IN A SQUARE PIPE

         Uniform Outlet Pressure Boundary Condition
                        zwangz.data
--------------------------------------------------------------
&geom
 ifres=1,
 nl1=124, nm1=48, nsurf=6,
 ify=0,
 imax=6, jmax=1, kmax=8,
 isolvr=1, nnzero=1065, nspace=5570,
 xnorml= 1.0,-1.0, 0.0, 0.0, 0.0, 0.0, 0.0,
 ynorml= 0.0, 0.0, 1.0,-1.0, 0.0, 0.0, 0.0,
 znorml= 0.0, 0.0, 0.0, 0.0, 1.0,-1.0,-1.0,
 dx=6*0.01,
 dy=0.01,
 dz=8*0.01,
 &end
reg -1.        1   1   1   1   1   8   1     left   +x
reg -1.        6   6   1   1   1   8   2     right  -x
reg -1.        1   6   1   1   1   8   3     front  +y
reg -1.        1   6   1   1   1   8   4     back   -y
reg -1.        1   6   1   1   1   1   5     inlet  +z
reg -1.        1   6   1   1   8   8   6     exit   -z
 &data
  alpha=1.0, eps3=1.e-6, omegav=1.0,
  iskew=0,  ifener=0, ifmom=1,
  idtime=0, dt=0.5,
  ntmax=200,  it=1,
  kpres(6)=1, pres(6)=1.0e05,
  kflow=     0,     0,    -3,    -3,     1,    -5,    -5,
  ktemp=     1,     1,     1,     1,     1,   400,   400,
  veloc=   0.0,   0.0,   0.0,   0.0,1.e-2,   0.0,   0.0,
  temp=   20.0,  20.0,  20.0,  20.0,  20.0,  20.0,  20.0,
  temp0= 20.0, pres0=1.0e5,
  matype=21, mattab=21, tablot=10.0, tabhit=200.0,
  gravz=-9.8,
  ntprnt=-9999,
  nthpr= 12001, 32001, 17201,
  &end
ul  0.0000     1   6   1   1   1   8
wl  1.0e-2     1   6   1   1   1   8
tl  20.000     1   6   1   1   1   8
```

Table 10.6. Output for zwangz.data presented in Table 10.5

```
*** X-Component of Velocity (m/s)                  ** ul ** j Plane  1 ** Time step  88 ** Time 4.40000E+01 s **

 k  i-->     0          1          2          3          4          5           6
 8      ( 0.000E+00) 1.555E-04  7.922E-05  1.060E-09 -7.922E-05 -1.555E-04 ( 0.000E+00)
 7      ( 0.000E+00) 1.613E-04  7.863E-05  7.534E-10 -7.863E-05 -1.613E-04 ( 0.000E+00)
 6      ( 0.000E+00) 1.659E-04  7.672E-05  5.043E-10 -7.672E-05 -1.659E-04 ( 0.000E+00)
 5      ( 0.000E+00) 1.689E-04  7.372E-05  3.202E-10 -7.372E-05 -1.689E-04 ( 0.000E+00)
 4      ( 0.000E+00) 1.685E-04  6.875E-05  1.904E-10 -6.875E-05 -1.685E-04 ( 0.000E+00)
 3      ( 0.000E+00) 1.612E-04  6.043E-05  1.030E-10 -6.043E-05 -1.612E-04 ( 0.000E+00)
 2      ( 0.000E+00) 1.422E-04  4.683E-05  4.536E-11 -4.683E-05 -1.422E-04 ( 0.000E+00)
 1      ( 0.000E+00) 1.072E-04  2.692E-05  4.129E-12 -2.692E-05 -1.072E-04 ( 0.000E+00)

*** Z-Component of Velocity (m/s)                  ** wl ** j Plane  1 ** Time step  88 ** Time 4.40000E+01 s **

 k  i-->     1            2            3            4            5            6
 8      ( 8.925E-03)( 1.064E-02)( 1.043E-02)( 1.043E-02)( 1.064E-02)( 8.925E-03)
 7        8.925E-03    1.064E-02    1.043E-02    1.043E-02    1.064E-02    8.925E-03
 6        9.086E-03    1.056E-02    1.035E-02    1.035E-02    1.056E-02    9.086E-03
 5        9.252E-03    1.047E-02    1.028E-02    1.028E-02    1.047E-02    9.252E-03
 4        9.421E-03    1.038E-02    1.020E-02    1.020E-02    1.038E-02    9.421E-03
 3        9.589E-03    1.028E-02    1.013E-02    1.013E-02    1.028E-02    9.589E-03
 2        9.751E-03    1.018E-02    1.007E-02    1.007E-02    1.018E-02    9.751E-03
 1        9.893E-03    1.008E-02    1.003E-02    1.003E-02    1.008E-02    9.893E-03
 0      ( 1.000E-02)( 1.000E-02)( 1.000E-02)( 1.000E-02)( 1.000E-02)( 1.000E-02)
```

10.2.2 Scalar Transport in Two Impinging Streams with Same Velocity and Different Temperatures

The streams enter a square domain from two adjacent edges and impinge along the diagonal with velocity = $\sqrt{0.02}$ (m/s) (two velocity components equal to 0.1 m/s). The temperatures of the inlet flows are 50 and 150°C. In this calculation, only the temperature analysis is performed in the prescribed flow field, where an artifically large value (1000) for the thermal conductivity is used, to confirm the symmetry property over the whole computational domain. If we use usual thermal conductivity, the temperature mixing is limited to the area near to the diagonal line. In this problem, the temperature of diagonal cells should be (50 + 150)/2 = 100°C. We confirm this.

Table 10.7 shows the input for the above problem. Table 10.8 shows the output for Table 10.7. Table 10.9 shows the temperature map. Tables 10.8 and 10.9 show that the temperatures of diagonal cells are 100°C.

10.2.3 Thermally Driven Cavity Flow

This is the natural-convection flow of air fluid in a square cavity with differentially heated vertical side walls. The driving temperature difference is 10°C and the Rayleigh number is 1000. We perform laminar analyses.

Table 10.10 shows the input in the x-y coordinate system. Table 10.11 shows the output for Table 10.10 Table 10.12 shows the input in the x-z coordinate system. Table 10.13 shows the output for Table 10.12. Comparison of Tables 10.11 and 10.13 shows the symmetry in both velocity and temperature with respect to exchanging the x-y system with the x-z system.

10.3 Validation of Implicitness Parameter

Table 10.14 shows the solutions that are obtained for α = 1.0 and α = 0.5 by using forced-channel-flow data (zwangz.data), Table 10.5.

In this calculation, Δt = 0.5 was used. The steady-state solutions used in the case of α = 0.5 are identical to those used in the case of α = 1.0. This means that programming implementation regarding the treatment of α = 0.5 is correct.

It is remarkable that the iteration numbers used in the case of α = 0.5 are smaller than α = 1.0.

10.4 Two-Dimensional Scalar Transport/Temperature Analysis in a Jet

Input data for this test case is the same as the data used in Sec. 10.2.2, Table 10.7.

Table 10.7. Input data for scalar transport in two impinging streams

```
-----------------------------------------------------------------
   INPUT DATA FOR SCALAR TRANSPORT IN TWO IMPINGING STREAMS

              Symmetry check for LECUSSO scheme
    15x15x1     u=v, or u different from v (change veloc)
               k=10**4 (conduction dominated)

                          <stran.data>
-----------------------------------------------------------------
&geom
 ifres=1,
 nl1=510, nm1=225, nsurf=6,
 ifz=0,
 imax=15, jmax=15, kmax=1,
 isolvr=1, nnzero=1065, nspace=5570,
 xnorml= 1.0,-1.0, 0.0, 0.0, 0.0, 0.0,
 ynorml= 0.0, 0.0, 0.0, 0.0,-1.0, 1.0,
 znorml= 0.0, 0.0,-1.0, 1.0, 0.0, 0.0,
 dx=15*0.1,
 dy=15*0.1,
 dz=   0.1,
 &end
reg -1.          1   1   1  15   1   1   1     inlet  +x
reg -1.         15  15   1  15   1   1   2     exit   -x
reg -1.          1  15   1  15   1   1   3     top    -z
reg -1.          1  15   1  15   1   1   4     bottom +z
reg -1.          1  15  15  15   1   1   5     exit   -y
reg -1.          1  15   1   1   1   1   6     inlet  +y
 &data
  alpha=1.0,
  iskew=0,  ifener=1, ifmom=0,
  idtime=0, dt=0.5,
  ntmax=200,  it=1,
  kpres(2)=1, kpres(5)=1, pres=6*1.01353e05
  kflow=    1,   -5,    -3,    -3,    -5,     1,
  ktemp=    1,  400,   400,   400,   400,     1,
  veloc=  0.10, -0.10,  0.0,  0.0, -0.1,  0.1,
  temp=  50.0,150.0, 50.0, 50.0, 50.0,150.0,
  temp0=100.0, pres0=1.0e5,
  matype=1, mattab=1, tablot=50.0, tabhit=150.0,
  c0h=0.0, c1h=1000.0,
  c0ro=1.0e3,
  c0k=1.0e+4,
  c0mu=1.0e-3,
  ntprnt=-9999,
  istpr= 13001, 23001, 53001,
  nthpr= 13001, 23001, 53001, 83001, 163001,
  &end
ul  0.1          1  15   1  15   1   1
vl  0.1          1  15   1  15   1   1
tl  100.0        1  15   1  15   1   1
```

Table 10.8. Output for stran.data presented in Table 10.7

*** Temperature (Celsius) ** tl ** k Plane 1 ** Time step 76 ** Time 3.80000E+01 s **

j \ i-->	0	1	2	3	4	5	6	7	8	9
16		(5.023E+01)	(5.144E+01)	(5.283E+01)	(5.478E+01)	(5.733E+01)	(6.050E+01)	(6.425E+01)	(6.851E+01)	(7.320E+01)
15	(5.000E+01)	5.023E+01	5.144E+01	5.283E+01	5.478E+01	5.733E+01	6.050E+01	6.425E+01	6.851E+01	7.320E+01
14	(5.000E+01)	5.026E+01	5.166E+01	5.325E+01	5.545E+01	5.829E+01	6.178E+01	6.586E+01	7.043E+01	7.538E+01
13	(5.000E+01)	5.032E+01	5.203E+01	5.394E+01	5.655E+01	5.988E+01	6.387E+01	6.845E+01	7.348E+01	7.882E+01
12	(5.000E+01)	5.040E+01	5.253E+01	5.489E+01	5.805E+01	6.199E+01	6.662E+01	7.180E+01	7.736E+01	8.313E+01
11	(5.000E+01)	5.051E+01	5.321E+01	5.614E+01	5.999E+01	6.468E+01	7.003E+01	7.587E+01	8.197E+01	8.814E+01
10	(5.000E+01)	5.066E+01	5.410E+01	5.777E+01	6.247E+01	6.802E+01	7.418E+01	8.069E+01	8.730E+01	9.379E+01
9	(5.000E+01)	5.086E+01	5.530E+01	5.991E+01	6.563E+01	7.216E+01	7.916E+01	8.630E+01	9.332E+01	1.000E+02
8	(5.000E+01)	5.114E+01	5.692E+01	6.273E+01	6.966E+01	7.726E+01	8.507E+01	9.274E+01	1.000E+02	1.067E+02
7	(5.000E+01)	5.155E+01	5.915E+01	6.649E+01	7.482E+01	8.350E+01	9.201E+01	1.000E+02	1.073E+02	1.137E+02
6	(5.000E+01)	5.217E+01	6.231E+01	7.154E+01	8.138E+01	9.104E+01	1.000E+02	1.080E+02	1.149E+02	1.208E+02
5	(5.000E+01)	5.319E+01	6.687E+01	7.837E+01	8.969E+01	1.000E+02	1.090E+02	1.165E+02	1.227E+02	1.278E+02
4	(5.000E+01)	5.508E+01	7.366E+01	8.762E+01	1.000E+02	1.103E+02	1.186E+02	1.252E+02	1.303E+02	1.344E+02
3	(5.000E+01)	5.899E+01	8.403E+01	1.000E+02	1.124E+02	1.216E+02	1.285E+02	1.335E+02	1.373E+02	1.401E+02
2	(5.000E+01)	6.816E+01	1.000E+02	1.160E+02	1.263E+02	1.331E+02	1.377E+02	1.408E+02	1.431E+02	1.447E+02
1	(5.000E+01)	1.000E+02	1.318E+02	1.410E+02	1.449E+02	1.468E+02	1.478E+02	1.485E+02	1.489E+02	1.491E+02
0		(1.500E+02)	(1.500E+02)	(1.500E+02)	(1.500E+02)	(1.500E+02)	(1.500E+02)	(1.500E+02)	(1.500E+02)	(1.500E+02)

j \ i-->	10	11	12	13	14	15	16
16	(7.817E+01)	(8.328E+01)	(8.835E+01)	(9.314E+01)	(9.726E+01)	(1.000E+02)	
15	7.817E+01	8.328E+01	8.835E+01	9.314E+01	9.726E+01	1.000E+02	(1.000E+02)
14	8.057E+01	8.584E+01	9.102E+01	9.586E+01	1.000E+02	1.027E+02	(1.027E+02)
13	8.432E+01	8.980E+01	9.511E+01	1.000E+02	1.041E+02	1.069E+02	(1.069E+02)
12	8.893E+01	9.461E+01	1.000E+02	1.049E+02	1.090E+02	1.117E+02	(1.117E+02)
11	9.420E+01	1.000E+02	1.054E+02	1.102E+02	1.142E+02	1.167E+02	(1.167E+02)
10	1.000E+02	1.058E+02	1.111E+02	1.157E+02	1.194E+02	1.218E+02	(1.218E+02)
9	1.062E+02	1.119E+02	1.169E+02	1.212E+02	1.246E+02	1.268E+02	(1.268E+02)
8	1.127E+02	1.180E+02	1.226E+02	1.265E+02	1.296E+02	1.315E+02	(1.315E+02)
7	1.193E+02	1.241E+02	1.282E+02	1.315E+02	1.341E+02	1.358E+02	(1.358E+02)
6	1.258E+02	1.300E+02	1.334E+02	1.361E+02	1.382E+02	1.395E+02	(1.395E+02)
5	1.320E+02	1.353E+02	1.380E+02	1.401E+02	1.417E+02	1.427E+02	(1.427E+02)
4	1.375E+02	1.400E+02	1.419E+02	1.434E+02	1.446E+02	1.452E+02	(1.452E+02)
3	1.422E+02	1.439E+02	1.451E+02	1.461E+02	1.468E+02	1.472E+02	(1.472E+02)
2	1.459E+02	1.468E+02	1.475E+02	1.480E+02	1.483E+02	1.486E+02	(1.486E+02)
1	1.493E+02	1.495E+02	1.496E+02	1.497E+02	1.497E+02	1.498E+02	(1.498E+02)
0	(1.500E+02)	(1.500E+02)	(1.500E+02)	(1.500E+02)	(1.500E+02)	(1.500E+02)	

Table 10.9. Temperature (°C) map for stran.data presented in Table 10.8

50.2	51.4	52.8	54.8	57.3	60.5	64.2	68.5	73.2	78.2	83.3	88.3	93.1	97.3	100.0
50.3	51.7	53.2	55.4	58.3	61.8	65.9	70.4	75.4	80.6	85.8	91.0	95.9	100.0	102.7
50.3	52.0	53.9	56.6	59.9	63.9	68.5	73.5	78.8	84.3	89.8	95.1	100.0	104.1	106.9
50.4	52.5	54.9	58.1	62.0	66.6	71.8	77.4	83.1	88.9	94.6	100.0	104.9	109.0	111.7
50.5	53.2	56.1	60.0	64.7	70.0	75.9	82.0	88.1	94.2	100.0	105.4	110.2	114.2	116.7
50.7	54.1	57.8	62.5	68.0	74.2	80.7	87.3	93.8	100.0	105.8	111.1	115.7	119.4	121.8
50.9	55.3	59.9	65.6	72.2	79.2	86.3	93.3	100.0	106.2	111.9	116.9	121.2	124.6	126.8
51.1	56.9	62.7	69.7	77.3	85.1	92.7	100.0	106.7	112.7	118.0	122.6	126.5	129.6	131.5
51.5	59.2	66.5	74.8	83.5	92.0	100.0	107.3	113.7	119.3	124.1	128.2	131.5	134.1	135.8
52.2	62.3	71.5	81.4	91.0	100.0	108.0	114.9	120.8	125.8	130.0	133.4	136.1	138.2	139.5
53.2	66.9	78.4	89.7	100.0	109.0	116.5	122.7	127.8	132.0	135.3	138.0	140.1	141.7	142.7
55.1	73.7	87.6	100.0	110.3	118.6	125.2	130.3	134.4	137.5	140.0	141.9	143.4	144.6	145.2
59.0	84.0	100.0	112.4	121.6	128.5	133.5	137.3	140.1	142.2	143.9	145.1	146.1	146.8	147.2
68.2	100.0	116.0	126.3	133.1	137.7	140.8	143.1	144.7	145.9	146.8	147.5	148.0	148.3	148.4
100.0	131.8	141.0	144.9	146.8	147.8	148.5	148.9	149.1	149.3	149.5	149.6	149.7	149.7	149.8

K = 1
Time: 38.00 s

LECUSSO Scheme

Table 10.10. Input data for natural convection in x-y coordinate system

```
------------------------------------------------------------------
 INPUT DATA FOR NATURAL CONVECTION IN THE x-y COORDINATE SYSTEM

                         <boxy.data>
natural convection of air in a square pipe with Rayleigh number of
       Ra = 1.00e+3, Th = 30.0, Tc = 20.0, L  = 1.0498
------------------------------------------------------------------
 &geom
  iturke=0,
  isolvr=1,  nnzero=1920, nspace=11042,
  ifres=1, ifz=0,
  nl1=880,  nml=400, nsurf=7,
  imax=10, jmax=10, kmax=1,
  dx=9*5.249e-4, 5.249e-04, dy=9*5.249e-4, 5.249e-04, dz=1.0,
  xnorml=  1.0, -1.0,  0.0,  0.0,  0.0,  0.0,  0.0,
  ynorml=  0.0,  0.0,  0.0,  0.0,  1.0, -1.0, -1.0,
  znorml=  0.0,  0.0,  1.0, -1.0,  0.0,  0.0,  0.0,
 &end
reg -1.0        1   1   1  10   1   1   1    +x surface
reg -1.0       10  10   1  10   1   1   2    -x surface
reg -1.0        1  10   1  10   1   1   3    +z surface
reg -1.0        1  10   1  10   1   1   4    -z surface
reg -1.0        1  10   1   1   1   1   5    +y surface
reg -1.0        1   9  10  10   1   1   6    -y surface
reg -1.0       10  10  10  10   1   1   7    -y surface
 &data
  alpha=1.0, eps3=5.0e-5, omega=1.3, omegav=1.0, omegae=1.0,
  itibug=1, iskew=0, nthcon=-1, ifener=1,
  idtime=0, dt=0.5,
  ntmax=300, it=1, trest=7200.0,
  gravy=-9.8,
  temp0=25.0, pres0=1.0e5,
  kflow=    0,     0,    -3,    -3,     0,   0,  0,
  kpres=    6*0,     1,  pres(7)=1.0e5,
  ktemp=    1,   1,   400,   400,   400,   400,  400,
  temp= 30.0,  20.0,
  veloc=  7*0.0,
  matype=1, mattab=1, tablot=20.0, tabhit=40.0,
  c0ro= 1.273738, c1ro=-3.588e-3,
  c0h=  0.0,  c1h=1005.7,
  c0k=  0.02624,
  c0mu= 1.846e-5,
  ntprnt=-9999,
  istpr=12001,22001,42001,52001,
  nthpr=13001,23001,43001,53001,
 &end
ul    0.001      1  10   1  10   1   1
vl    0.001      1  10   1  10   1   1
tl    25.00      1  10   1  10   1   1
```

Table 10.11. Output for boxy.data presented in Table 10.10

*** X-Component of Velocity (m/s) ** u1 ** k Plane 1 ** Time step 63 ** Time 3.15000E+01 s **

j i-->	0	1	2	3	4	5	6	7	8	9
10	(0.000E+00)	2.440E-04	6.303E-04	9.734E-04	1.195E-03	1.269E-03	1.191E-03	9.704E-04	6.319E-04	2.483E-04
9	(0.000E+00)	3.854E-04	1.008E-03	1.584E-03	1.969E-03	2.100E-03	1.964E-03	1.578E-03	1.006E-03	3.870E-04
8	(0.000E+00)	3.462E-04	9.254E-04	1.472E-03	1.843E-03	1.968E-03	1.832E-03	1.456E-03	9.109E-04	3.392E-04
7	(0.000E+00)	2.314E-04	6.252E-04	9.986E-04	1.251E-03	1.333E-03	1.233E-03	9.686E-04	5.945E-04	2.141E-04
6	(0.000E+00)	8.773E-05	2.306E-04	3.608E-04	4.442E-04	4.657E-04	4.226E-04	3.237E-04	1.913E-04	6.460E-05
5	(0.000E+00)	-6.661E-05	-1.957E-04	-3.288E-04	-4.264E-04	-4.667E-04	-4.423E-04	-3.573E-04	-2.273E-04	-8.626E-05
4	(0.000E+00)	-2.197E-04	-6.064E-04	-9.818E-04	-1.241E-03	-1.333E-03	-1.242E-03	-9.854E-04	-6.136E-04	-2.262E-04
3	(0.000E+00)	-3.486E-04	-9.305E-04	-1.477E-03	-1.845E-03	-1.966E-03	-1.826E-03	-1.449E-03	-9.048E-04	-3.366E-04
2	(0.000E+00)	-3.998E-04	-1.032E-03	-1.605E-03	-1.979E-03	-2.097E-03	-1.947E-03	-1.553E-03	-9.800E-04	-3.719E-04
1	(0.000E+00)	-2.596E-04	-6.530E-04	-9.913E-04	-1.203E-03	-1.265E-03	-1.178E-03	-9.481E-04	-6.068E-04	-2.319E-04

j i-->	10
10	(0.000E+00)
9	(0.000E+00)
8	(0.000E+00)
7	(0.000E+00)
6	(0.000E+00)
5	(0.000E+00)
4	(0.000E+00)
3	(0.000E+00)
2	(0.000E+00)
1	(0.000E+00)

*** y-Component of Velocity (m/s) ** v1 ** k Plane 1 ** Time step 63 ** Time 3.15000E+01 s **

j i-->	1	2	3	4	5	6	7	8	9	10
10	(0.000E+00)	(0.000E+00)	(0.000E+00)	(0.000E+00)	(0.000E+00)	(0.000E+00)	(0.000E+00)	(0.000E+00)	(0.000E+00)	(0.000E+00)
9	2.444E-04	3.876E-04	3.455E-04	2.246E-04	7.745E-05	-7.370E-05	-2.175E-04	-3.360E-04	-3.823E-04	-2.479E-04
8	6.303E-04	1.012E-03	9.252E-04	6.149E-04	2.152E-04	-2.043E-04	-5.978E-04	-9.042E-04	-9.990E-04	-6.343E-04
7	9.770E-04	1.593E-03	1.476E-03	9.900E-04	3.468E-04	-3.347E-04	-9.688E-04	-1.446E-03	-1.569E-03	-9.730E-04
6	1.209E-03	1.988E-03	1.851E-03	1.245E-03	4.328E-04	-4.309E-04	-1.229E-03	-1.817E-03	-1.948E-03	-1.187E-03
5	1.297E-03	2.131E-03	1.982E-03	1.329E-03	4.555E-04	-4.725E-04	-1.327E-03	-1.949E-03	-2.074E-03	-1.251E-03
4	1.230E-03	2.002E-03	1.848E-03	1.230E-03	4.138E-04	-4.494E-04	-1.243E-03	-1.819E-03	-1.933E-03	-1.165E-03
3	1.010E-03	1.613E-03	1.469E-03	9.674E-04	3.184E-04	-3.624E-04	-9.892E-04	-1.449E-03	-1.547E-03	-9.391E-04
2	6.605E-04	1.029E-03	9.185E-04	5.947E-04	1.909E-04	-2.279E-04	-6.162E-04	-9.085E-04	-9.801E-04	-6.029E-04
1	2.601E-04	3.949E-04	3.410E-04	2.148E-04	6.659E-05	-8.430E-05	-2.264E-04	-3.391E-04	-3.738E-04	-2.316E-04
0	(0.000E+00)	(0.000E+00)	(0.000E+00)	(0.000E+00)	(0.000E+00)	(0.000E+00)	(0.000E+00)	(0.000E+00)	(0.000E+00)	(0.000E+00)

*** Temperature (Celsius) ** t1 ** k Plane 1 ** Time step 63 ** Time 3.15000E+01 s **

j i-->	0	1	2	3	4	5	6	7	8	9
11		(2.951E+01)	(2.852E+01)	(2.755E+01)	(2.658E+01)	(2.560E+01)	(2.461E+01)	(2.361E+01)	(2.259E+01)	(2.156E+01)
10	(3.000E+01)	2.951E+01	2.852E+01	2.755E+01	2.658E+01	2.560E+01	2.461E+01	2.361E+01	2.259E+01	2.156E+01
9	(3.000E+01)	2.950E+01	2.852E+01	2.754E+01	2.657E+01	2.559E+01	2.460E+01	2.360E+01	2.259E+01	2.156E+01
8	(3.000E+01)	2.950E+01	2.850E+01	2.751E+01	2.653E+01	2.555E+01	2.456E+01	2.357E+01	2.256E+01	2.154E+01
7	(3.000E+01)	2.949E+01	2.847E+01	2.747E+01	2.648E+01	2.549E+01	2.450E+01	2.351E+01	2.252E+01	2.151E+01
6	(3.000E+01)	2.948E+01	2.844E+01	2.742E+01	2.641E+01	2.541E+01	2.442E+01	2.344E+01	2.246E+01	2.148E+01
5	(3.000E+01)	2.947E+01	2.841E+01	2.736E+01	2.633E+01	2.533E+01	2.434E+01	2.337E+01	2.240E+01	2.144E+01
4	(3.000E+01)	2.945E+01	2.837E+01	2.730E+01	2.626E+01	2.525E+01	2.426E+01	2.330E+01	2.235E+01	2.141E+01
3	(3.000E+01)	2.944E+01	2.834E+01	2.726E+01	2.621E+01	2.519E+01	2.420E+01	2.325E+01	2.231E+01	2.139E+01
2	(3.000E+01)	2.944E+01	2.832E+01	2.723E+01	2.618E+01	2.515E+01	2.417E+01	2.322E+01	2.229E+01	2.137E+01
1	(3.000E+01)	2.944E+01	2.832E+01	2.723E+01	2.617E+01	2.515E+01	2.416E+01	2.321E+01	2.228E+01	2.137E+01
0		(2.944E+01)	(2.832E+01)	(2.723E+01)	(2.617E+01)	(2.515E+01)	(2.416E+01)	(2.321E+01)	(2.228E+01)	(2.137E+01)

j i-->	10	11
11	(2.052E+01)	
10	2.052E+01	(2.000E+01)
9	2.052E+01	(2.000E+01)
8	2.051E+01	(2.000E+01)
7	2.050E+01	(2.000E+01)
6	2.049E+01	(2.000E+01)
5	2.048E+01	(2.000E+01)
4	2.047E+01	(2.000E+01)
3	2.046E+01	(2.000E+01)
2	2.046E+01	(2.000E+01)
1	2.045E+01	(2.000E+01)
0	(2.045E+01)	

****

Table 10.12. Input data for natural convection in x-z coordinate system

```
-----------------------------------------------------------------
 INPUT DATA FOR NATURAL CONVECTION IN THE x-z COORDINATE SYSTEM

                          <boxz.data>
natureal convection of air in a square pipe with Rayleigh number of
        Ra = 1.00e+3, Th = 30.0, Tc = 20.0, L = 1.0498
-----------------------------------------------------------------
 &geom
  iturke=0,
  isolvr=1,  nnzero=1920, nspace=11042,
  ifres=1, ify=0,
  nl1=880,  nm1=400, nsurf=7,
  imax=10, jmax=1, kmax=10,
  dx=10*5.249e-4,  dy=1.0,  dz=10*5.249e-4,
  xnorml=  1.0, -1.0,  0.0,  0.0,  0.0,  0.0,  0.0,
  ynorml=  0.0,  0.0,  1.0, -1.0,  0.0,  0.0,  0.0,
  znorml=  0.0,  0.0,  0.0,  0.0,  1.0, -1.0, -1.0,
 &end
reg -1.0         1   1   1   1   1  10   1    +x surface
reg -1.0        10  10   1   1   1  10   2    -x surface
reg -1.0         1  10   1   1   1  10   3    +y surface
reg -1.0         1  10   1   1   1  10   4    -y surface
reg -1.0         1  10   1   1   1   1   5    +z surface
reg -1.0         1   9   1   1  10  10   6    -z surface
reg -1.0        10  10   1   1  10  10   7    -z surface
 &data
  alpha=1.0, eps3=5.0e-5, omega=1.3, omegav=1.0, omegae=1.0,
  itibug=1, iskew=0, nthcon=-1, ifener=1,
  idtime=0, dt=0.5,
  ntmax=500, it=1, trest=7200.0,
  gravz=-9.8,
  temp0=25.0, pres0=1.0e5,
  kflow=    0,    0,   -3,    -3,    0,   0,  0,
  kpres=    6*0,      1,  pres(7)=1.0e5,
  ktemp=    1,  1,  400,  400,  400,  400, 400,
  temp= 30.0,  20.0,
  veloc=  7*0.0,
  matype=1, mattab=1, tablot=20.0, tabhit=40.0,
  c0ro= 1.273738, c1ro=-3.588e-3,
  c0h=  0.0,  c1h=1005.7,
  c0k=  0.02624,
  c0mu= 1.846e-5,
  ntprnt=-9999,
  istpr=12001,32001,42001,52001,82001,
  nthpr=12001,32001,42001,52001,82001,
 &end
ul    0.001       1  10   1   1   1  10
wl    0.001       1  10   1   1   1  10
tl    25.00       1  10   1   1   1  10
```

Table 10.13. Output for boxz.data presented in Table 10.12

*** X-Component of Velocity (m/s) ** ul ** j Plane 1 ** Time step 63 ** Time 3.15000E+01 s **

k i-->	0	1	2	3	4	5	6	7	8	9
10	(0.000E+00)	2.440E-04	6.303E-04	9.734E-04	1.195E-03	1.269E-03	1.191E-03	9.704E-04	6.319E-04	2.483E-04
9	(0.000E+00)	3.854E-04	1.008E-03	1.584E-03	1.969E-03	2.100E-03	1.964E-03	1.578E-03	1.006E-03	3.870E-04
8	(0.000E+00)	3.462E-04	9.254E-04	1.472E-03	1.843E-03	1.968E-03	1.832E-03	1.456E-03	9.109E-04	3.392E-04
7	(0.000E+00)	2.314E-04	6.252E-04	9.986E-04	1.251E-03	1.333E-03	1.233E-03	9.686E-04	5.945E-04	2.141E-04
6	(0.000E+00)	8.773E-05	2.306E-04	3.608E-04	4.442E-04	4.657E-04	4.226E-04	3.237E-04	1.913E-04	6.460E-05
5	(0.000E+00)	-6.661E-05	-1.957E-04	-3.288E-04	-4.264E-04	-4.667E-04	-4.423E-04	-3.573E-04	-2.273E-04	-8.626E-05
4	(0.000E+00)	-2.197E-04	-6.064E-04	-9.818E-04	-1.241E-03	-1.333E-03	-1.242E-03	-9.854E-04	-6.136E-04	-2.262E-04
3	(0.000E+00)	-3.486E-04	-9.305E-04	-1.477E-03	-1.845E-03	-1.966E-03	-1.826E-03	-1.449E-03	-9.048E-04	-3.366E-04
2	(0.000E+00)	-3.998E-04	-1.032E-03	-1.605E-03	-1.979E-03	-2.097E-03	-1.947E-03	-1.553E-03	-9.800E-04	-3.719E-04
1	(0.000E+00)	-2.596E-04	-6.530E-04	-9.913E-04	-1.203E-03	-1.265E-03	-1.178E-03	-9.481E-04	-6.068E-04	-2.319E-04

k i-->	10
10	(0.000E+00)
9	(0.000E+00)
8	(0.000E+00)
7	(0.000E+00)
6	(0.000E+00)
5	(0.000E+00)
4	(0.000E+00)
3	(0.000E+00)
2	(0.000E+00)
1	(0.000E+00)

*** Z-Component of Velocity (m/s) ** wl ** j Plane 1 ** Time step 63 ** Time 3.15000E+01 s **

k i-->	1	2	3	4	5	6	7	8	9	10
10	(0.000E+00)	(0.000E+00)	(0.000E+00)	(0.000E+00)	(0.000E+00)	(0.000E+00)	(0.000E+00)	(0.000E+00)	(0.000E+00)	(0.000E+00)
9	2.444E-04	3.876E-04	3.455E-04	2.246E-04	7.745E-05	-7.370E-05	-2.175E-04	-3.360E-04	-3.823E-04	-2.479E-04
8	6.303E-04	1.012E-03	9.252E-04	6.149E-04	2.152E-04	-2.043E-04	-5.978E-04	-9.042E-04	-9.990E-04	-6.343E-04
7	9.770E-04	1.593E-03	1.476E-03	9.900E-04	3.468E-04	-3.347E-04	-9.688E-04	-1.446E-03	-1.569E-03	-9.730E-04
6	1.209E-03	1.988E-03	1.851E-03	1.245E-03	4.328E-04	-4.309E-04	-1.229E-03	-1.817E-03	-1.948E-03	-1.187E-03
5	1.297E-03	2.131E-03	1.982E-03	1.329E-03	4.555E-04	-4.725E-04	-1.327E-03	-1.949E-03	-2.074E-03	-1.251E-03
4	1.230E-03	2.002E-03	1.848E-03	1.230E-03	4.138E-04	-4.494E-04	-1.243E-03	-1.819E-03	-1.933E-03	-1.165E-03
3	1.010E-03	1.613E-03	1.469E-03	9.674E-04	3.184E-04	-3.624E-04	-9.892E-04	-1.449E-03	-1.547E-03	-9.391E-04
2	6.605E-04	1.029E-03	9.185E-04	5.947E-04	1.909E-04	-2.279E-04	-6.162E-04	-9.085E-04	-9.801E-04	-6.029E-04
1	2.601E-04	3.949E-04	3.410E-04	2.148E-04	6.659E-05	-8.430E-05	-2.264E-04	-3.391E-04	-3.738E-04	-2.316E-04
0	(0.000E+00)	(0.000E+00)	(0.000E+00)	(0.000E+00)	(0.000E+00)	(0.000E+00)	(0.000E+00)	(0.000E+00)	(0.000E+00)	(0.000E+00)

*** Temperature (Celsius) ** tl ** j Plane 1 ** Time step 63 ** Time 3.15000E+01 s **

k i-->	0	1	2	3	4	5	6	7	8	9
11		(2.951E+01)	(2.852E+01)	(2.755E+01)	(2.658E+01)	(2.560E+01)	(2.461E+01)	(2.361E+01)	(2.259E+01)	(2.156E+01)
10	(3.000E+01)	2.951E+01	2.852E+01	2.755E+01	2.658E+01	2.560E+01	2.461E+01	2.361E+01	2.259E+01	2.156E+01
9	(3.000E+01)	2.950E+01	2.852E+01	2.754E+01	2.657E+01	2.559E+01	2.460E+01	2.360E+01	2.259E+01	2.156E+01
8	(3.000E+01)	2.950E+01	2.850E+01	2.751E+01	2.653E+01	2.555E+01	2.456E+01	2.357E+01	2.256E+01	2.154E+01
7	(3.000E+01)	2.949E+01	2.847E+01	2.747E+01	2.648E+01	2.549E+01	2.450E+01	2.351E+01	2.252E+01	2.151E+01
6	(3.000E+01)	2.948E+01	2.844E+01	2.742E+01	2.641E+01	2.541E+01	2.442E+01	2.344E+01	2.246E+01	2.148E+01
5	(3.000E+01)	2.947E+01	2.841E+01	2.736E+01	2.633E+01	2.533E+01	2.434E+01	2.337E+01	2.240E+01	2.144E+01
4	(3.000E+01)	2.945E+01	2.837E+01	2.730E+01	2.626E+01	2.525E+01	2.426E+01	2.330E+01	2.235E+01	2.141E+01
3	(3.000E+01)	2.944E+01	2.834E+01	2.726E+01	2.621E+01	2.519E+01	2.420E+01	2.325E+01	2.231E+01	2.139E+01
2	(3.000E+01)	2.944E+01	2.832E+01	2.723E+01	2.618E+01	2.515E+01	2.417E+01	2.322E+01	2.229E+01	2.137E+01
1	(3.000E+01)	2.944E+01	2.832E+01	2.723E+01	2.617E+01	2.515E+01	2.416E+01	2.321E+01	2.228E+01	2.137E+01
0		(2.944E+01)	(2.832E+01)	(2.723E+01)	(2.617E+01)	(2.515E+01)	(2.416E+01)	(2.321E+01)	(2.228E+01)	(2.137E+01)

k i-->	10	11
11	(2.052E+01)	
10	2.052E+01	(2.000E+01)
9	2.052E+01	(2.000E+01)
8	2.051E+01	(2.000E+01)
7	2.050E+01	(2.000E+01)
6	2.049E+01	(2.000E+01)
5	2.048E+01	(2.000E+01)
4	2.047E+01	(2.000E+01)
3	2.046E+01	(2.000E+01)
2	2.046E+01	(2.000E+01)
1	2.045E+01	(2.000E+01)
0	(2.045E+01)	

Table 10.14. Comparison of α = 1.0 and α = 0.5 for zwangz.data presented in Table 10.5

Case 1 alpha=1.0 zwangz.data iter=88

*** Z-Component of Velocity (m/s) ** wl ** j Plane 1

k	i--> 1	2	3	4	5	6
8	(8.925E-03)	(1.064E-02)	(1.043E-02)	(1.043E-02)	(1.064E-02)	(8.925E-03)
7	8.925E-03	1.064E-02	1.043E-02	1.043E-02	1.064E-02	8.925E-03
6	9.086E-03	1.056E-02	1.035E-02	1.035E-02	1.056E-02	9.086E-03
5	9.252E-03	1.047E-02	1.028E-02	1.028E-02	1.047E-02	9.252E-03
4	9.421E-03	1.038E-02	1.020E-02	1.020E-02	1.038E-02	9.421E-03
3	9.589E-03	1.028E-02	1.013E-02	1.013E-02	1.028E-02	9.589E-03
2	9.751E-03	1.018E-02	1.007E-02	1.007E-02	1.018E-02	9.751E-03
1	9.893E-03	1.008E-02	1.003E-02	1.003E-02	1.008E-02	9.893E-03
0	(1.000E-02)	(1.000E-02)	(1.000E-02)	(1.000E-02)	(1.000E-02)	(1.000E-02)

Case 2 alpha=0.5 zwangz.data iter=70

*** Z-Component of Velocity (m/s) ** wl ** j Plane 1

k	i--> 1	2	3	4	5	6
8	(8.925E-03)	(1.064E-02)	(1.043E-02)	(1.043E-02)	(1.064E-02)	(8.925E-03)
7	8.925E-03	1.064E-02	1.043E-02	1.043E-02	1.064E-02	8.925E-03
6	9.086E-03	1.056E-02	1.035E-02	1.035E-02	1.056E-02	9.086E-03
5	9.252E-03	1.047E-02	1.028E-02	1.028E-02	1.047E-02	9.252E-03
4	9.421E-03	1.038E-02	1.020E-02	1.020E-02	1.038E-02	9.421E-03
3	9.589E-03	1.028E-02	1.013E-02	1.013E-02	1.028E-02	9.589E-03
2	9.751E-03	1.018E-02	1.007E-02	1.007E-02	1.018E-02	9.751E-03
1	9.893E-03	1.008E-02	1.003E-02	1.003E-02	1.008E-02	9.893E-03
0	(1.000E-02)	(1.000E-02)	(1.000E-02)	(1.000E-02)	(1.000E-02)	(1.000E-02)

Case 1: $v_x = 0.1$ m/s, $v_y = 0.1$ m/s, and velocity skewness $v_y/v_x = 1$. Figure 10.5 shows the velocity field for Case 1. Figures 10.6–10.8 show the isotherms for Case 1, obtained by using the first-order upwind scheme, optimized FMSUD scheme, and QUICK scheme, respectively.

Case 2: $v_x = 0.126$ m/s, $v_y = 0.0632$ m/s, and velocity skewness $v_y/v_x = 0.5$. Figure 10.9 shows the velocity field for Case 2. Figures 10.10–10.12 show the isotherms for Case 2, obtained by using the original FMSUD scheme, optimized FMSUD scheme, and QUICK scheme, respectively.

In Case 1, original and optimized FMSUD gave exact solutions.

In Case 2, QUICK scheme shows the best solutions among the above schemes.

Optimized FMSUD scheme shows better solutions than the original FMSUD scheme.

10.5 Von Karmann Vortex Shedding

We performed a Von Karmann vortex shedding analysis by using the LECUSSO scheme and compared the results with experimental data of Davis et al.[32] This is a test problem of momentum transport. Figure 10.13 shows the configuration of the experiment by Davis et al.[32] and the computational modeling. Table 10.15 shows the input data for the Von Karmann vortex shedding analysis.

Case 1

Computational conditions

Fluid: Air,
Square obstacle: length $D = 0.2$ m,
Flow channel: confined channel
channel width $H = 4 \times D = 0.8$ m,
Inlet velocity distribution: measurement with maximum velocity $U_0 = 0.0422$ m/s,
and $Re = U_0 \times D/\nu = 0.0422 \times 0.2/1.536E{-5} = 550$ (at 20°C).

Computational results

Fig. 10.14: Velocity vector plot.
Fig. 10.15: Experimentally determined and predicted flow fields.
Fig. 10.16 Experimentally determined and predicted streak lines.
Fig. 10.17: Enlarged view of computed streakline.
Fig. 10.18: Time variation of fluctuating axial velocity in the wake region.
Fig. 10.19: Predicted and experimentally determined Strouhal numbers.

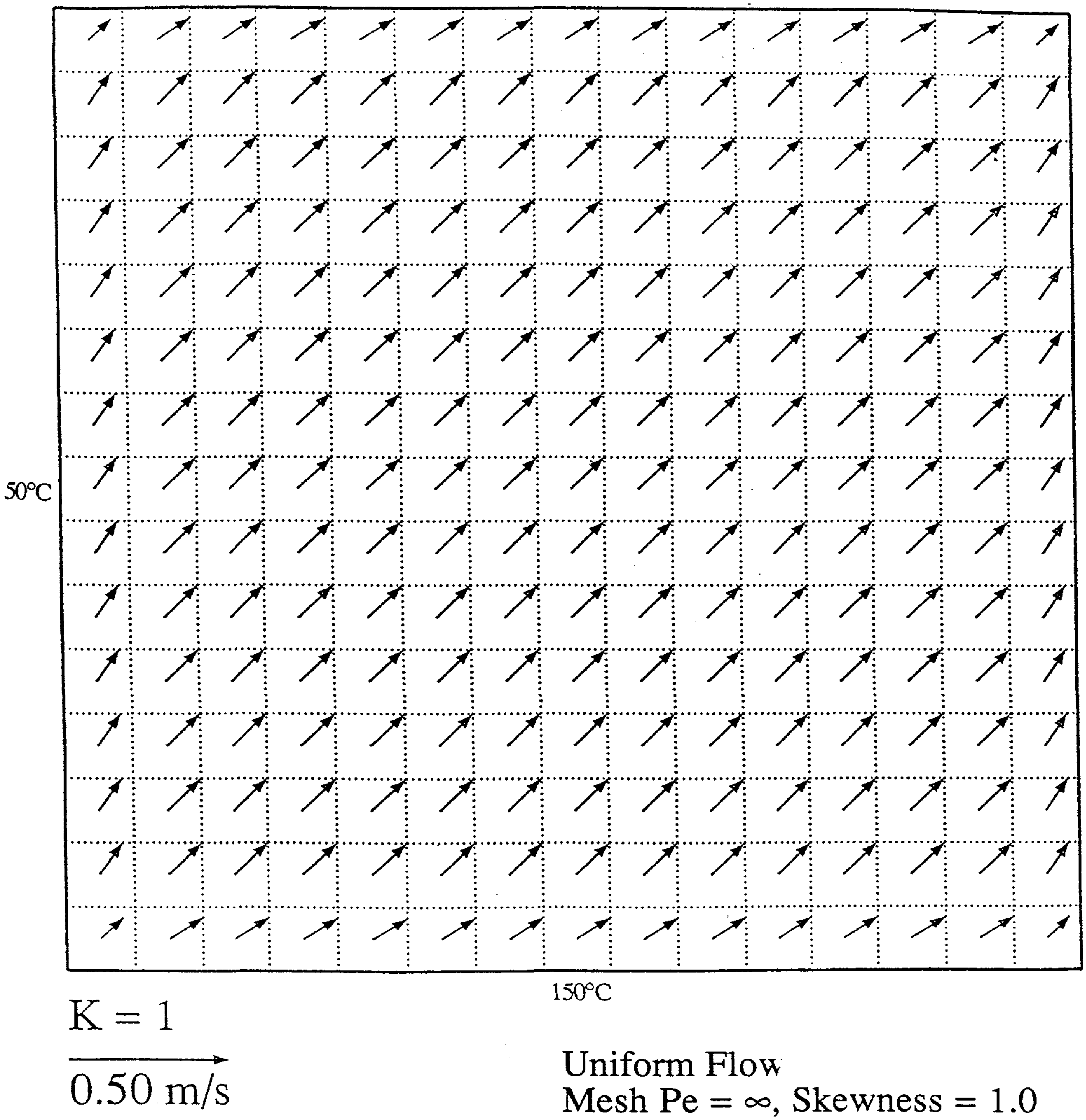

Fig. 10.5. Velocity field for scalar transport (Case 1: $v_y/v_x = 1$)

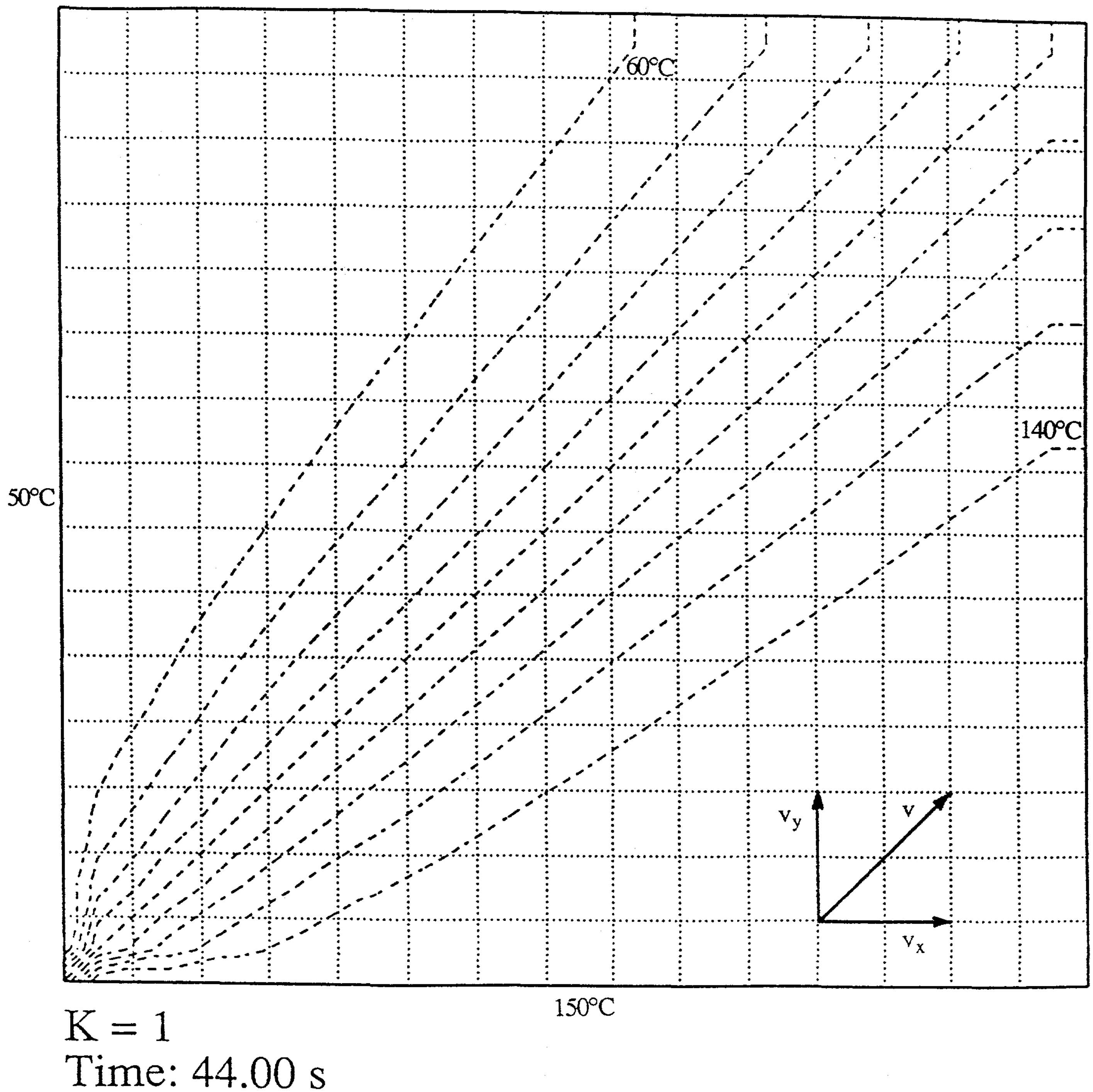

Fig. 10.6. Isotherms obtained by first-order upwind scheme (Case 1: $v_y/v_x = 1$)

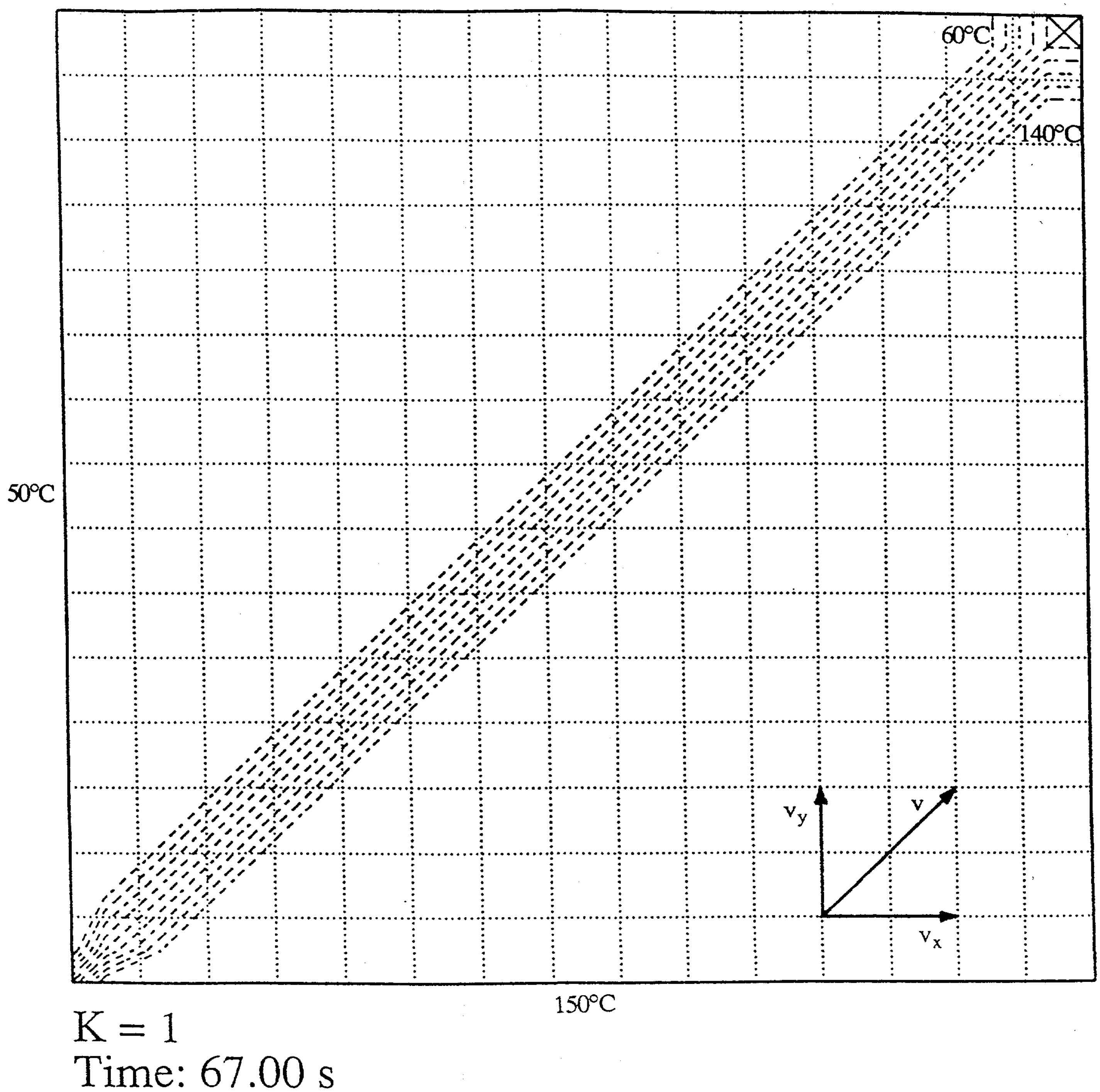

Fig. 10.7. Isotherms obtained by optimized and original FMSUD (Case 1: v_y/v_x = 1)

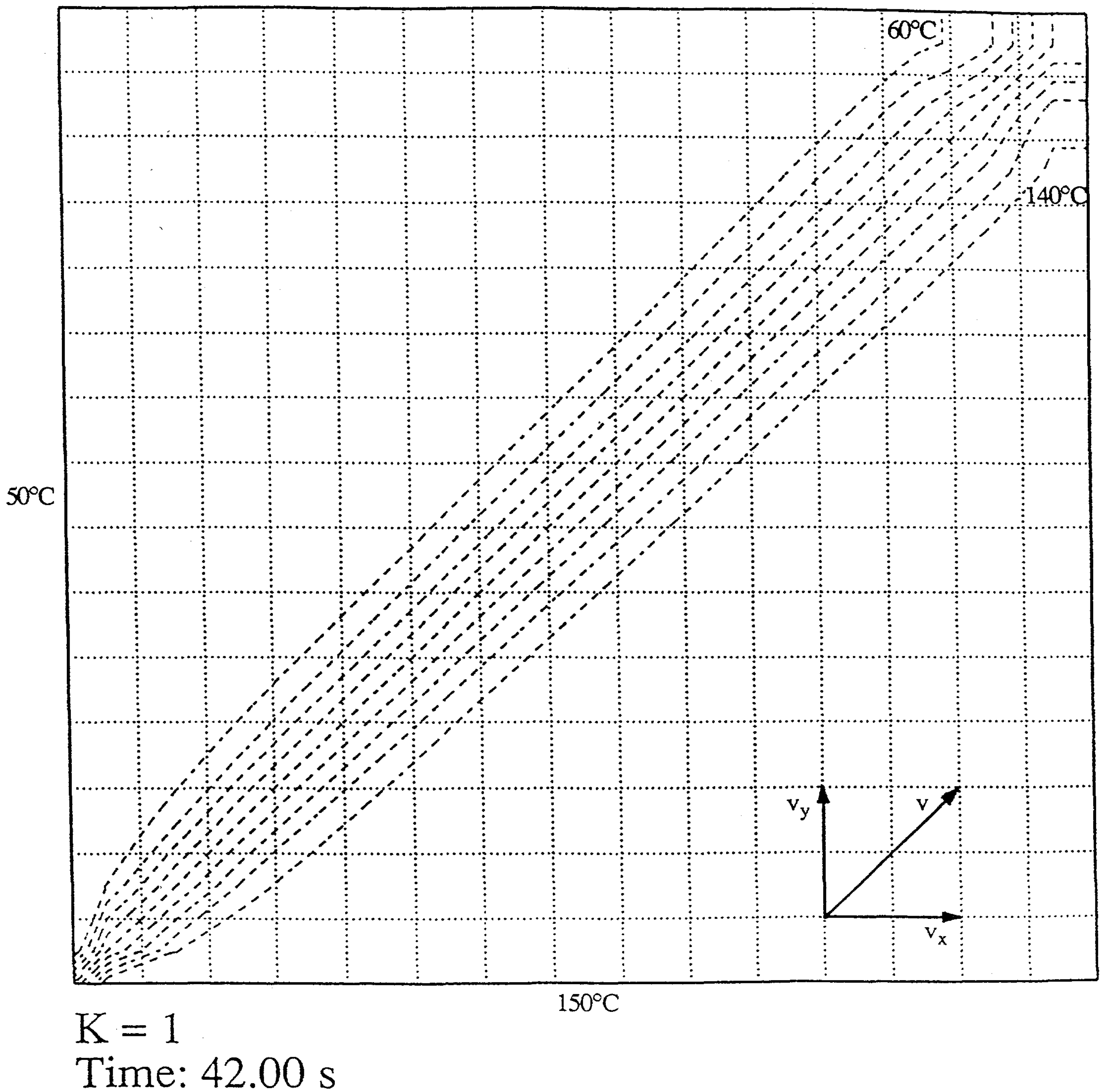

Fig. 10.8. Isotherms obtained by QUICK (Case 1: v_y/v_x = 1)

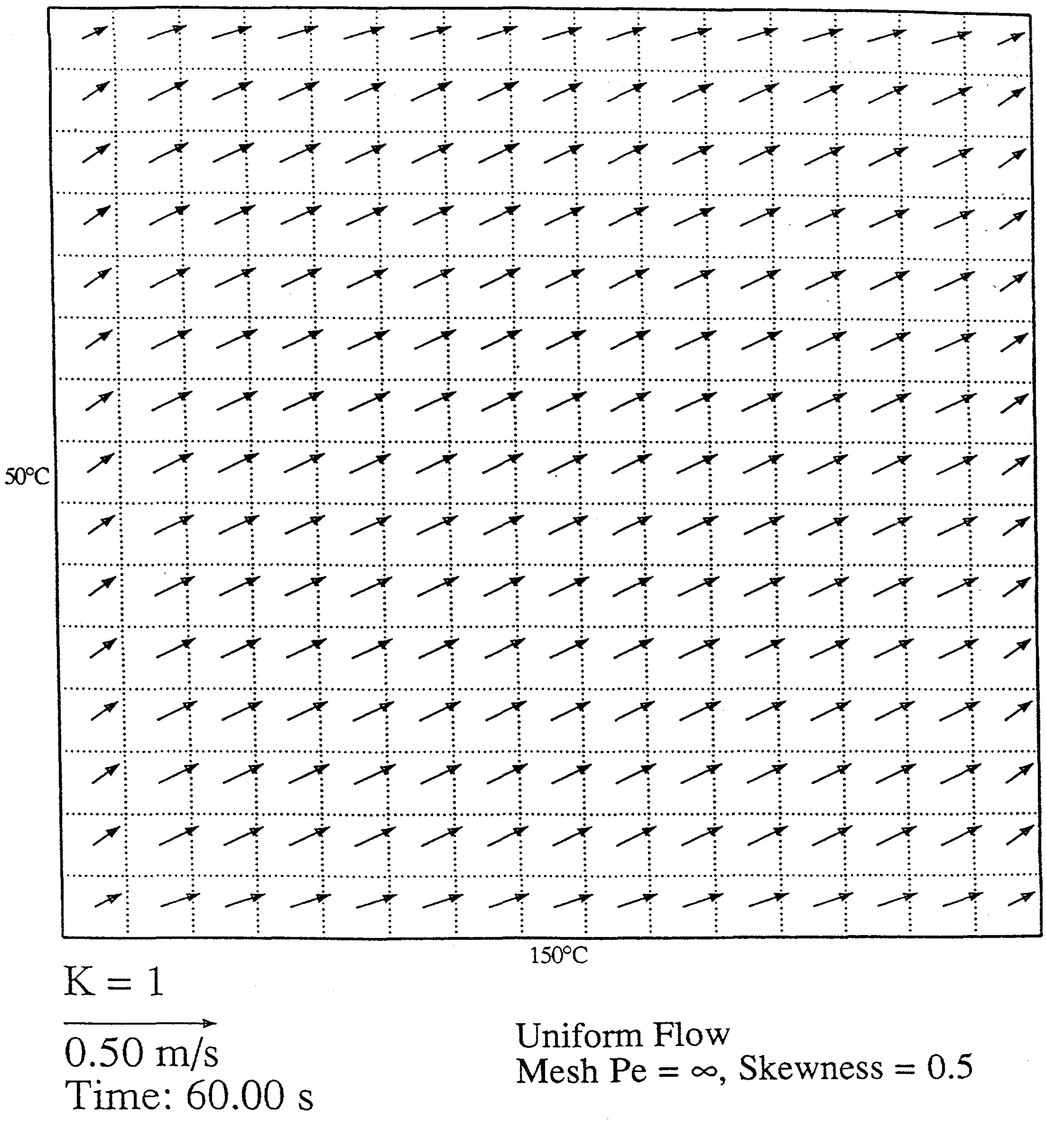

Fig. 10.9. Velocity field for scalar transport (Case 2: $v_y/v_x = 0.5$)

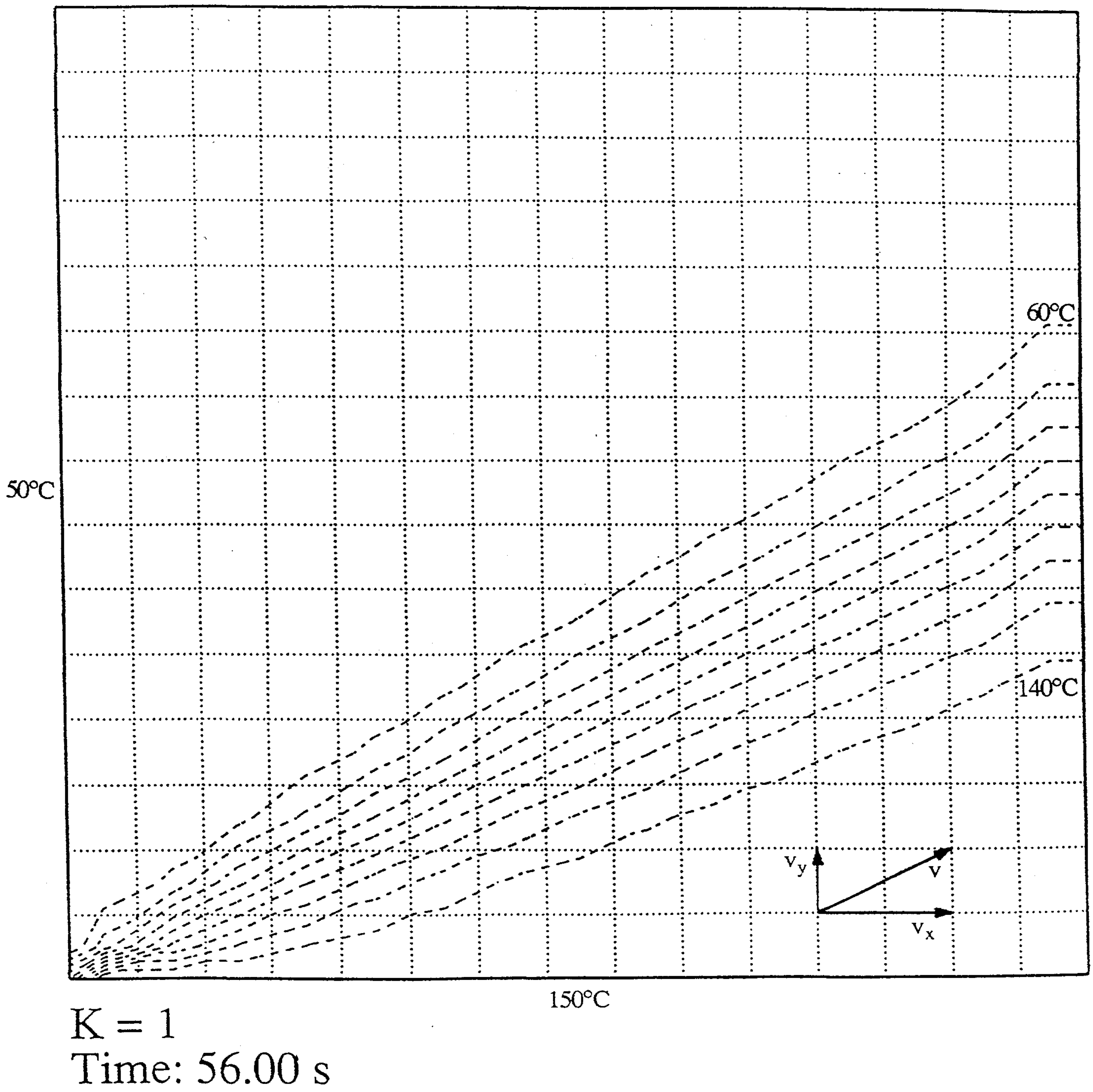

Fig. 10.10. Isotherms obtained by original FMSUD (Case 2: v_y/v_x = 0.5)

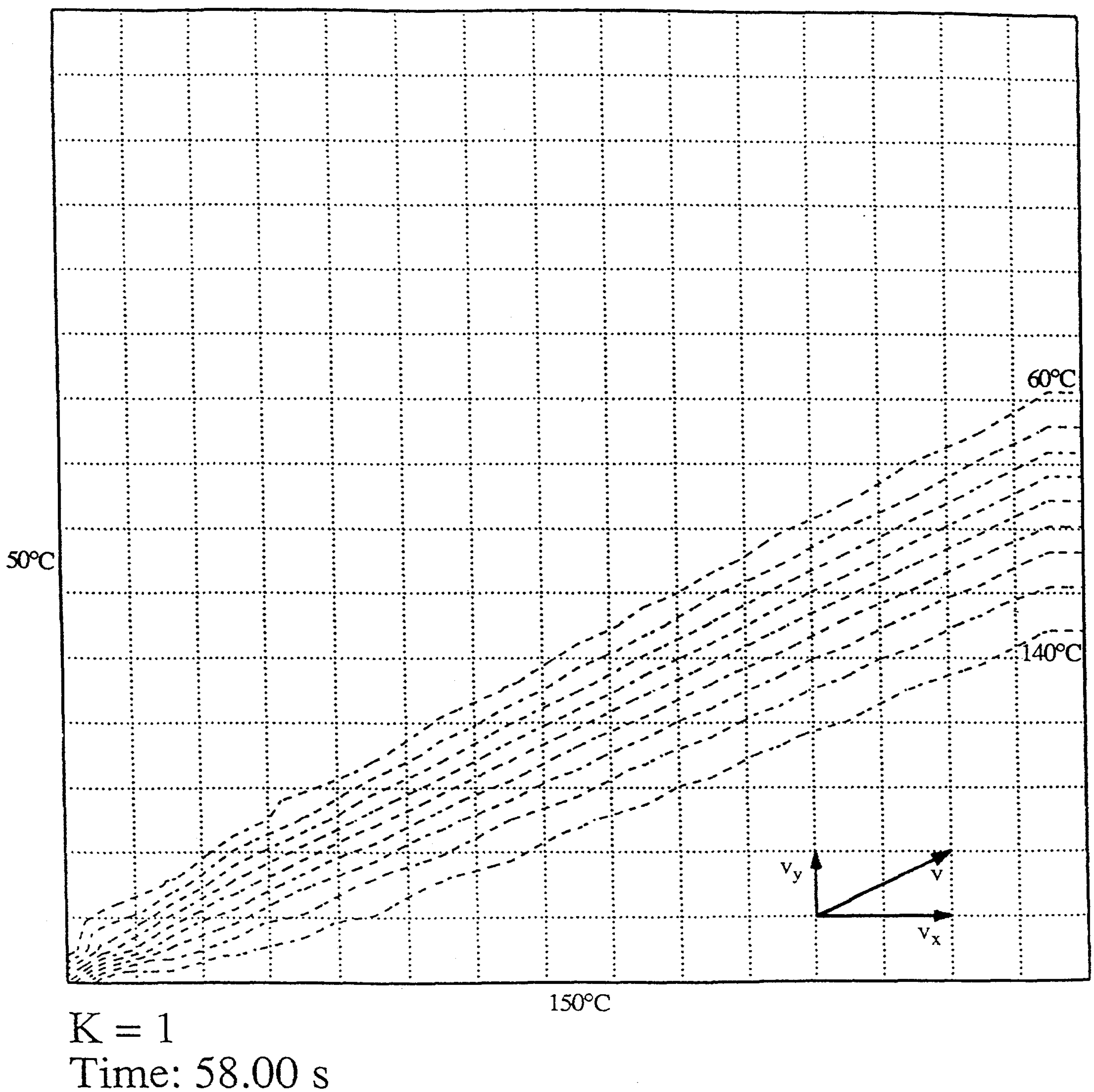

Fig. 10.11. Isotherms obtained by optimized FMSUD (Case 2: v_y/v_x = 0.5)

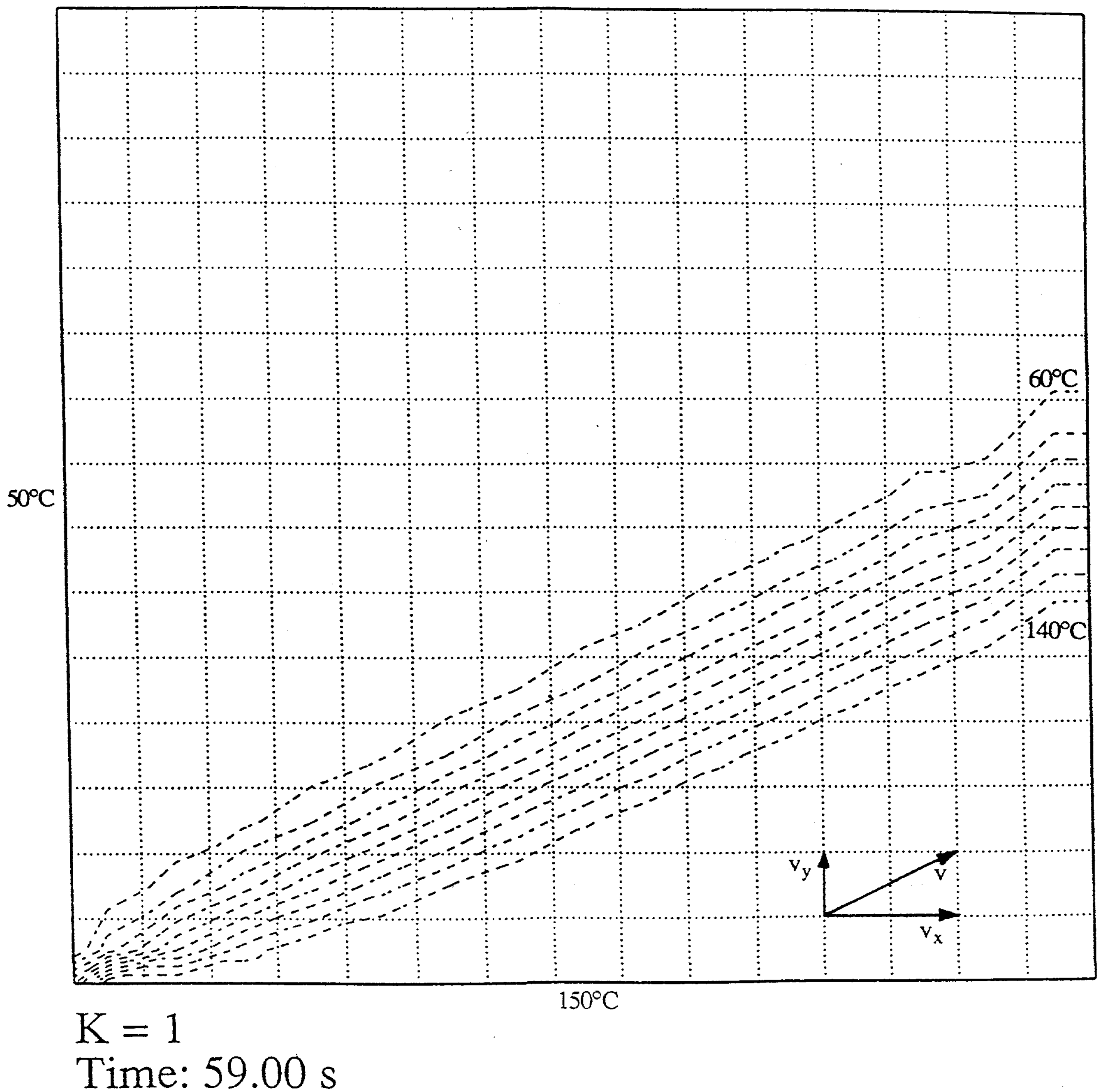

Fig. 10.12. Isotherms obtained by QUICK (Case 2: $v_y/v_x = 0.5$)

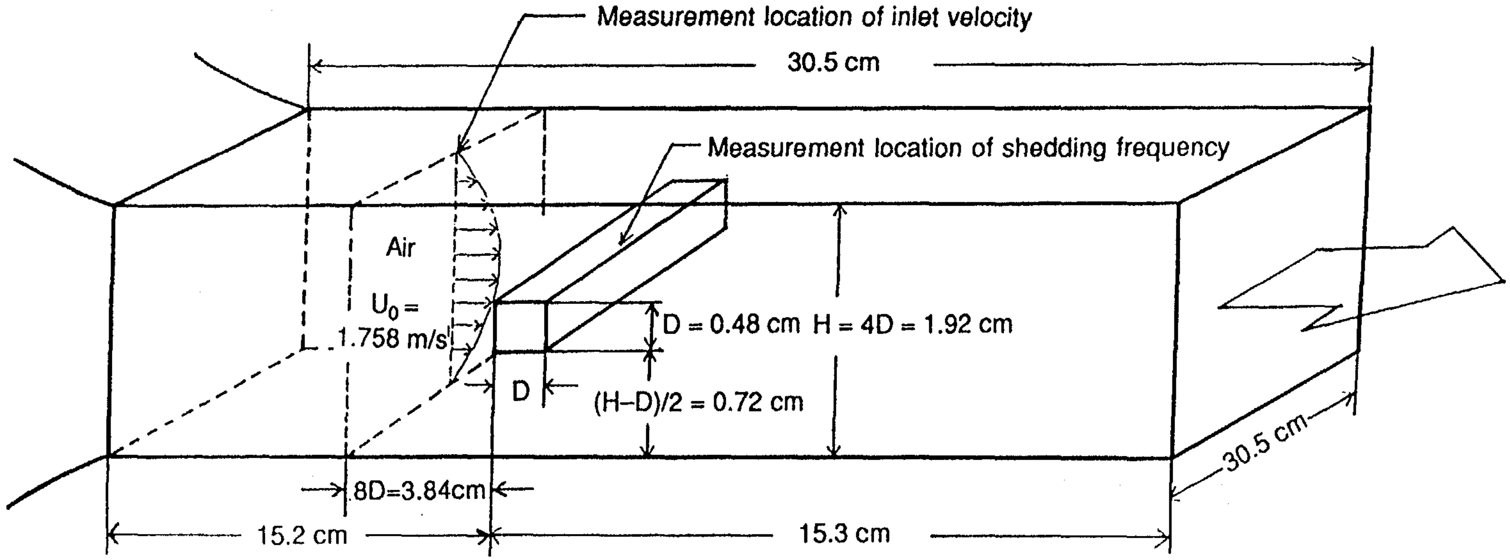

(a) Configuration of experiment (NBS Low Velocity Airflow Facility)
$Re = U_0D/\nu = 550$ (at 20°C)

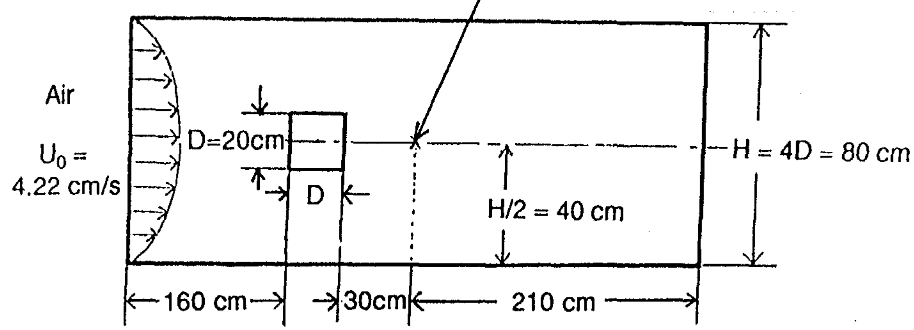

(b) 2–D model of computation
$Re = U_0D/\nu = 550$ (at 20°C)

Fig. 10.13. Configuration of experimental facility and computational modeling for Von Karmann vortex shedding analysis

Table 10.15. Input data for Von Karmann vortex shedding analysis

```
---------------------------------------------------------------------
  Sample Input Data for Von Karmann Vortex Shedding Analysis
  square channel with a square obstacle, H=0.8m, D=0.2m, H/D=4
  76x40 meshes, air, Re=500, erf inlet velocity, u0=3.7931cm/s

                        <vortxzd4.data>
---------------------------------------------------------------------
&geom
 isolvr=1,nnzero=14428, nspace=110938,
 ifres=1, ify=0,
 nl1=6152,  nml=2940,
 imax=76, jmax=1, kmax=40, nsurf=11,
 dx= 5*0.2, 4*0.1, 6*0.05, 0.03, 18*0.02,
     0.03, 6*0.05, 25*0.1, 9*0.2, 0.2,
 dy=0.1,
 dz= 39*0.02, 0.02,
 xnorml=1.0,-1.0, 0.0, 0.0, 0.0, 0.0,-1.0, 1.0, 0.0, 0.0,-1.0,
 ynorml=0.0, 0.0, 0.0, 0.0, 1.0,-1.0, 0.0, 0.0, 0.0, 0.0, 0.0,
 znorml=0.0, 0.0, 1.0,-1.0, 0.0, 0.0, 0.0, 0.0,-1.0, 1.0, 0.0,
&end
reg -1.0        1   1   1   1   1  40   1    +x surface inlet
reg -1.0       76  76   1   1   1  39   2    -x surface exit
reg -1.0        1  76   1   1   1   1   3    +z surface
reg -1.0        1  76   1   1  40  40   4    -z surface
reg -1.0        1  20   1   1   1  40   5    +y surface
reg -1.0       21  30   1   1   1  15   5
reg -1.0       21  30   1   1  26  40   5
reg -1.0       31  76   1   1   1  40   5
reg -1.0        1  20   1   1   1  40   6    -y surface
reg -1.0       21  30   1   1   1  15   6
reg -1.0       21  30   1   1  26  40   6
reg -1.0       31  76   1   1   1  40   6
reg -1.0       20  20   1   1  16  25   7    -x obstacle
reg -1.0       31  31   1   1  16  25   8    +x
reg -1.0       21  30   1   1  15  15   9    -z
reg -1.0       21  30   1   1  26  26  10    +z
reg -1.0       76  76   1   1  40  40  11    -x exit press.
&data
 alpha=1.0, itibug=0, iskew=0,
 idtime=0, dt=0.00001, it=1,
 nthcon=-1, ifener=0, eps3=1.0e-6, omegav=1.0,
 ntmax=1,  ntprnt=-9999, trest=720000.0,
 temp0=20.0, pres0=1.0e5,
 kflow=    1,  -5,  2*0,  -3,  -3,  4*0,  -5,
 ktemp=    1,  9*400, 400,
 kpres(11)=1,    pres(11)=1.0e5,
 temp=  20.0, 9*20.0, 20.0,
 veloc= 0.037931,  9*0.0, 0.0,
 matype=1,
 c0k = 0.0241,    c1k = 7.6e-5,
 c0h = 2.74e+5,   c1h = 1003.5,
 c0ro= 0.0,       c1ro= 0.0,     c2ro=0.0034843,
 c0mu= 1.71e-5,   c1mu= 4.7e-8,
 wtmol = 28.97,
&end
```

Table 10.15. Input data for Von Karmann vortex shedding analysis (Contd.)

velb	0.003747	1	1	1	1	1	1	1
velb	0.011015	1	1	1	1	2	2	1
velb	0.017645	1	1	1	1	3	3	1
velb	0.023333	1	1	1	1	4	4	1
velb	0.027921	1	1	1	1	5	5	1
velb	0.031403	1	1	1	1	6	6	1
velb	0.033889	1	1	1	1	7	7	1
velb	0.035556	1	1	1	1	8	8	1
velb	0.036610	1	1	1	1	9	9	1
velb	0.037235	1	1	1	1	10	10	1
velb	0.037584	1	1	1	1	11	11	1
velb	0.037764	1	1	1	1	12	12	1
velb	0.037857	1	1	1	1	13	13	1
velb	0.037898	1	1	1	1	14	14	1
velb	0.037917	1	1	1	1	15	15	1
velb	0.037926	1	1	1	1	16	16	1
velb	0.037929	1	1	1	1	17	17	1
velb	0.037931	1	1	1	1	18	23	1
velb	0.037929	1	1	1	1	24	24	1
velb	0.037926	1	1	1	1	25	25	1
velb	0.037917	1	1	1	1	26	26	1
velb	0.037898	1	1	1	1	27	27	1
velb	0.037857	1	1	1	1	28	28	1
velb	0.037764	1	1	1	1	29	29	1
velb	0.037584	1	1	1	1	30	30	1
velb	0.037235	1	1	1	1	31	31	1
velb	0.036610	1	1	1	1	32	32	1
velb	0.035556	1	1	1	1	33	33	1
velb	0.033889	1	1	1	1	34	34	1
velb	0.031403	1	1	1	1	35	35	1
velb	0.027921	1	1	1	1	36	36	1
velb	0.023333	1	1	1	1	37	37	1
velb	0.017645	1	1	1	1	38	38	1
velb	0.011015	1	1	1	1	39	39	1
velb	0.003747	1	1	1	1	40	40	1

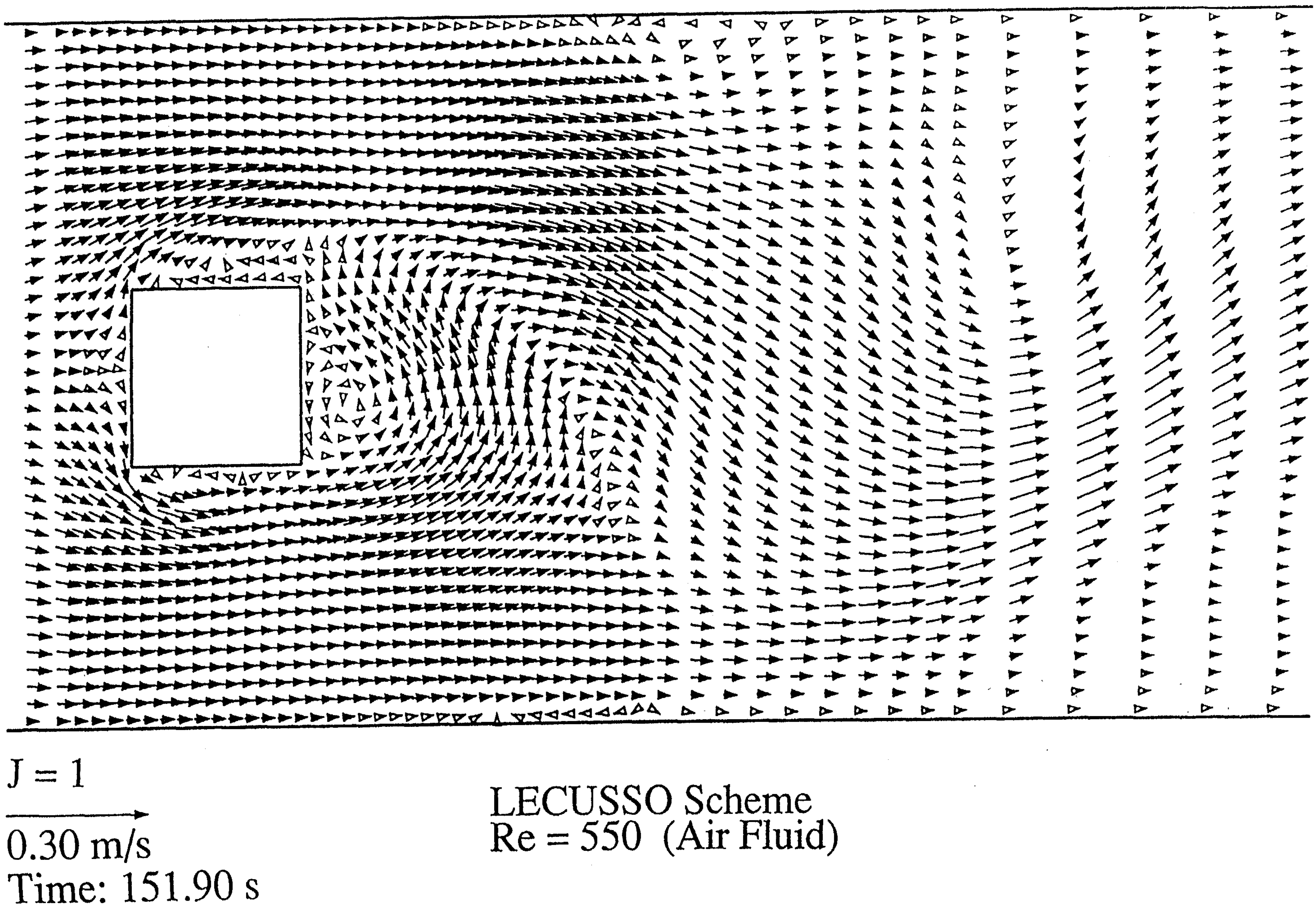

Fig. 10.14. Velocity vector plot from Von Karmann vortex shedding analysis

(a) Experiment (streakline)

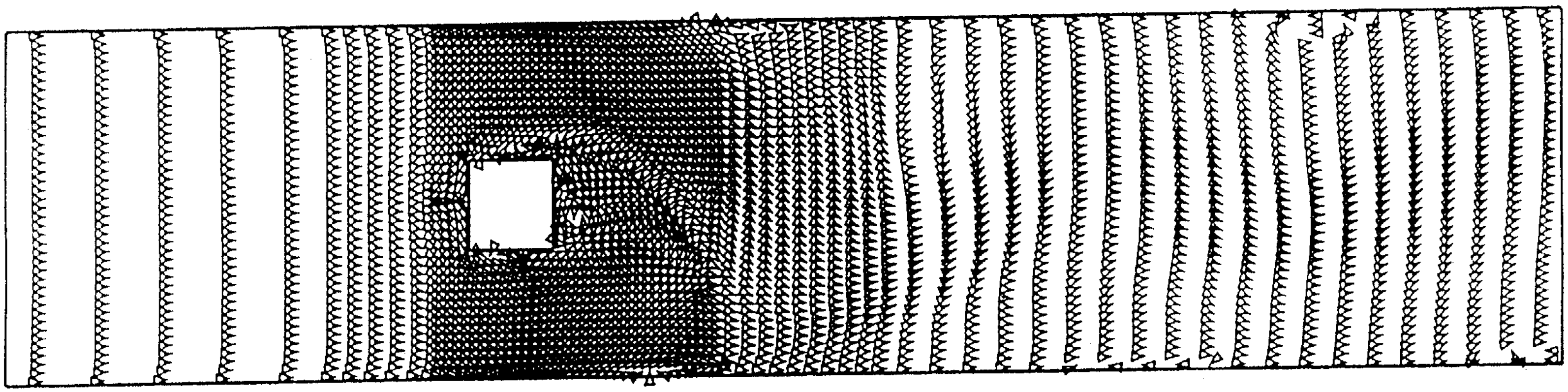

J = 1

1.00 m/s

Time: 151.90 s

(b) Prediction (velocity vector)

LECUSSO Scheme
Re = 550 (Air Fluid)

Fig. 10.15. Experimentally determined streakline and predicted velocity vector

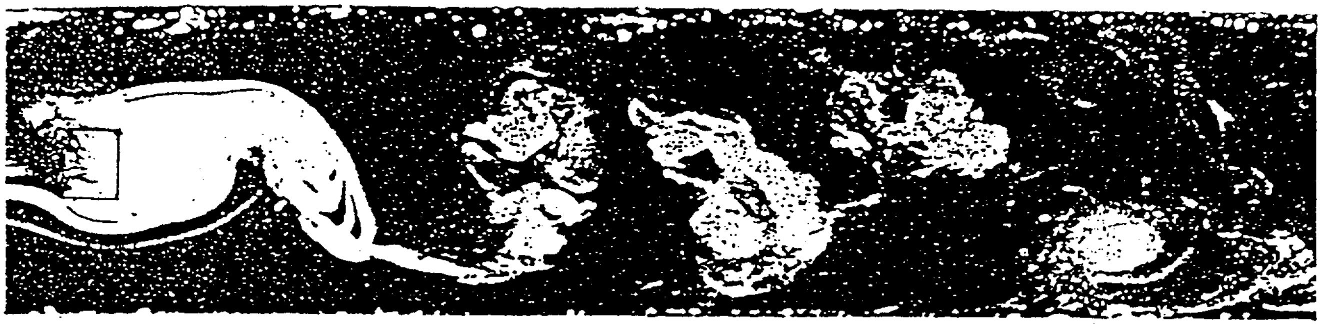

(a) Experiment

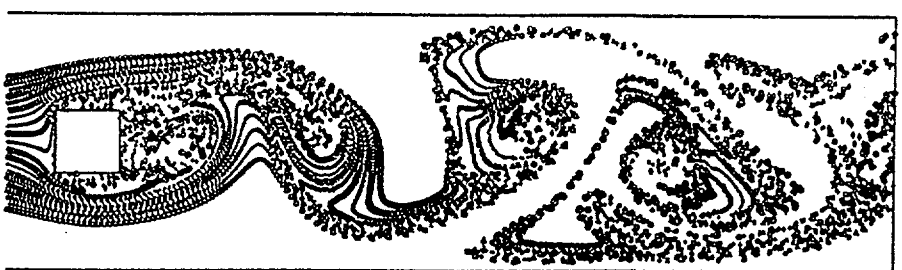

J = 1
Time: 125.00 s

LECUSSO Scheme
Re = 550 (Air Fluid)

(b) Prediction

Fig. 10.16. Experimentally determined and predicted streaklines from Von Karmann vortex shedding analysis

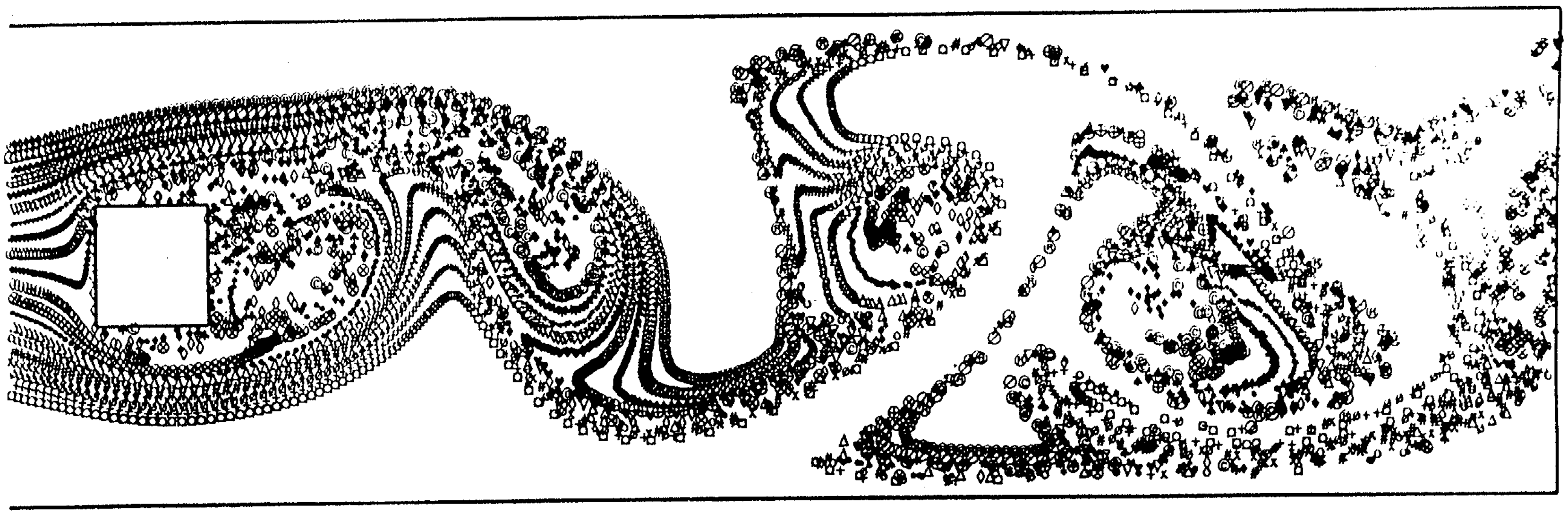

Fig. 10.17. Enlarged view of computed streaklines shown in Fig. 10.16

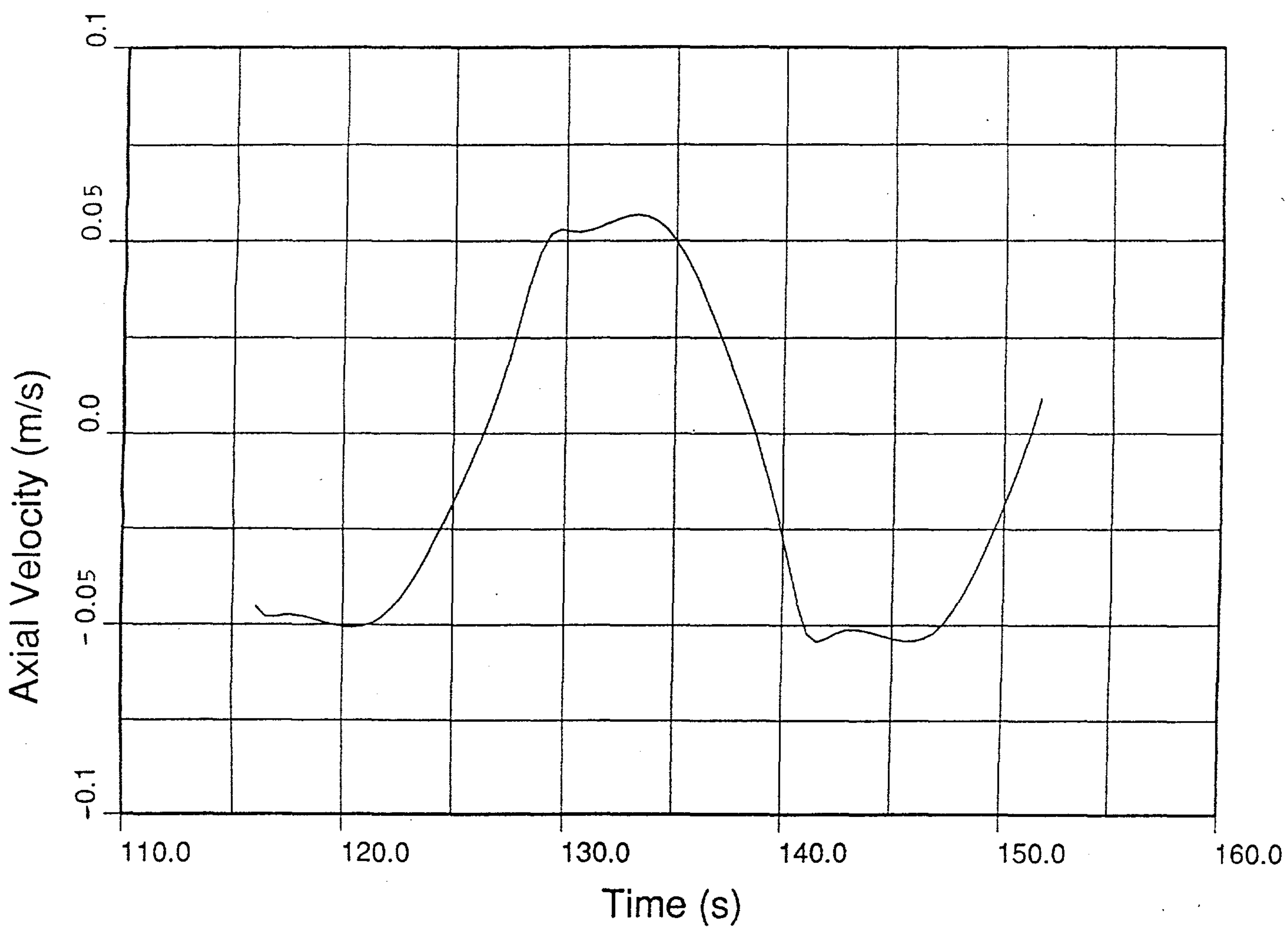

Fig. 10.18. Time variation of fluctuating axial velocity in the wake region at Re = 550 during Von Karmann vortex shedding analysis

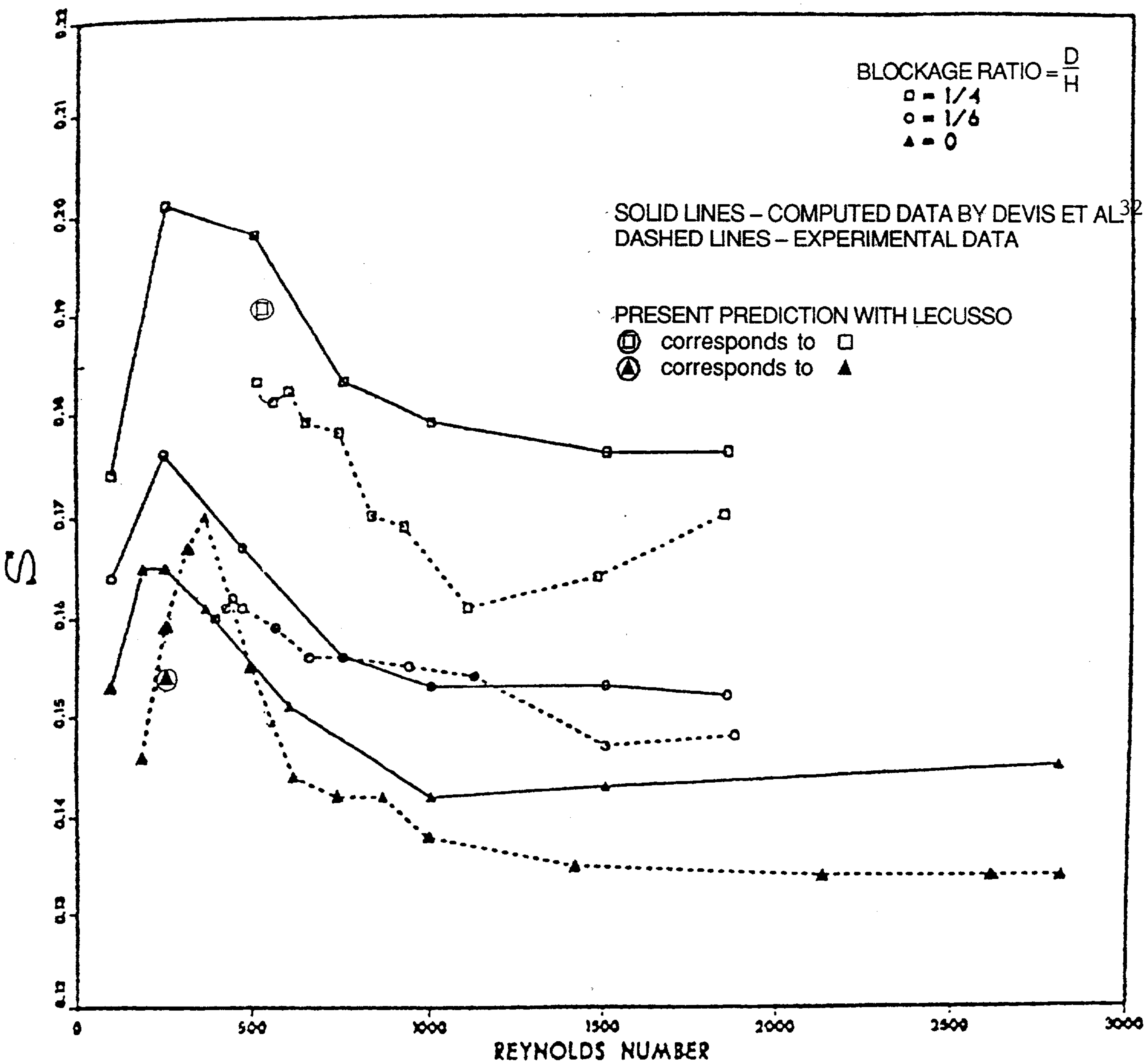

Fig. 10.19. Strouhal numbers experimentally determined and computed by Davis et al[32] *and predicted by current LECUSSO*

Prediction of Strouhal number S:
$S = f \times D/U_0 = 0.04032 \times 0.2/0.0422 = 0.191$
f = frequency = $1/T = 1/24.8 = 0.04032$.
T = period = (151.3 – 126.5) sec = 24.8 sec (from Fig. 10.18).
Measurement of Strouhal number S = 0.182 (from Fig. 10.19).

Case 2

Computational conditions

Fluid: Air,
Square obstacle: length D = 0.02 m,
Flow channel: open channel
channel width $H = 6 \times D = 0.12$ m,
Inlet velocity distribution: measurement with maximum velocity $U_0 = 0.0127$ m/s,
and $Re = U_0 \times D/\nu = 0.0127 \times 0.2/1.011E{-}6 = 251$ (at 20°C).

Computational results

Fig. 10.19: Predicted and experimentally determined Strouhal numbers.
Fig. 10.20: Time variation of fluctuating axial velocity in the wake region.

Prediction of Strouhal number S:
$S = f \times D/U_0 = 0.0980 \times 0.2/0.0127 = 0.154$
f = frequency = $1/T = 1/10.2 = 0.0980$.
T = period = (114.5 – 104.3) sec = 10.2 sec (from Fig. 10.20).
Measurement of Strouhal number S = 0.159 (from Fig. 10.19).

10.6 Shear-Driven Cavity Flow

Numerical calculations were performed for the two-dimensional shear-driven cavity flow by using the QUICK and LECUSSO schemes.

Two-dimensional shear-driven cavity flow represents an excellent test for evaluating convective differencing schemes because of the large streamline-to-grid skewness present over most of the flow region and the existence of several relatively large recirculation regions. The calculational results were compared with those of Ghia et al.,[33] who used grids that were quite fine, such as 257 x 257 mesh, and whose results can be considered almost exact solutions.

Figure 10.21 shows the computational region for a shear-driven cavity flow. Table 10.16 shows the input data for the above shear-driven cavity flow with 40 x 40 meshes.

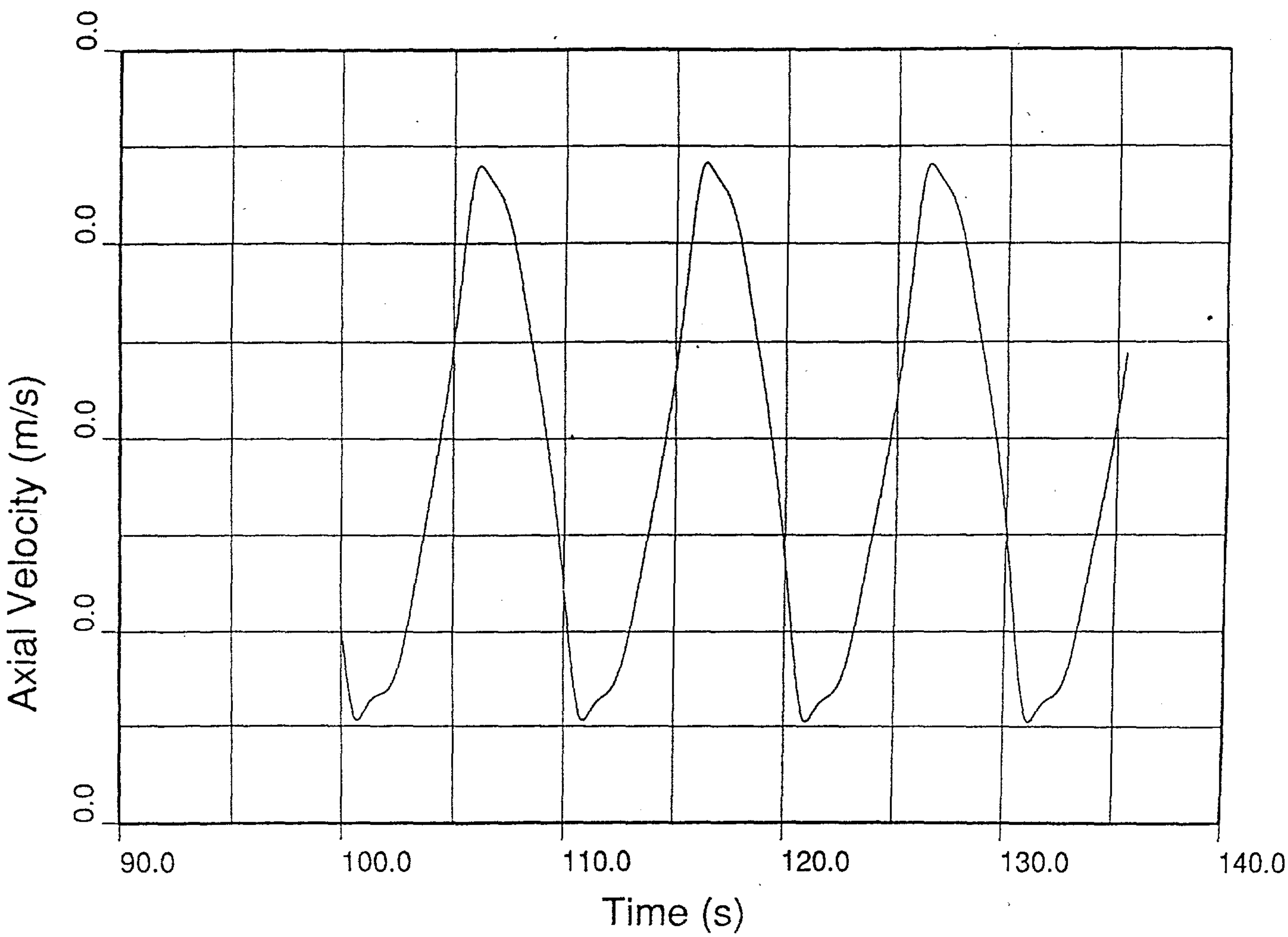

Fig. 10.20. Time variation of fluctuating axial velocity in the wake region at Re = 251 during Von Karmann vortex shedding analysis

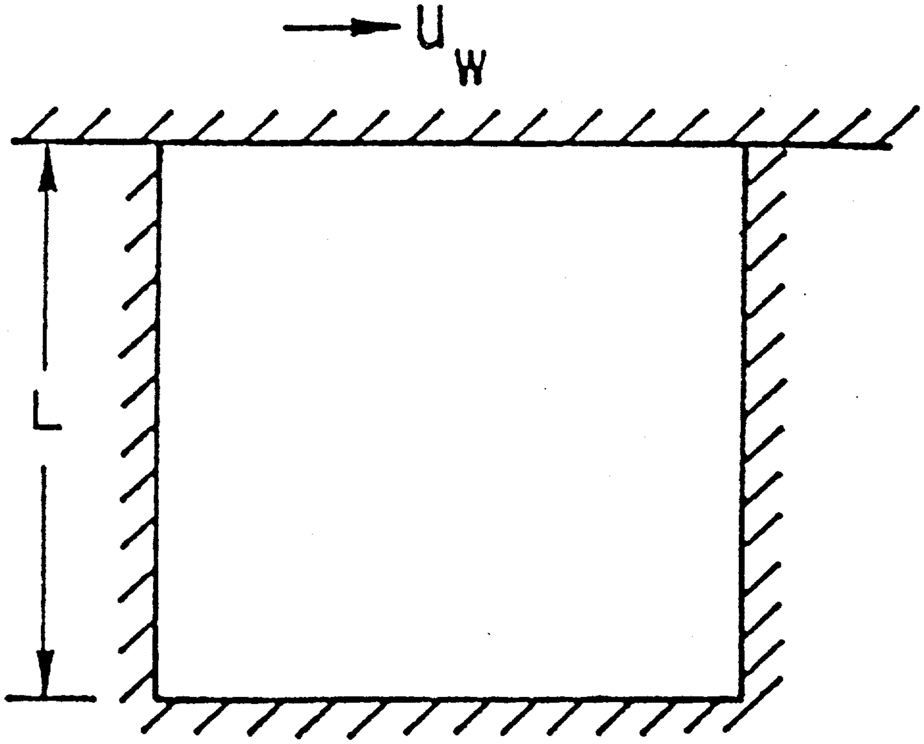

$$Re = \frac{\rho U_W L}{\mu}$$

Fig. 10.21. Computational region for shear-driven cavity flows

Table 10.16. Cavity flow analysis data under shear flow boundary conditions

```
-----------------------------------------------------------------------
    CAVITY FLOW ANALYSIS DATA WITH SHEAR FLOW BOUNDARY CONDITION
                           at Re = 5000

                           <cavity.data>
-----------------------------------------------------------------------
&geom
 ifres=1,
 nl1=4800, nml=1600, nsurf=7,
 ify=0,
 imax=40, jmax=1, kmax=40,
 isolvr=1, nnzero=7840, nspace=57428,
 xnorml= 1.0,-1.0, 0.0, 0.0, 0.0, 0.0, 0.0,
 ynorml= 0.0, 0.0, 1.0,-1.0, 0.0, 0.0, 0.0,
 znorml= 0.0, 0.0, 0.0, 0.0, 1.0,-1.0,-1.0,
 dx=40*12.5e-3,
 dy=12.5e-3,
 dz=40*12.5e-3,
 &end
reg -1.         1   1   1   1   1  40   1     left    +x
reg -1.        40  40   1   1   1  40   2     right   -x
reg -1.         1  40   1   1   1  40   3     front   +y
reg -1.         1  40   1   1   1  40   4     back    -y
reg -1.         1  40   1   1   1   1   5     bottom  +z
reg -1.         1  39   1   1  40  40   6     upper   -z (shear flow)
reg -1.        40  40   1   1  40  40   7     upper   -z (shear flow)
 &data
  alpha=1.0, eps3=1.e-6, omegav=1.0,
  iskew=0,  ifener=0, ifmom=1,
  idtime=0, dt=0.1,
  ntmax=50000,  it=1, trest=9999999.0,
  kpres(7)=1, pres(7)=1.0e05,
  kflow=    0,    0,   -3,   -3,    0,    0,    0,
  ktemp=    1,    1,    1,    1,    1,  400,  400,
  veloc=  0.0,  0.0,  0.0,  0.0,  0.0,  0.0,  0.0,
  temp=  20.0, 20.0, 20.0, 20.0, 20.0, 20.0, 20.0,
  temp0= 20.0, pres0=1.0e5,
  matype=1, mattab=1, tablot=20.0, tabhit=40.0,
  c0ro= 1000.,
  c0h=  0.0,     c1h=1005.7,
  c0k=  0.624,
  c0mu= 1.000e-3,
  ntprnt=-9999,
  nthpr= 12001, 32001, 17201,
  &end
ul  0.0000       1  40   1   1   1  40
wl  0.0000       1  40   1   1   1  40
tl  20.000       1  40   1   1   1  40
```

10.6.1 Calculational Results with 20 x 20 Meshes

Figures 10.22, 10.23, and 10.24 show the velocity vectors obtained at Re = 400, 1000, and 5000, respectively, with 20 x 20 computational cells.

Figures 10.25, 10.26, and 10.27 show the lateral component of velocity obtained from the present calculations and Ghia et al.'s calculations at Re = 400, 1000, and 5000, respectively.

In these calculations, $\varepsilon_3 = 10^{-6}$ was used for the convergence criterion of the velocities.

10.6.2 Calculational Results with 40 x 40 Meshes

Figures 10.28, 10.29, and 10.30 show the velocity vector obtained at Re = 400, 1000, and 5000, respectively, with 40 x 40 computational cells.

Figures 10.31, 10.32, and 10.33 show the results of Ghia et al.'s calculations and the present calculations with 40 x 40 meshes.

10.6.3 50 x 50 Meshes at Re = 10000

Figure 10.34 shows the velocity vector at Re = 10000. At this high Reynolds number, one may observe whether the schemes show.

a stable and converged steady-state solution and

a tertial vortex at the corner of the lower right-hand side.

In Fig. 10.34, a stable and converged solution was obtained with the LECUSSO scheme. Moreover, we can clearly see a tertial vortex at the lower right–hand side corner.

It is remarkable that the LECUSSO scheme gives quite a stale solution at Re = 10000.

Figure 10.35 shows the streamline pattern calculated by Ghia et al.[33]

By using the QUICK scheme, we could not obtain stable solutions at this high Reynolds number flow.

10.6.4 50 x 50 Meshes at Re = 30,000

Figures 10.36 and 10.37 show the velocity vectors at 6×10^4 and 6.17×10^4 s after the beginning of the calculations, respectively, for Re = 30000.

In this calculation, a convergence rate of velocity (ε_3) was $\approx 3 \times 10^{-5}$.

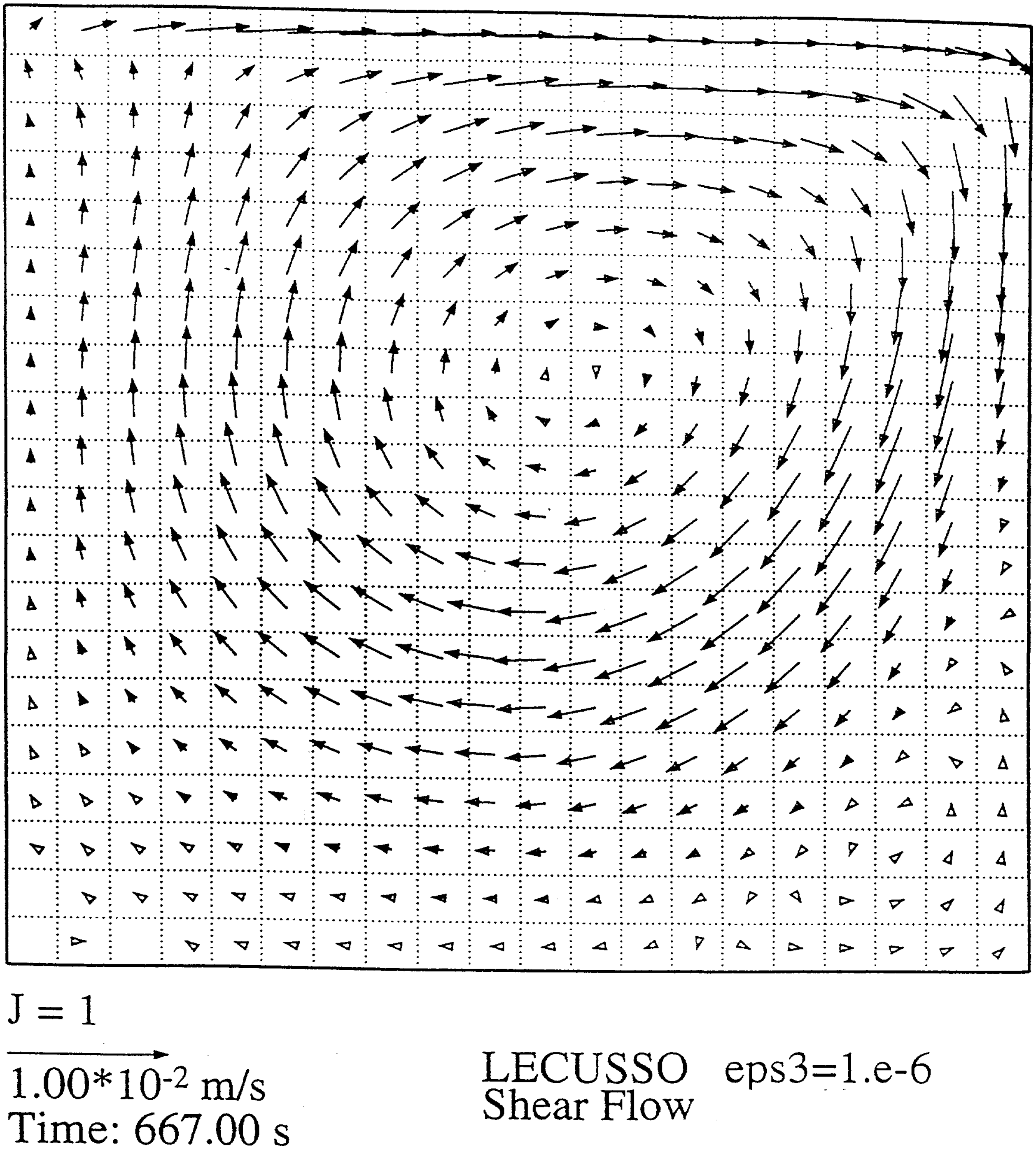

Fig. 10.22. Velocity vector at Re = 400 (20x20 meshes) for shear-driven cavity flow

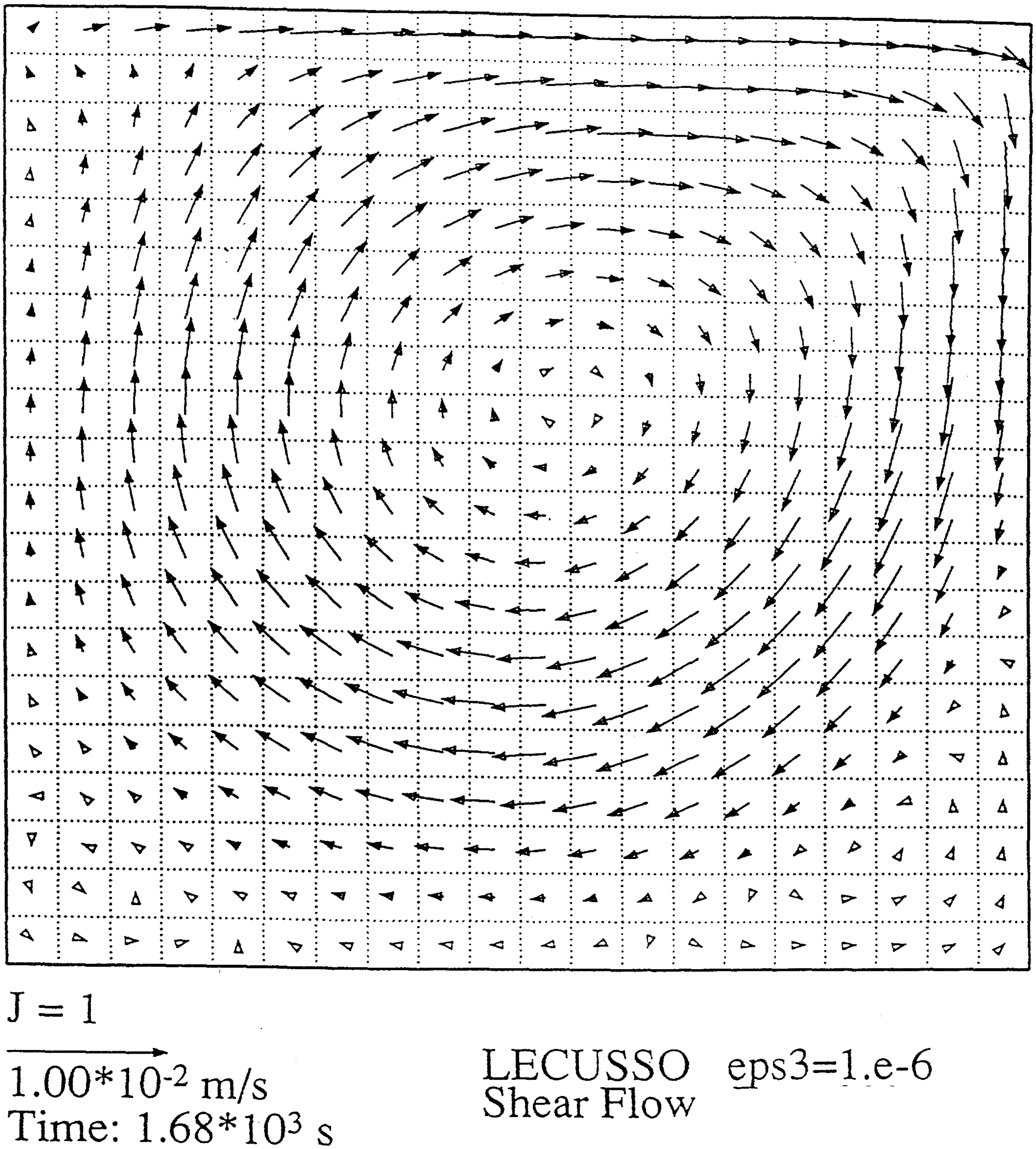

Fig. 10.23. Velocity vector at Re = 1000 (20x20 meshes) for shear-driven cavity flow

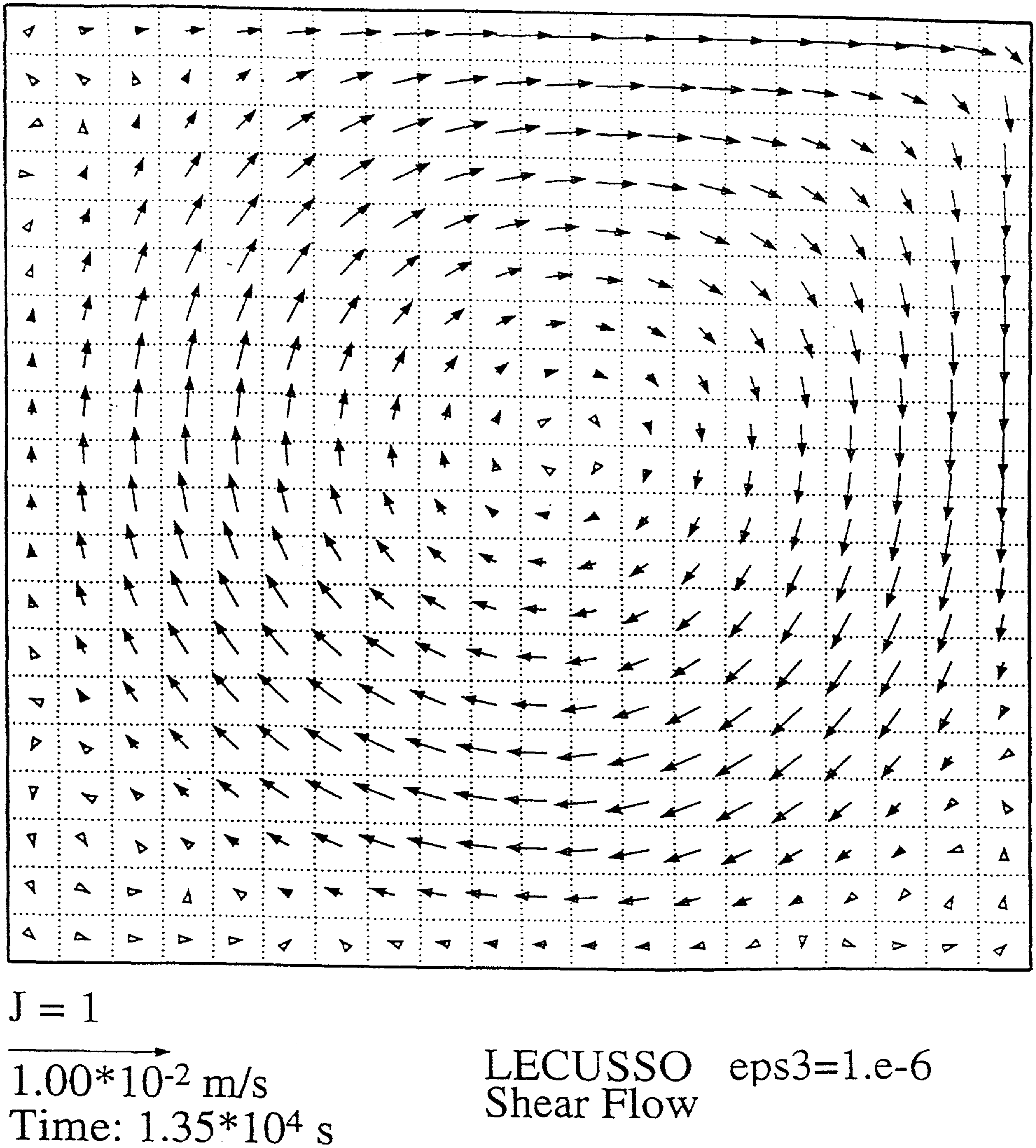

Fig. 10.24. Velocity vector at Re = 5000 (20x20 meshes) for shear-driven cavity flow

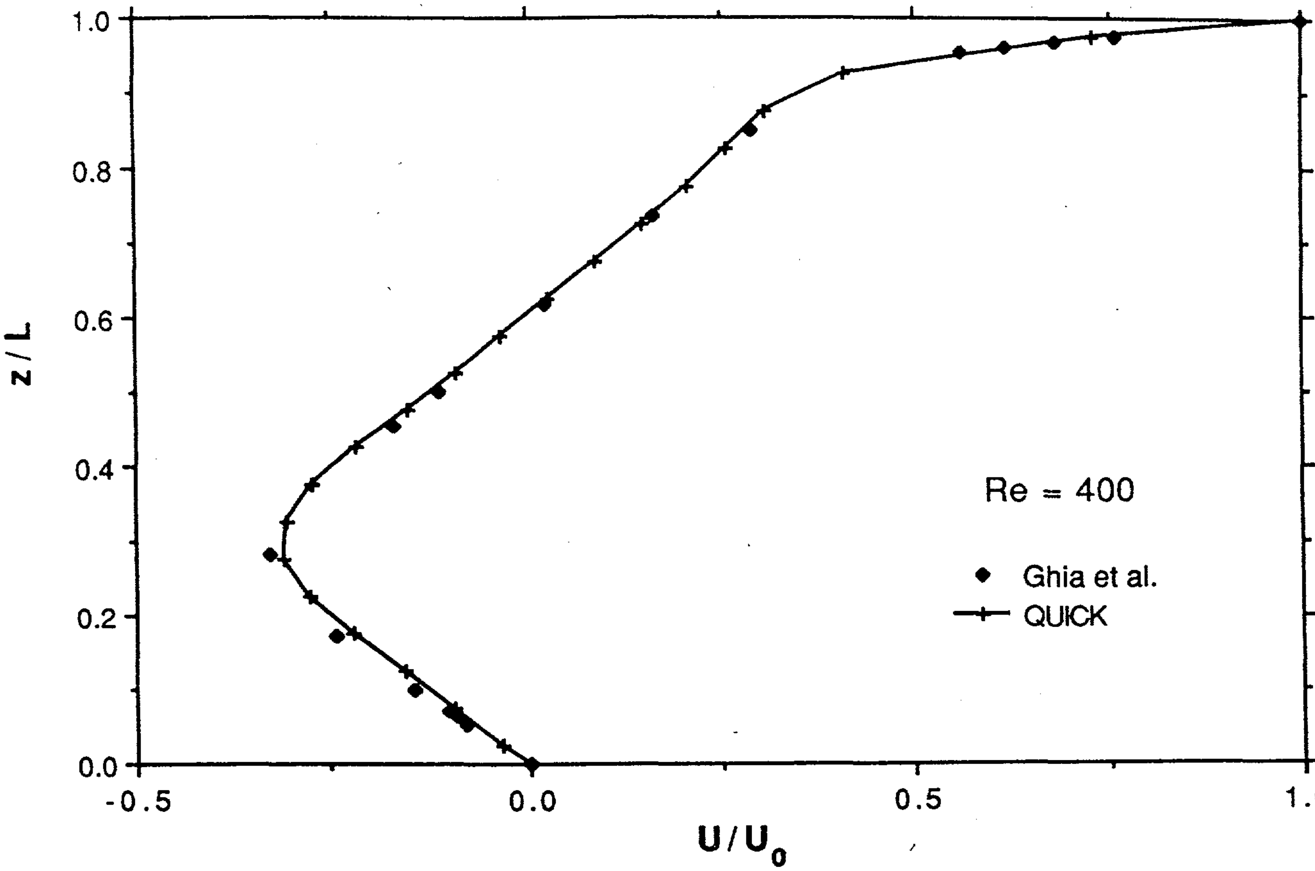

Fig. 10.25. Lateral component of velocity from the present calculations and from the calculations of Ghia et al.[33] *at Re = 400 (20x20 meshes) for shear-driven cavity flows*

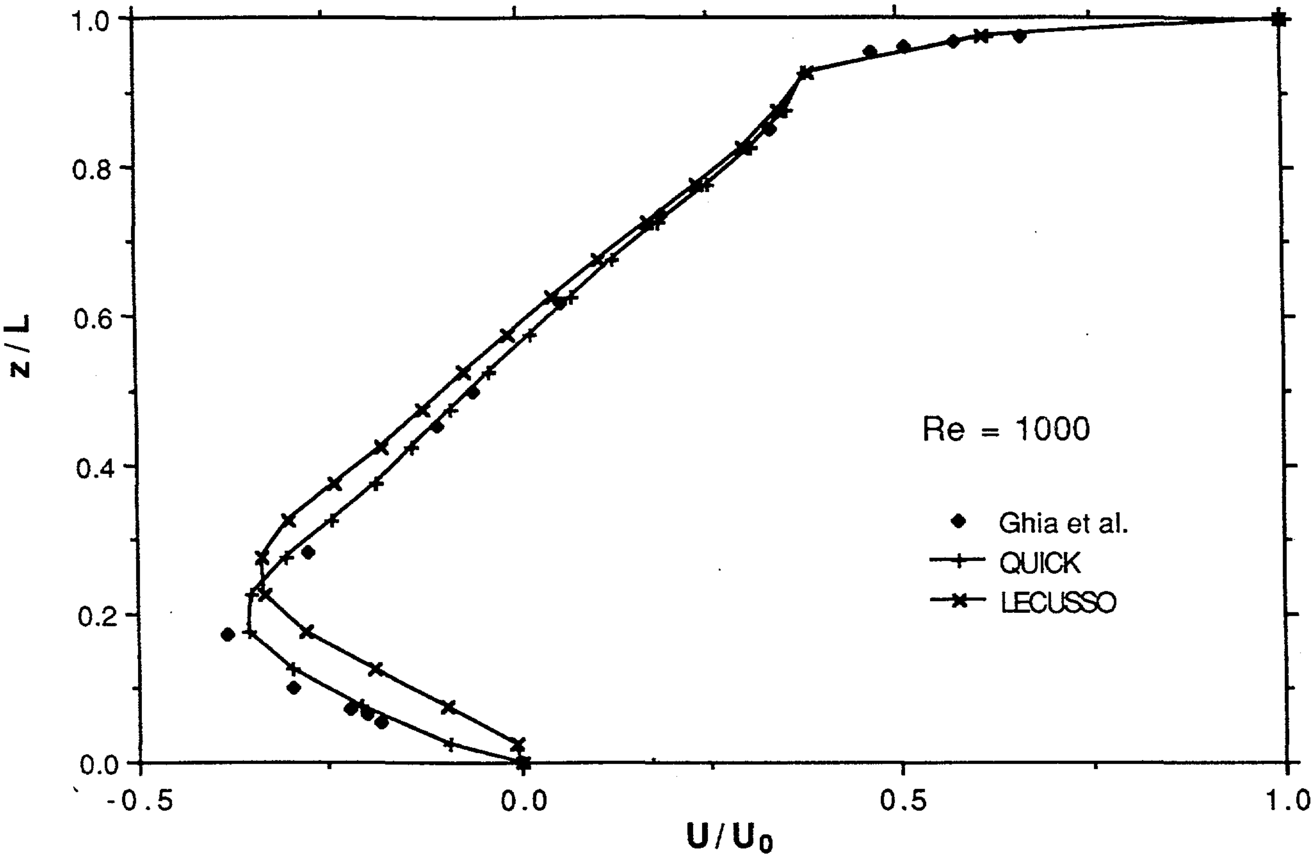

Fig. 10.26. Lateral component of velocity from the present calculations and from the calculations of Ghia et al.[33] at Re = 1000 (20x20 meshes) for shear-driven cavity flows

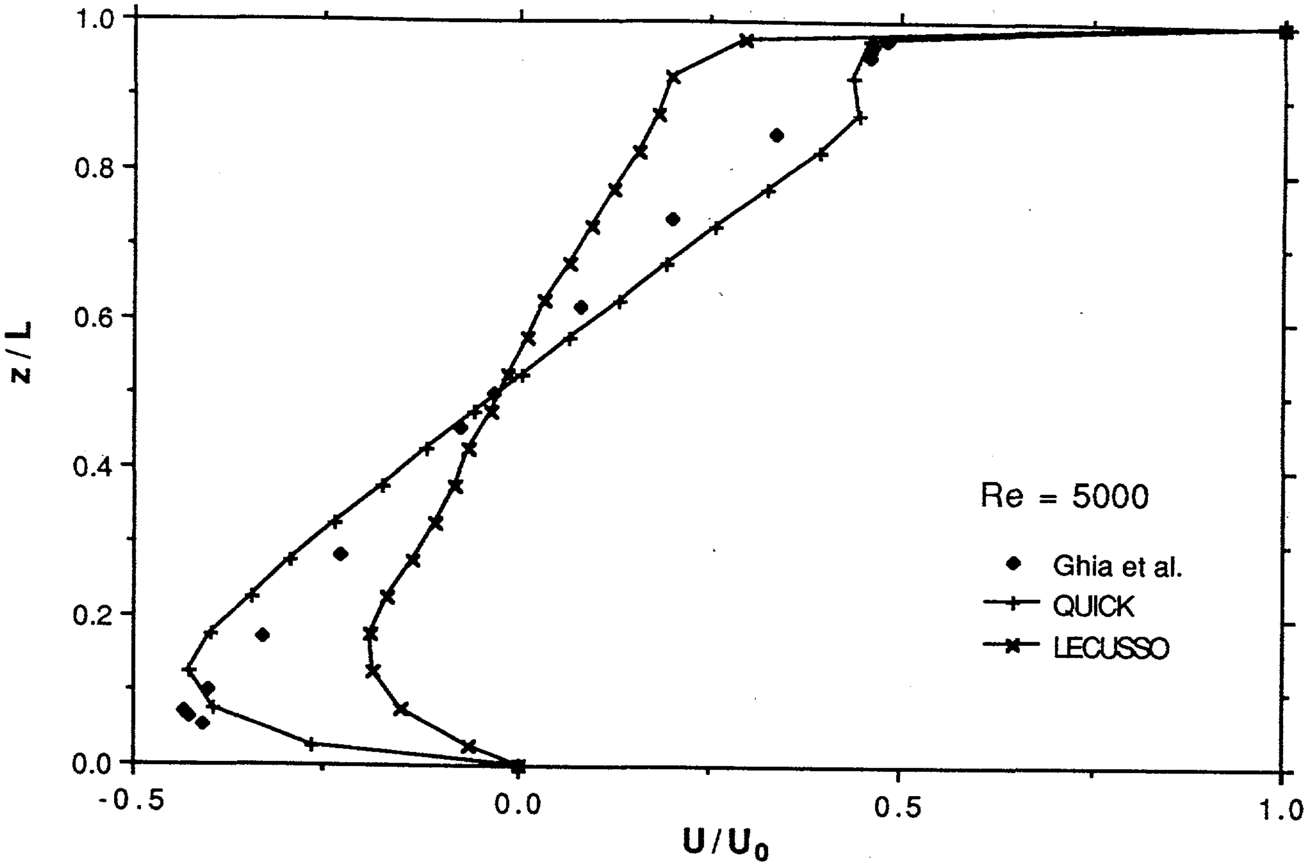

Fig. 10.27. Lateral component of velocity from the present calculations and from the calculations of Ghia et al.[33] *at Re = 5000 (20x20 meshes) for shear-driven cavity flows*

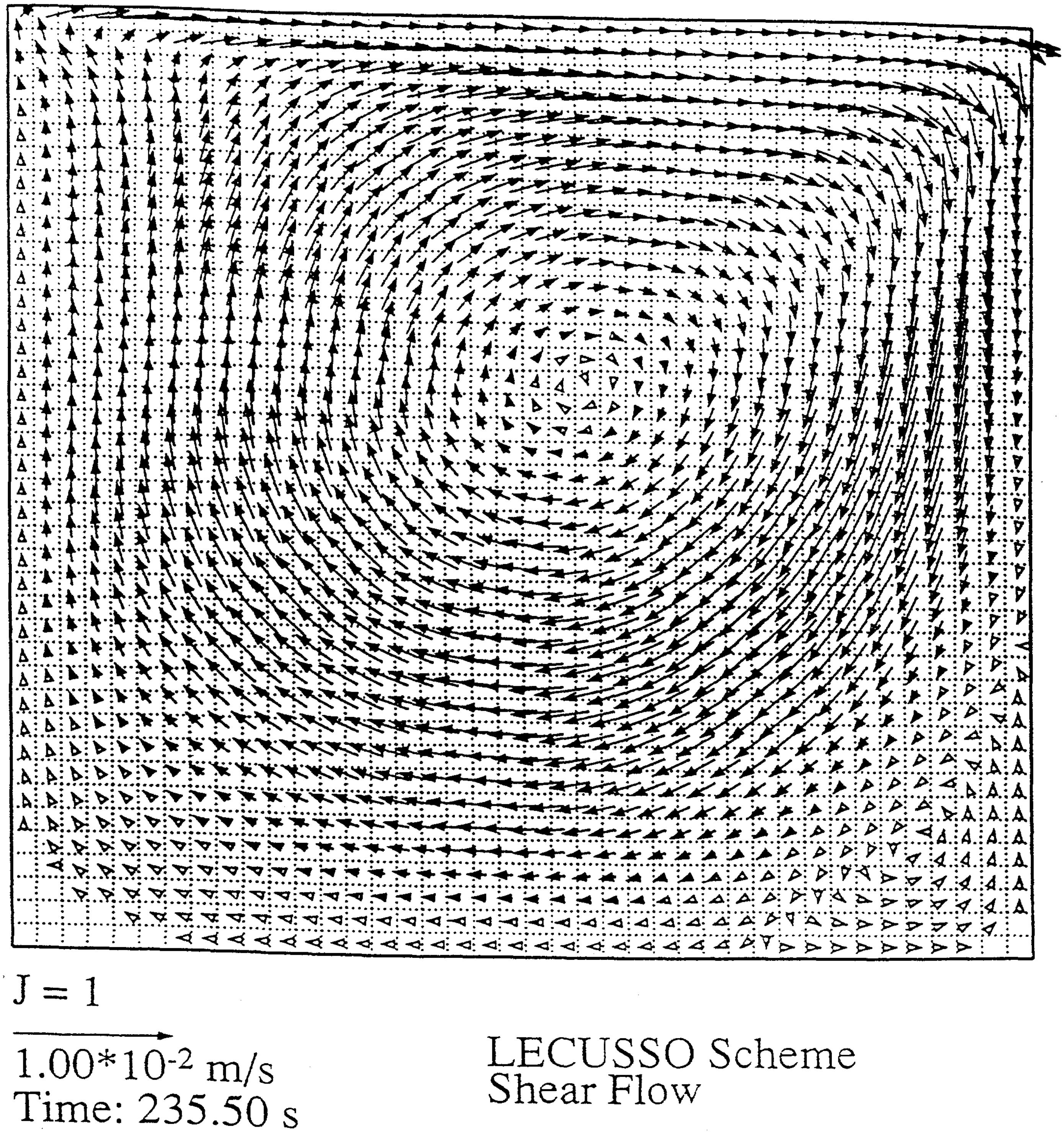

Fig. 10.28. Velocity vector at Re = 400 (40x40 meshes) for shear-driven cavity flow

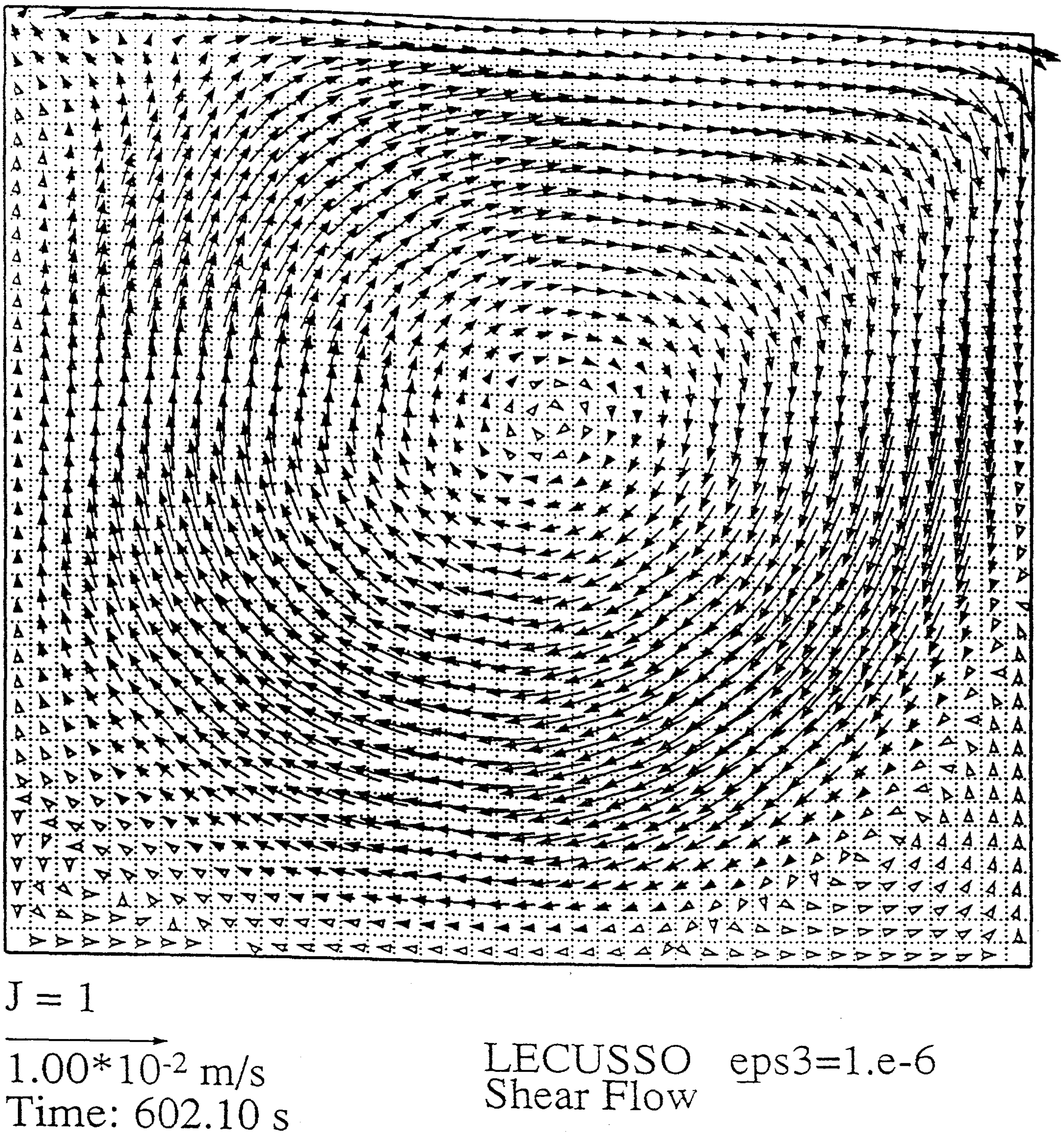

Fig. 10.29. Velocity vector at Re = 1000 (40x40 meshes) for shear-driven cavity flow

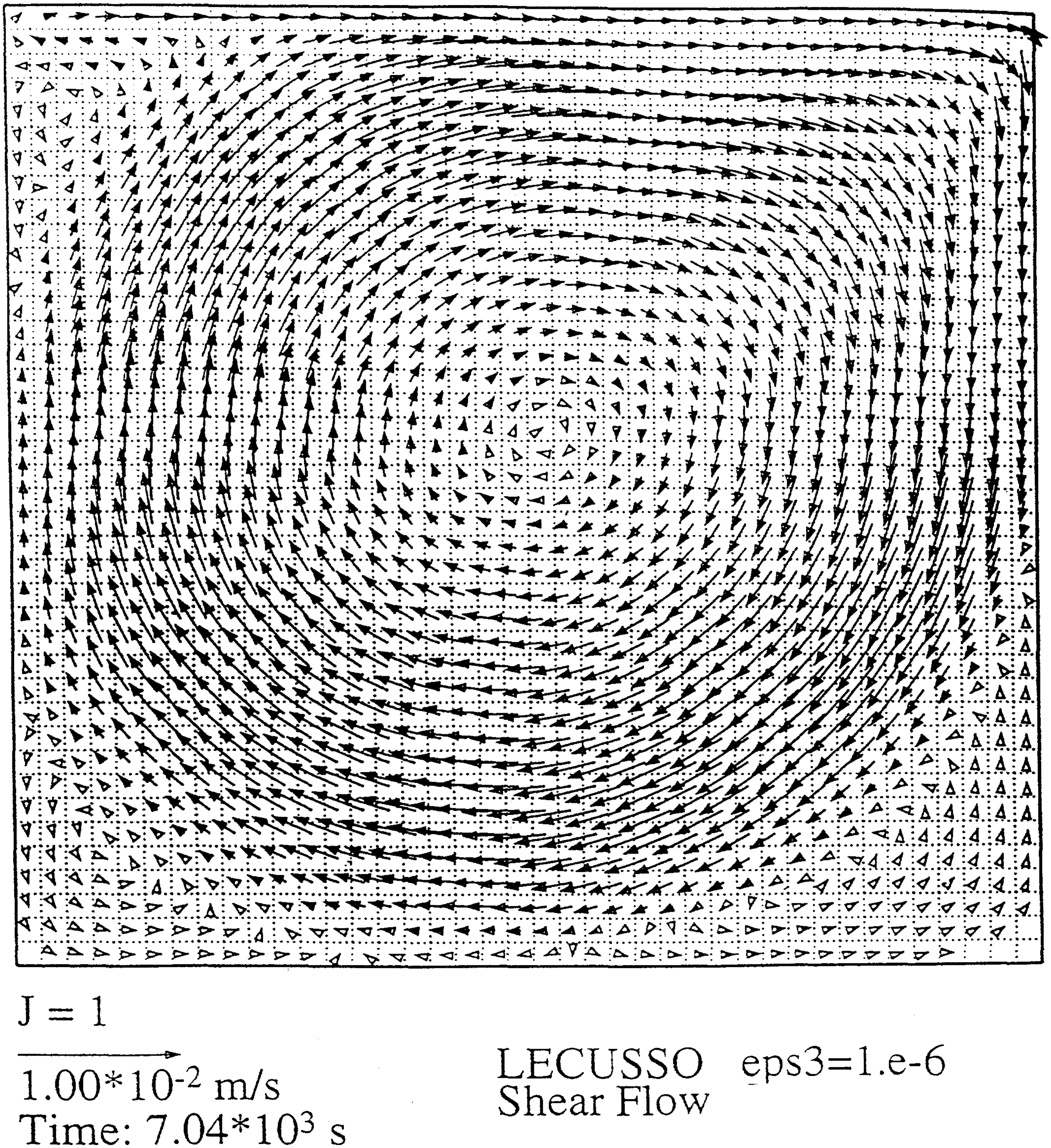

Fig. 10.30. Velocity vector at Re = 5000 (40x40 meshes) for shear-driven cavity flow

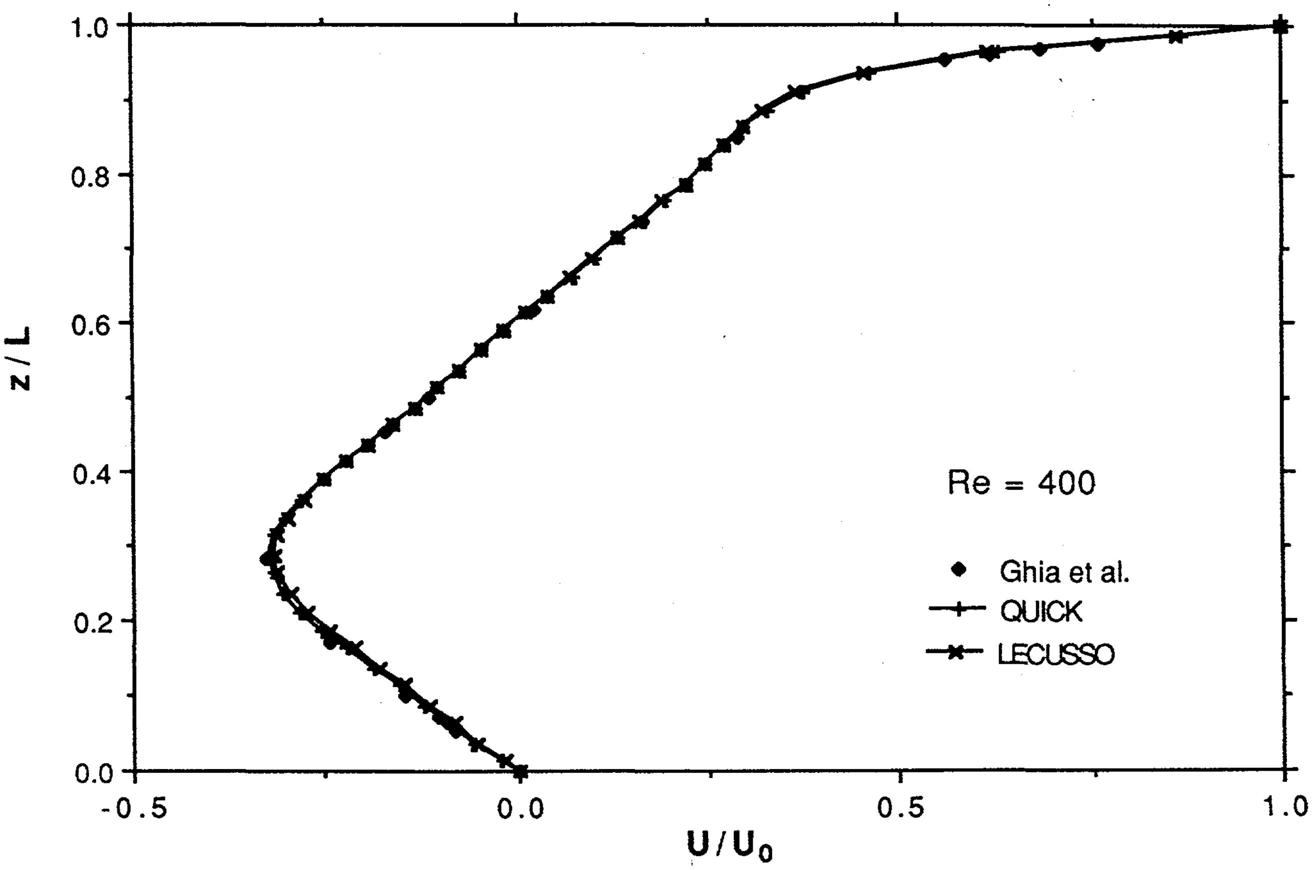

Fig. 10.31. Lateral velocity component from the present calculations and from the calculations of Ghia et al.[33] at Re = 400 (40x40 meshes) for shear-driven cavity flows

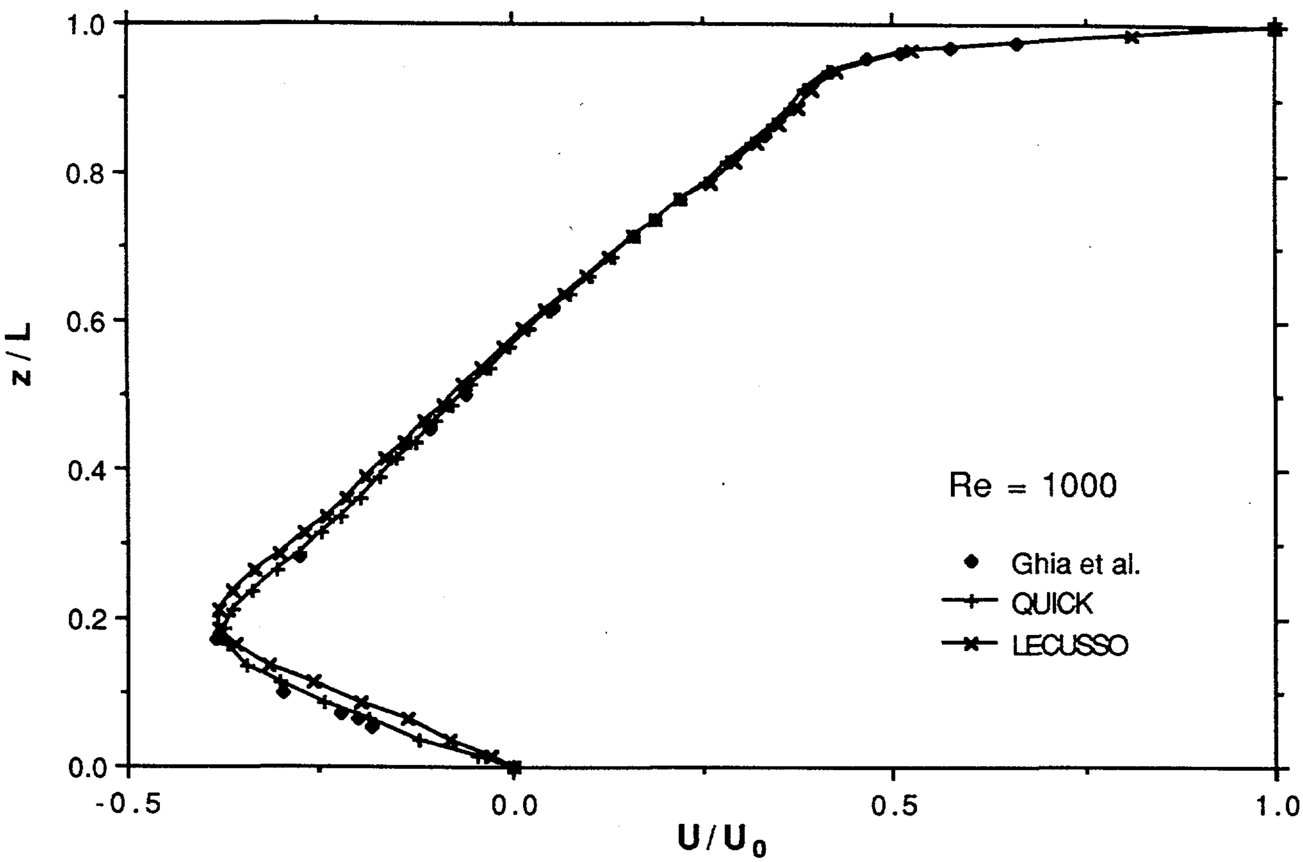

Fig. 10.32. Lateral velocity component from the present calculations and from the calculations of Ghia et al.[33] *at Re = 1000 (40x40 meshes) for shear-driven cavity flows*

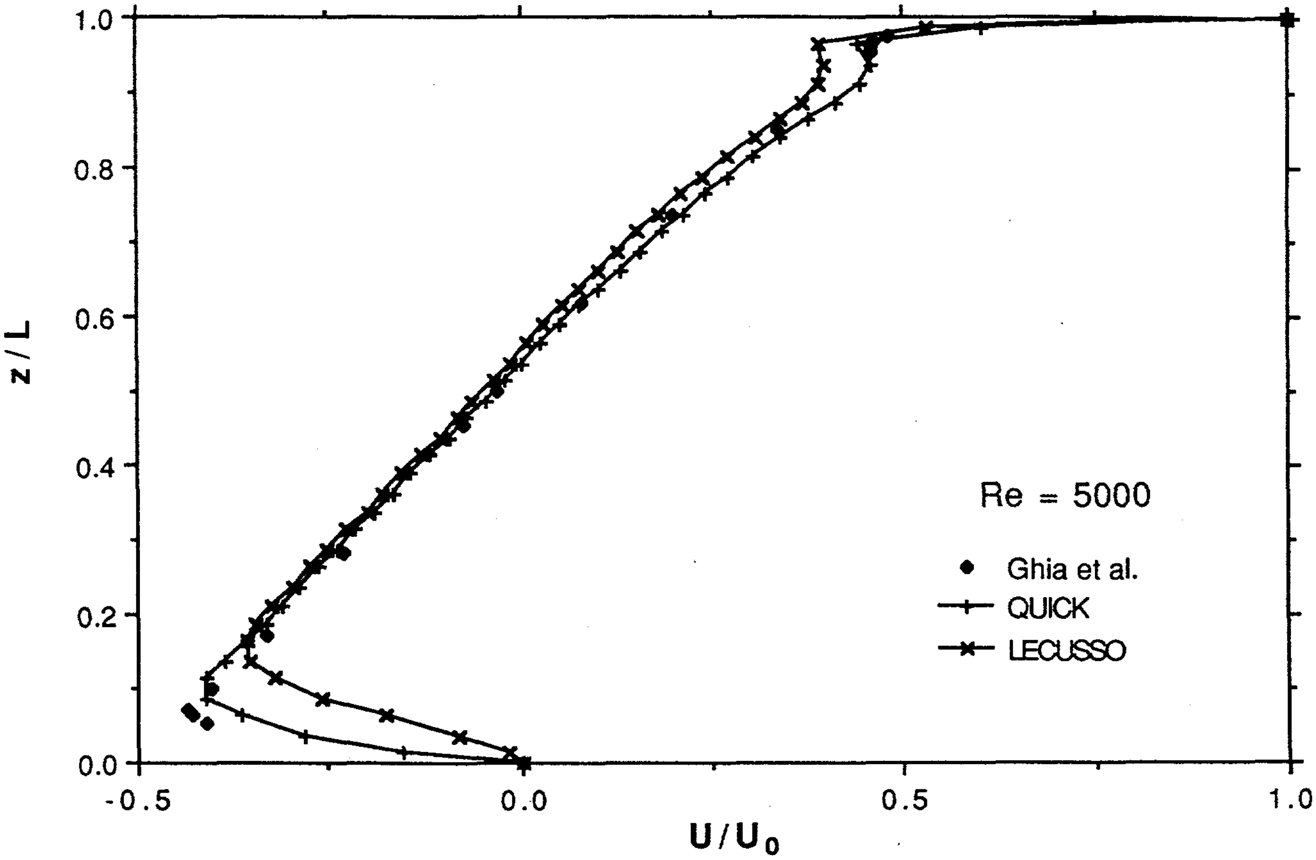

Fig. 10.33. Lateral velocity component from the present calculations and from the calculations of Ghia et al.[33] *at Re = 5000 (40x40 meshes) for shear-driven cavity flows*

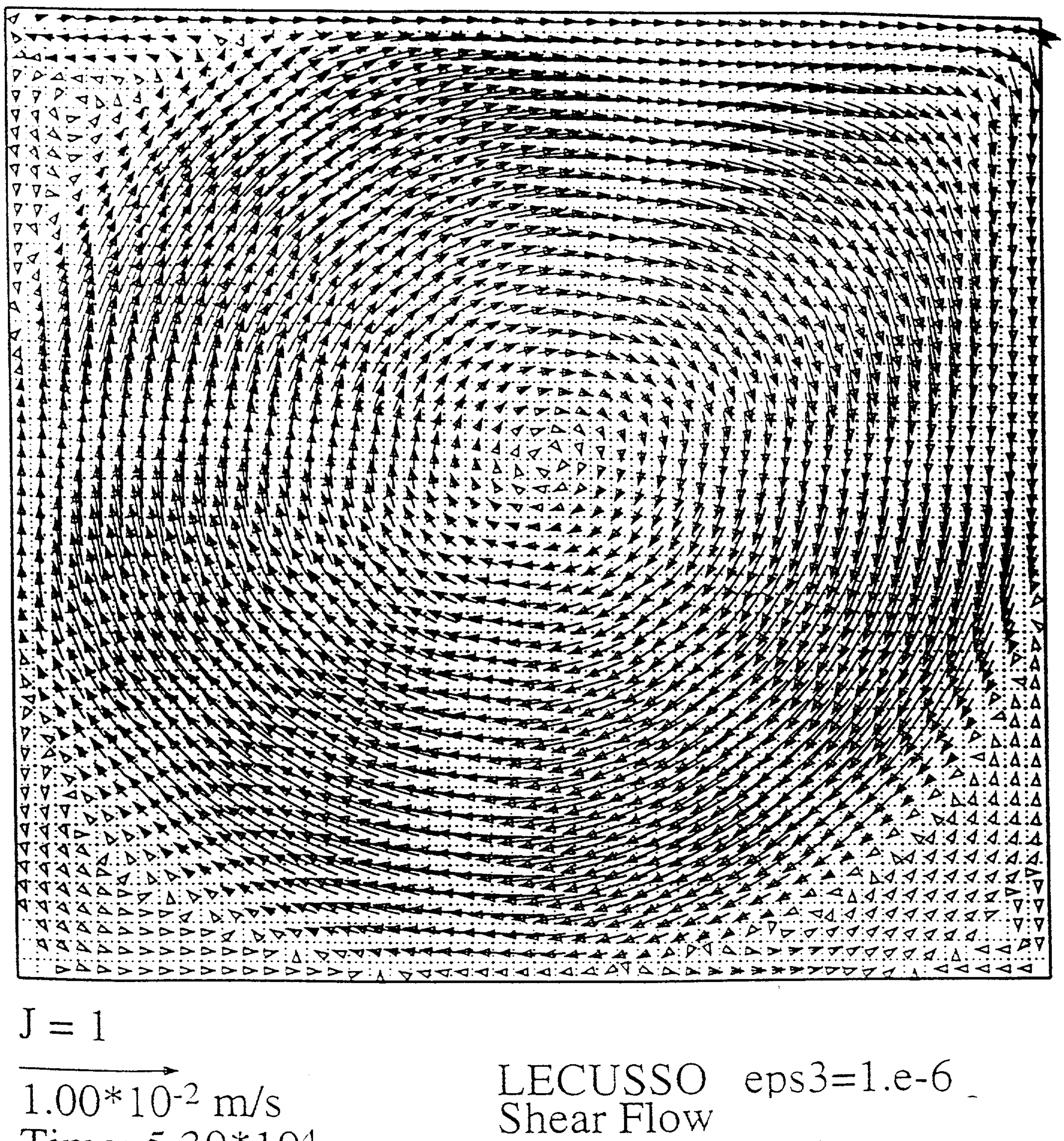

Fig. 10.34. Velocity vector at Re = 10000 for shear-driven cavity flow

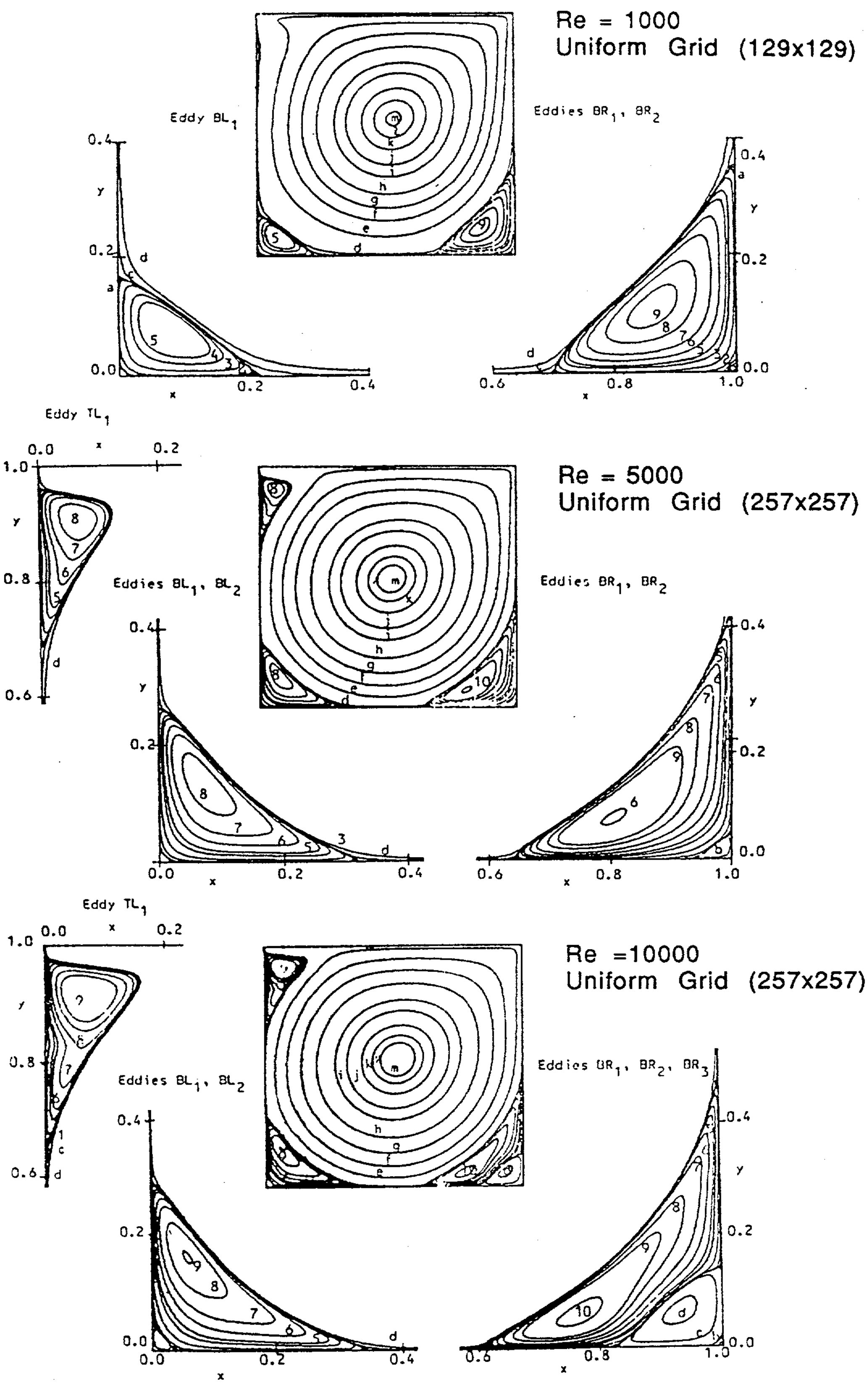

Fig. 10.35. Streamline pattern for primary, secondary, and additional corner vortices obtained by Ghia et al.[33]

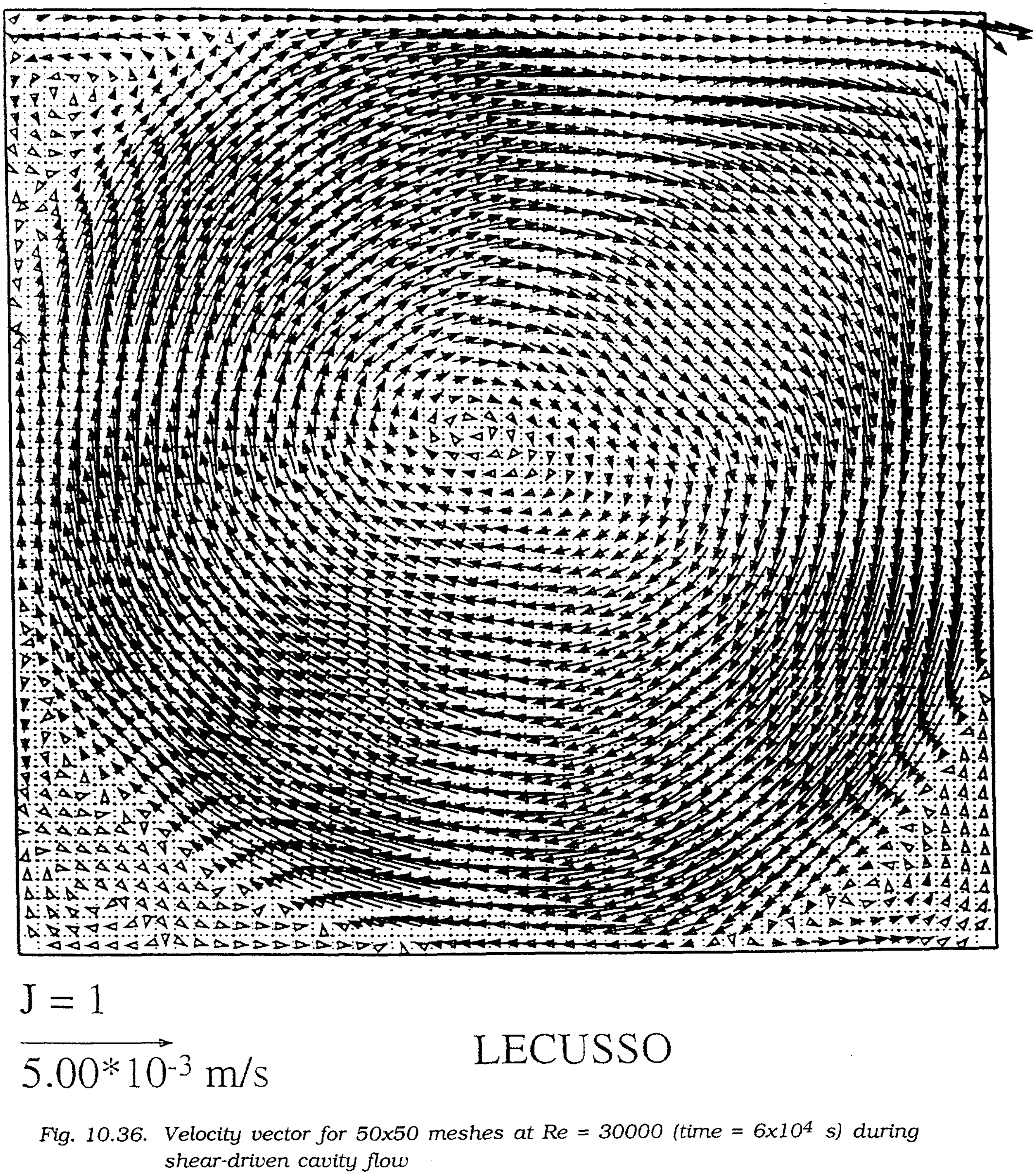

Fig. 10.36. Velocity vector for 50x50 meshes at Re = 30000 (time = 6x10⁴ s) during shear-driven cavity flow

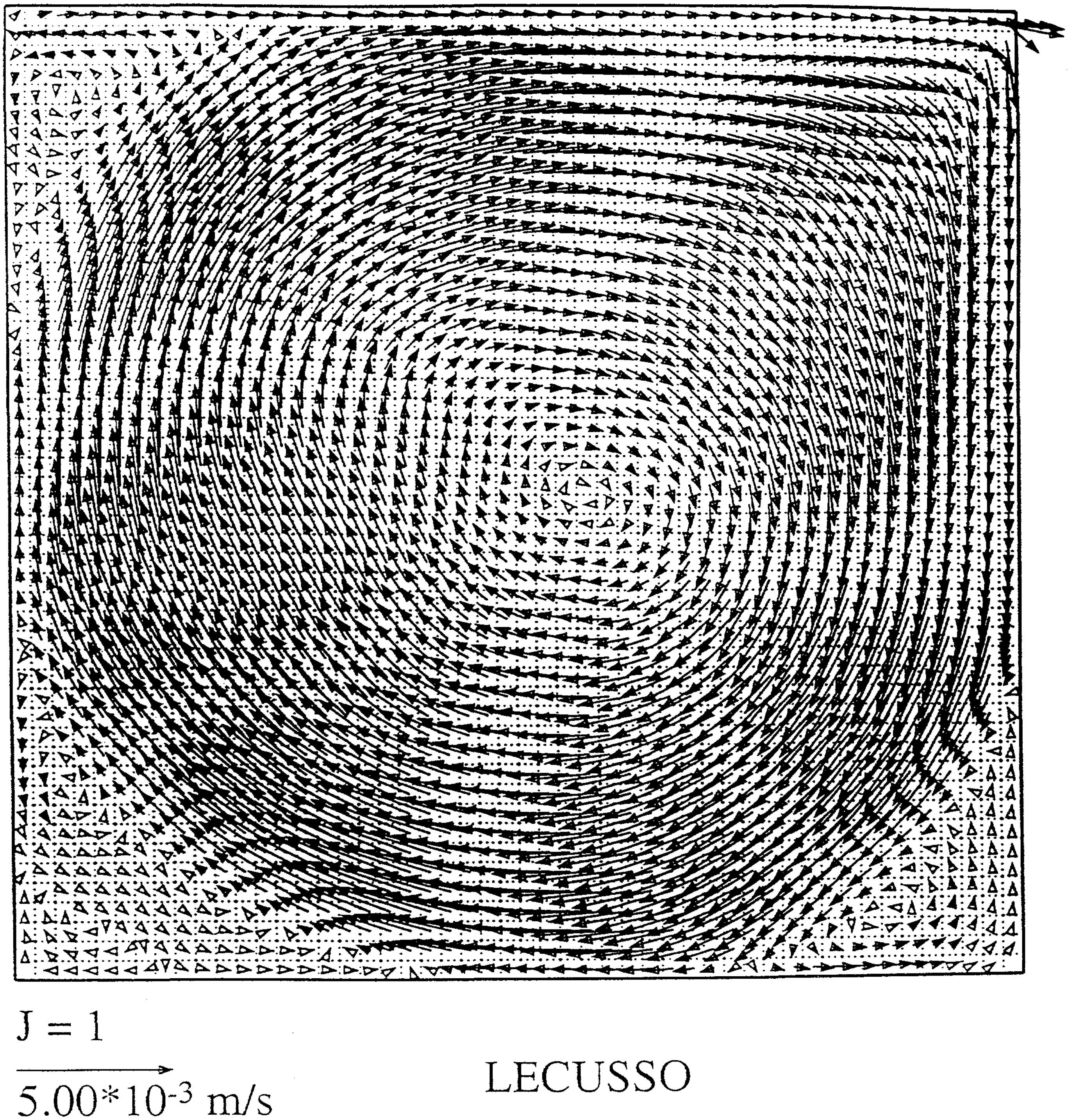

Fig. 10.37. Velocity vector for 50x50 meshes at Re = 30000 (time = $6.17x10^4$ s) during shear-driven cavity flow

Ghia et al.[33] did not perform laminar analysis for this high Re flow, but Huser and Biringen[34] tried. They obtained fluctuating solutions, in which the velocity field never converged, a finding that may be attributed to flow fluctuations due to turbulence.

In Figs. 10.36 and 10.37, the center of a large primary vortex is also fluctuating. Considering the results of Huser and Biringen,[34] our results are reasonable. In these fluctuating, turbulent flows, it is difficult to compare our calculations with their calculations. It is necessary to compare statistical quantities such as Reynolds stress ($\overline{u'v'}$), turbulence kinetic energy (u_1^2, v_1^2), two-point velocity correlation of functions, etc. by using finer mesh sizes to realize small-scale turbulent motions.

10.7 Couette and Circular-Pipe Flow

In this section, the Couette flow and circular-pipe flow in an entrance region are calculated with the QUICK scheme. The results are compared with the theoretical and experimental results.

10.7.1 Couette Flow

In the analysis of Couette flow, the fluid is confined in the two-dimensional x-z plane. The flow is in the x-direction bounded by parallel plates at a distance H, with the upper plate moving at a constant velocity. To simulate infinite length in the x-direction, the velocity distribution at the inlet is assigned to be equal to the exit condition. Table 10.17 shows the input data for the Couette flow analysis. There are 20 partitions in the transverse direction and 20 partitions in the flow direction.

The steady-state solution of velocity with the QUICK scheme is shown in Fig. 10.38. A comparison of this result with the theoretical solution of linear velocity distribution is plotted in Fig. 10.39. It is seen that the agreement is good. The maximum difference between the theoretical and the computational results is <0.1%. The first-order upwind scheme gives the same result as the QUICK scheme.

10.7.2 Circular-Pipe Flow in an Entrance Region

The pipe flow is modeled in a two-dimensional (axisymmetric) cylindrical pipe of radius R = 0.5 m. The flow is in the z-direction. The input data for the pipe flow is listed in Table 10.18. The Reynolds number Re (= $2R\rho V/\mu$), based on the pipe diameter (2R) and the mean flow velocity (V), is 1000 so that the flow is laminar. There are 20 uniform partitions in the radius direction and 50 nonuniform partitions in the flow direction.

Figure 10.40 shows the calculated velocity distributions at various locations z^* (= $\frac{z}{2R \cdot Re}$) with the QUICK scheme and the first-order upwind scheme and the theoretical results of Langhaar.[35] Langhaar's theory, and all other theories to be cited later, were based on the assumption that pressure is uniform over the cross section of the pipe. Although this is true for fully developed flow, the numerical solution showed that the pressure is not uniform near the inlet of the pipe. The nonuniformity of the pressure at the inlet is due to the development of the boundary layer near the pipe wall, resulting in an inward flow of the fluid toward the centerline. Near the inlet, e.g, at z^* = 0.00205, the location of maximum

Table 10.17. Input data for Couette flow analysis

```
-----------------------------------------------------------------
                INPUT DATA FOR COUETTE FLOW ANALYSIS
upper wall velocity is set to 0.01m/s in specic.f (surface No. 6)

                         <couette.data>
-----------------------------------------------------------------
&geom
 ifres=1,
 nll=840, nml=400, nsurf=6,
 ify=0,
 imax=20, jmax=1, kmax=20,
 isolvr=1, nnzero=1960, nspace=12224,
 xnorml= 0.0, 0.0, 0.0, 0.0, 0.0, 0.0,
 ynorml= 1.0,-1.0, 0.0, 0.0, 0.0, 0.0,
 znorml= 0.0, 0.0, 1.0, 1.0, 1.0,-1.0,
 dx=20*2.5e-3,
 dy=2.5e-3,
 dz=20*1.25e-3,
 &end
reg -1.          1  20   1   1   1  20   1     front  +y
reg -1.          1  20   1   1   1  20   2     back   -y
reg -1.          1   7   1   1   1   1   3     bottom +z
reg -1.          8  14   1   1   1   1   4     bottom +z
reg -1.         15  20   1   1   1   1   5     bottom +z
reg -1.          1  20   1   1  20  20   6     upper  -z (shear flow)
 &data
  alpha=1.0, eps3=1.e-6,
  iskew=0,  ifener=0, ifmom=1, ilink=1,
  idtime=0, dt=1.0,
  ntmax=20000,   it=1,
  trest=9999999.0,
  kflow=    -3,    -3,     0,     0,
  ktemp=     1,     1,     1,     1,
  veloc=   0.0,   0.0,   0.0,   0.0,
  temp=   20.0, 20.0, 20.0, 20.0,
  temp0= 20.0, pres0=1.0e5,
  matype=21, mattab=21, tablot=10.0, tabhit=40.0,
  ntprnt=-9999,
  nthpr= 12001, 32001,
  &end
```

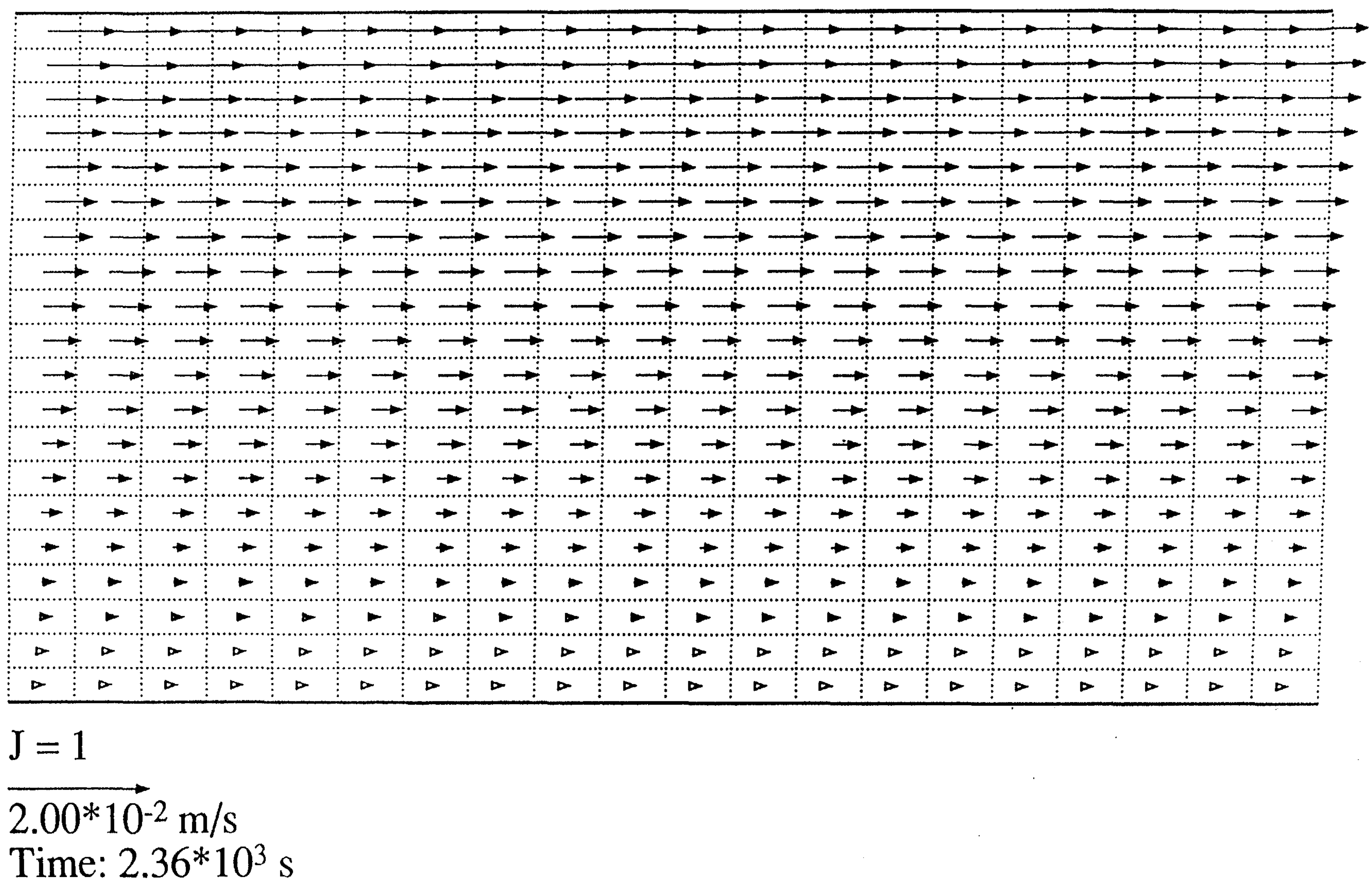

Fig. 10.38. *Velocity distribution of computed Couette flow*

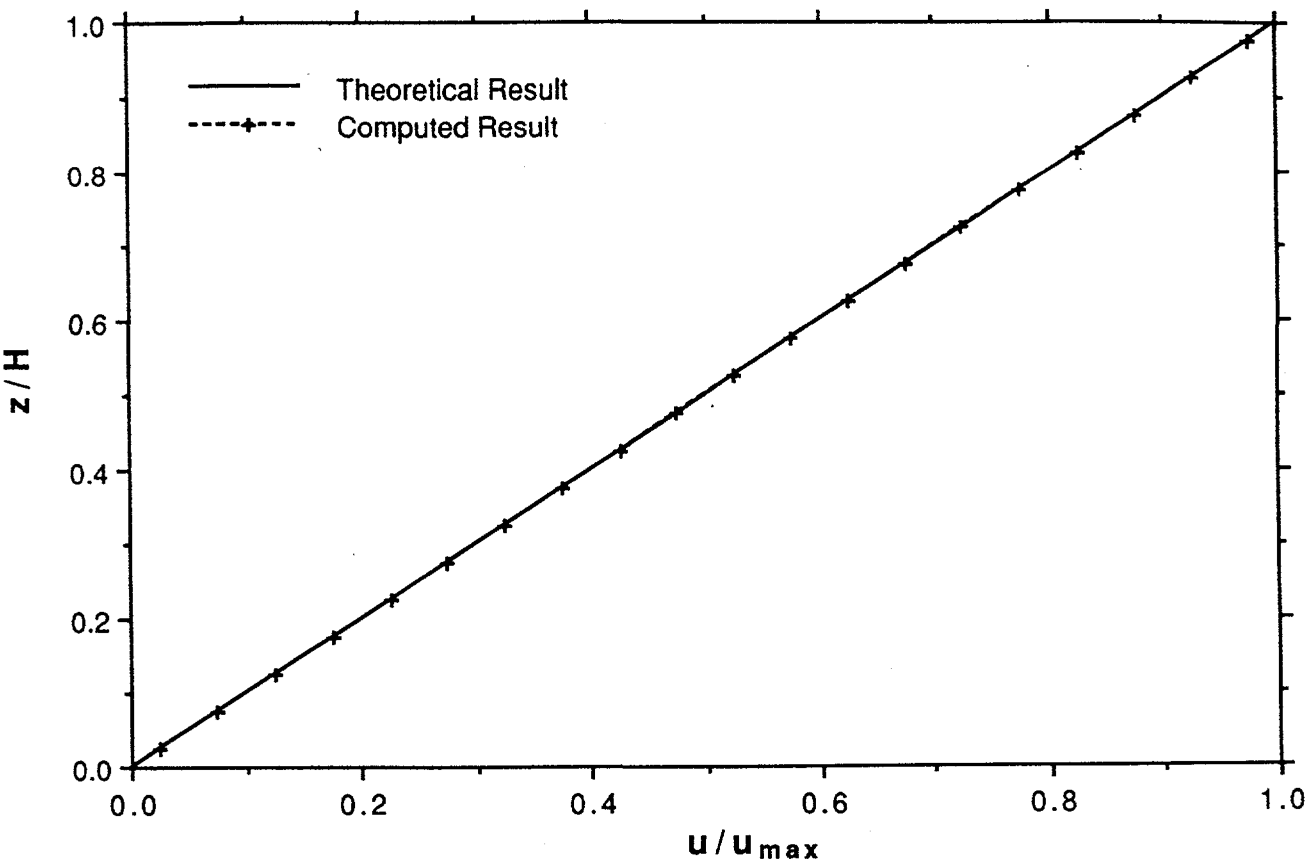

Fig. 10.39. Theoretical and computed velocity profiles for Couette flow

Table 10.18. Input data for analysis of entrance flow in a circular pipe

```
------------------------------------------------------------------
    INPUT DATA FOR ANALYSIS OF ENTRANCE FLOW IN A CIRCULAR PIPE
                            Re = 1000

                          <tube.data>
------------------------------------------------------------------
&geom
 ifres=1, igeom=-1, ify=0,
 nl1=140, nm1=1000, nsurf=5,
 imax=20, jmax=1, kmax=50,
 isolvr=1, nnzero=4860, nspace=30886,
 xnorml=1.0, -1.0, 3*0.0, ynorml=5*0.0, znorml=2*0.0, 1.0,-1.0,-1.0,
 dx=20*0.025, dy=6.28318531,
 dz= 0.0002, 0.0004, 0.0008, 0.0016, 0.0032, 0.0076, 0.0124, 0.0236,
     0.0324, 0.0356, 0.0504, 0.0836, 0.1364, 0.2236, 0.2364, 0.3036,
     0.5564, 0.7836, 1.4164, 2.1836, 2.4164, 2.9836, 12*2.5, 8*5.0,
     4*10.0, 4*20.0,
 &end
reg -1.         1   1   1   1   1  50   1     left   +x
reg -1.        20  20   1   1   1  50   2     right  -x
reg -1.         1  20   1   1   1   1   3     front  +z (inlet)
reg -1.         2  20   1   1  50  50   4     back   -z (outlet)
reg -1.         1   1   1   1  50  50   5     back   -z (outlet)

&data
 alpha=1.0, eps3=1.e-7, omegav=1.0,
 iskew=0,  ifener=0, ifmom=1,
 idtime=0, dt=100.0,
 ntmax=4000,   it=1,
 trest=9999999.0,
 kpres(5)=1, pres(5)=1.0e05,
 kflow=     -3,  0,  1,    -5, -5,
 ktemp=     5*400,
 veloc=  0.0,  0.0,  0.001,  2*0.0,
 temp=  5*20.0,
 temp0= 20.0, pres0=1.0e5,
 matype=1,
 c0ro= 1000.,
 c0h=  0.0,  c1h=1005.7,
 c0k=  0.624,
 c0mu= 1.000e-3,
 ntprnt=-9999,
 nthpr= 12001, 32001, 172001,
 &end
ul  0.0000      1  20   1   1   1  50
wl  0.0010      1  20   1   1   1  50
```

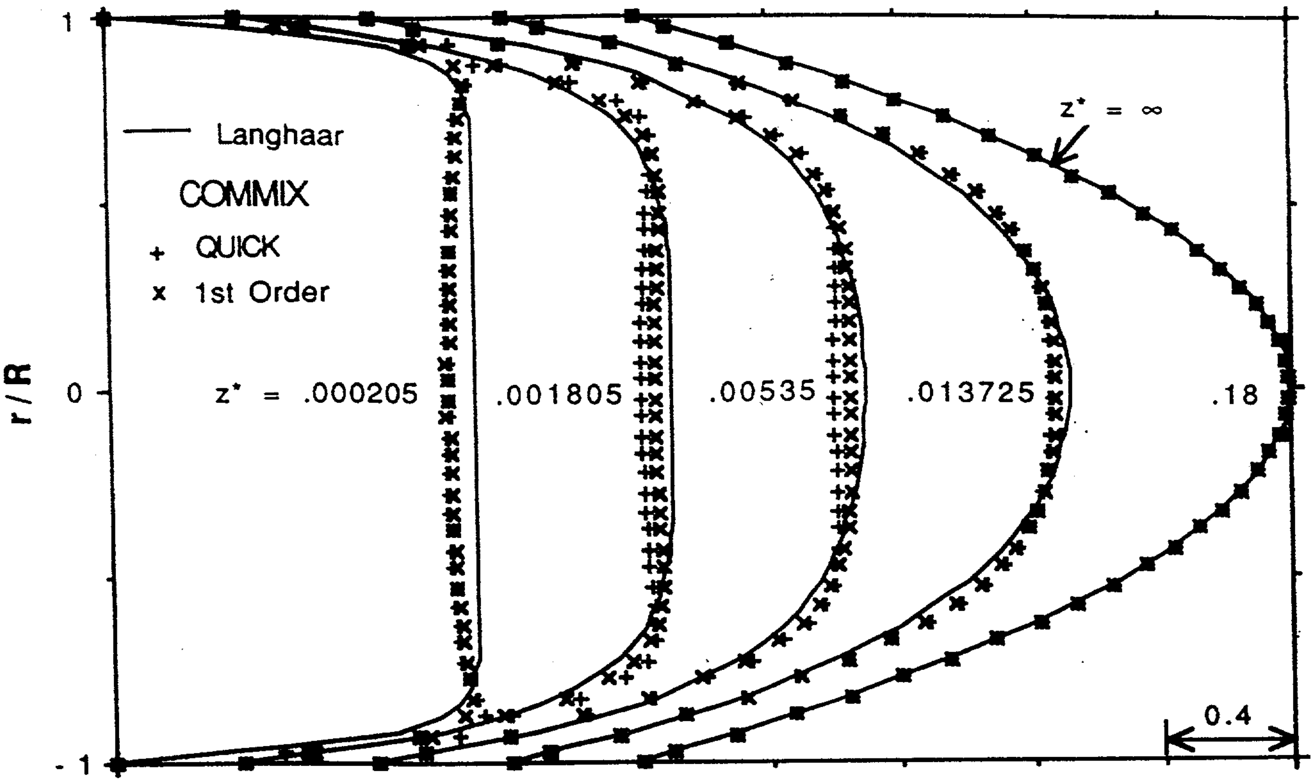

Fig. 10.40. Velocity profiles at various locations for circular-pipe flow in an entrance region

velocity is close to the wall, as shown in Fig. 10.40. At large z*, e.g., z* = 0.18, the velocity distribution approaches parabolic distribution. In general, however, the calculational results and the Langhaar's results agree well.

The centerline velocity and the pressure increase with z*, plotted in Figs. 10.41 and 10.42, respectively, are compared with the results of Campbell and Slattery[36] and others. It is seen that both the QUICK scheme and the first-order upwind scheme give good results. Close examination of Fig. 10.41 reveals that the results with the QUICK scheme agrees better with the experimental results of Pfenninger and of Reshotko.[36]

10.8 Analysis of Two-Dimensional Flow for Scalar Transport with FRAM

This analysis uses the same condition as Case 1 in Sec. 10.4. The velocity distribution and the inlet temperature condition are shown in Fig. 10.5.

With the QUICK scheme, the temperature contour of the steady-state solution is shown in Fig. 10.43. It is seen that the calculated temperature of <50°C or >150°C exists in some regions. This is not physically realistic because the inlet temperature is in the 50–150° range. The reason for this finding is that the QUICK scheme results in oscillatory solutions at regions of large gradient, as described in Sec. 7. To remove the spurious oscillations, the FRAM scheme is used together with the QUICK scheme. The resulting temperature contour

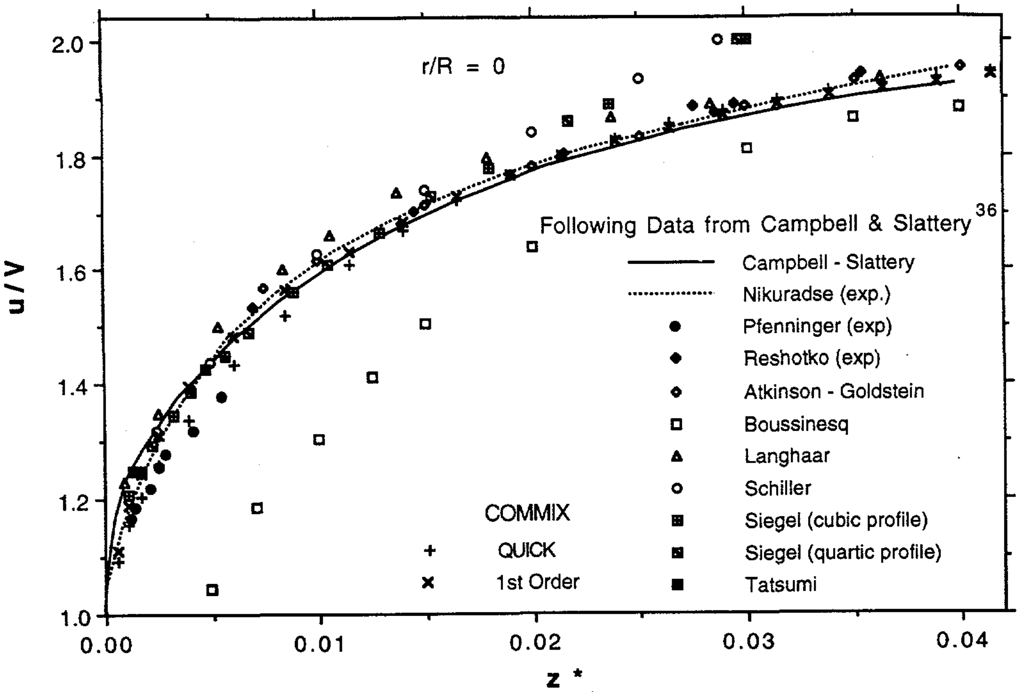

Fig. 10.41. Velocity versus axial position for r/R = 0.0 for circular-pipe flow in an entrance region

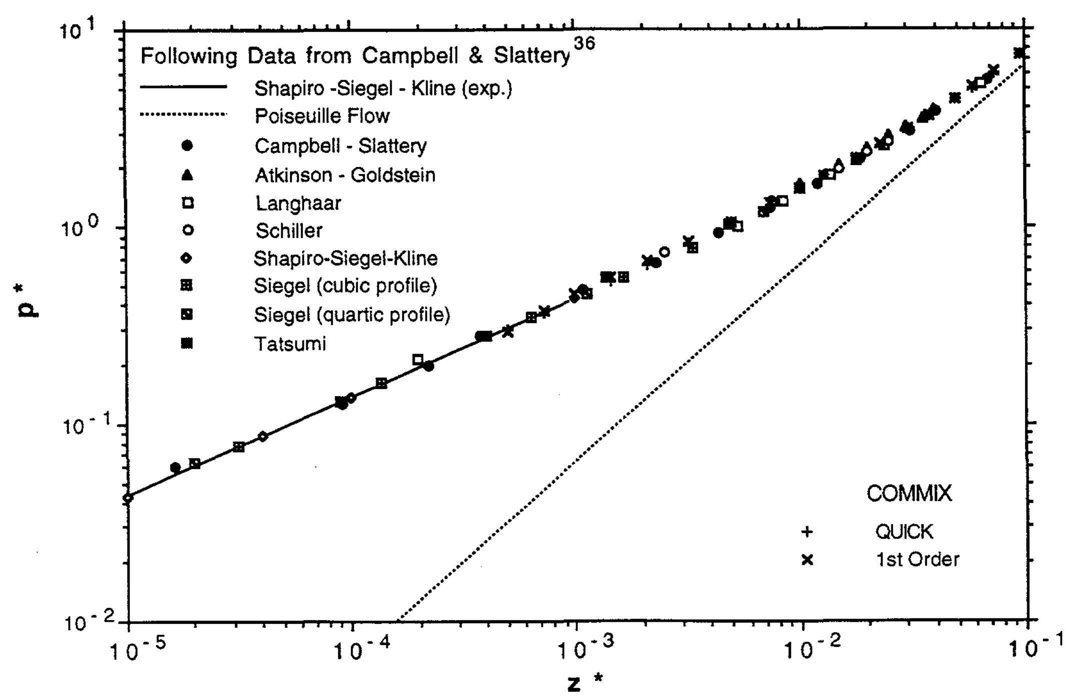

Fig. 10.42. Pressure versus axial position for circular-pipe flow in an entrance region

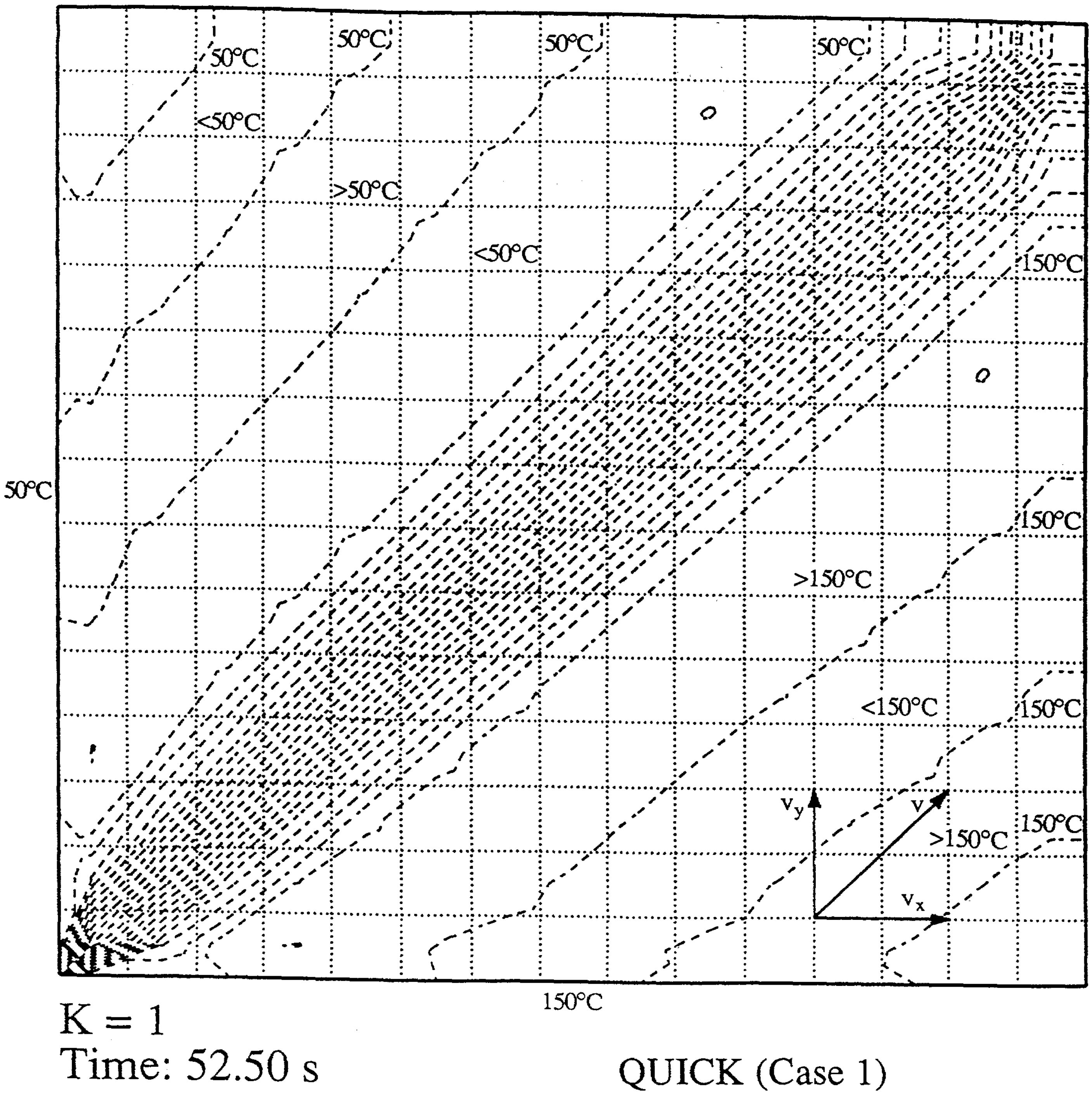

Fig. 10.43. Isotherms calculated with QUICK scheme

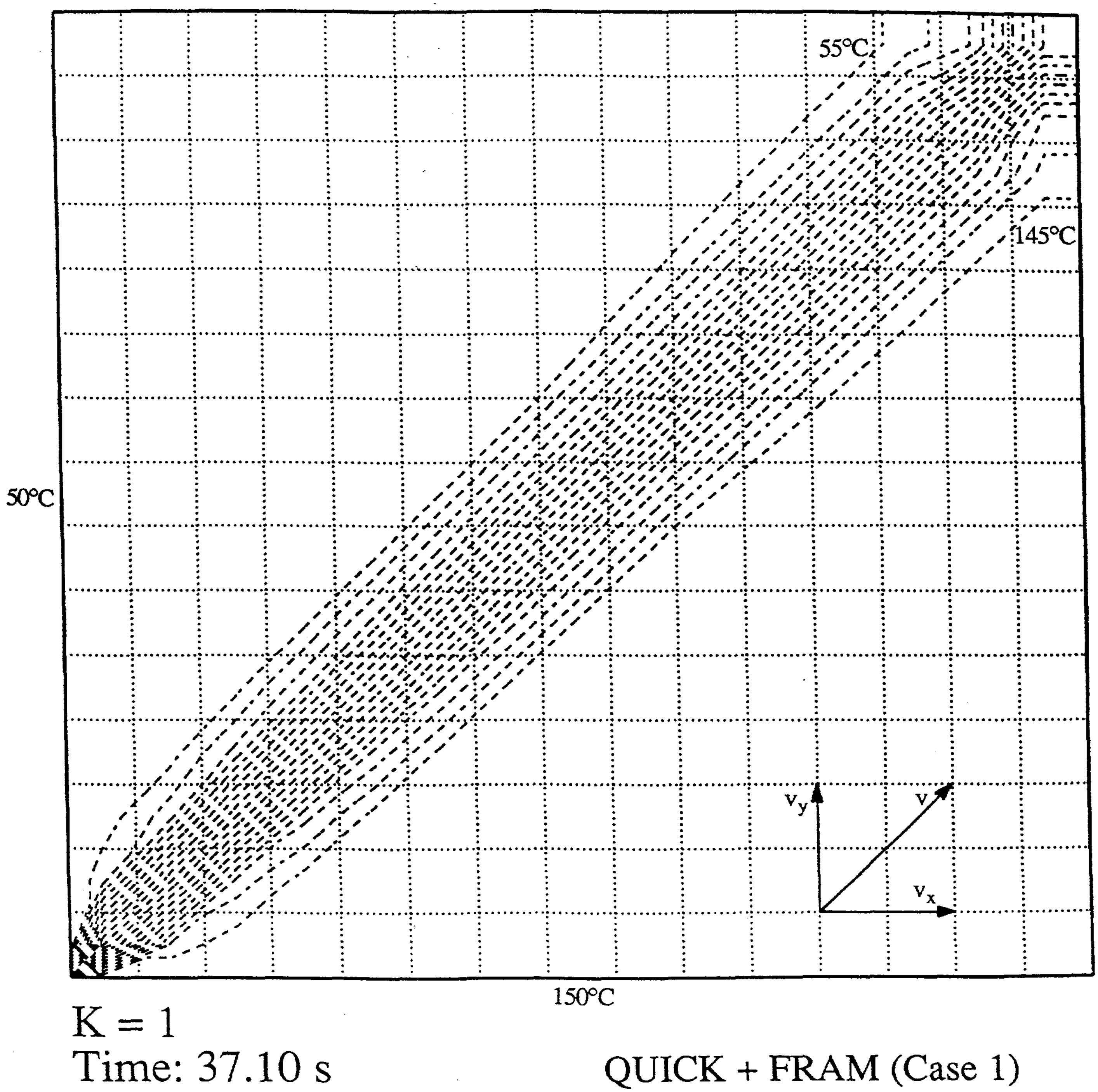

Fig. 10.44. Isotherms calculated with QUICK+FRAM scheme

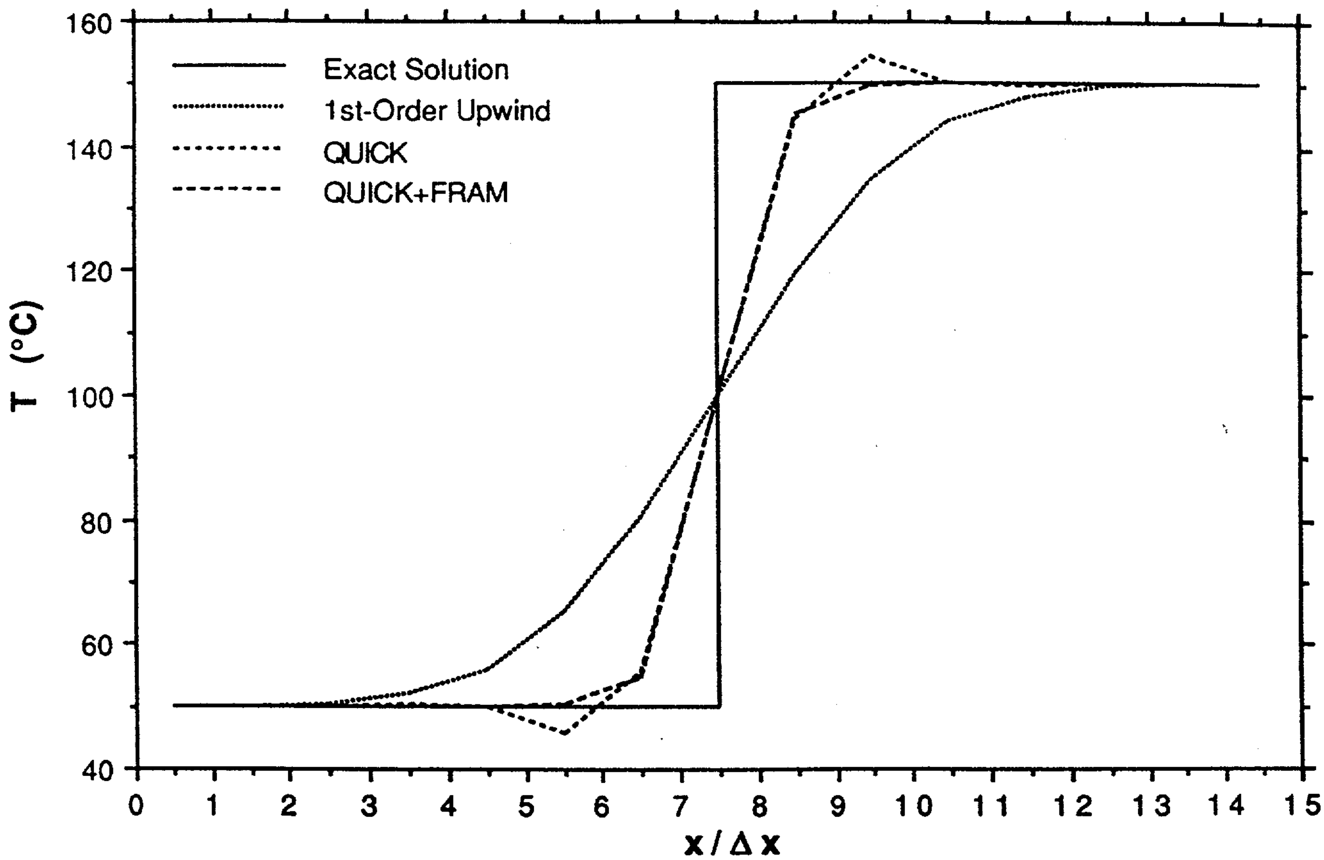

Fig. 10.45. Temperature profiles calculated with various numerical schemes

is shown in Fig. 10.44. The oscillation is eliminated. It is also noticeable that the QUICK+FRAM scheme used fewer iteration time steps (37.1 s) to reach steady state than the QUICK scheme (52.5 s). To further examine the accuracy of the various solutions, the temperature distribution across the temperature gradient is plotted in Fig. 10.45 for solutions with the first-order upwind, QUICK, and QUICK+FRAM schemes. It is clear that the QUICK+FRAM scheme gives the best result.

11 Description of Programming

11.1 Main Features

- QUICK and LECUSSO schemes for convection terms in all governing equations (mass, momentum, energy, kinetic energy of turbulence and dissipation of turbulence kinetic energy).

- Three-dimensional.
- Nonuniform-mesh-size grids.
- All values between 0 and 1 for implicitness parameter α.
- Shear flow (or tangential velocity) boundary conditions.
- Second-order boundary conditions for velocity.

11.2 Subroutines Changed or Newly Added

11.2.1 Changed Subroutines

alladd	
amain	
timstp	
moloop	
tkloop	only dynamical arguments are changed
tdloop	only dynamical arguments are changed
enloop	
xmomi	
ymomi	
zmomi	
xmom1	
ymom1	
zmom1	
zmomx	
zmomz	
peqn	

11.2.2 Added subroutines

specic	specification of newly added options regarding QUICK and LECUSSO
specle	specification of newly added options regarding LECUSSO scheme
coefqe	QUICK coefficients for main control volume
coefmx	QUICK coefficients for x–x term in momentum
coefmy	QUICK coefficients for y–y term in momentum
coefmz	QUICK coefficients for z–z term in momentum
cofmox	QUICK coefficients for cross terms in momentum
rlquik	density calculation with QUICK scheme
encon1	copy of original encon0
encofm	optimized FMSUD

11.3 Newly Added Options

The following options are specified in specic.

ihighm	= 1	high–order (QUICK) mass continuity for momentum equation
	= 0	1st–order upwind mass continuity for momentum equation

ihighe	= 1	high–order (QUICK) mass continuity for energy equation
	= 0	1st–st order upwind mass continuity for energy equation This option is available only for $a_0(2)$ form. For $a_0(1)$ form, this option does not work.

ifa012	= 1	$a_0(1)$ form for momentum calculation
	= 2	$a_0(2)$ form for momentum calculation
iea012	= 1	$a_0(1)$ form for energy calculation
	= 2	$a_0(2)$ form for energy calculation
ifunix	= 1	uniform mesh grid in x–axis
	= 0	nonuniform mesh grid in x–axis
ifuniy	= 1	uniform mesh grid in y–axis
	= 0	nonuniform mesh grid in y–axis
ifuniz	= 1	uniform mesh grid in z–axis
	= 0	nonuniform mesh grid in z–axis
iunifo	= 1	uniform mesh grid in all axes
	= 0	nonuniform mesh grid in any axis This option, used for energy calculation, is automatically determined by ifunix, ifuniy, and ifuniz in subroutine specic.
ishear	= 1	shear flow boundary condition
	= 0	no shear Shear flow boundary is available for x–z domain. For ishear = 1, next data should be given in subroutine specic by using initial data statements. lflow(nsurf) = 1: surface number=nsurf is shear flow boundary = 0: surface number=nsurf is no shear flow boundary velbt(nsurf) = tangential velocity on the surface nsurf (m/s)
ishord	= 1	first–order for shear flow boundary condition
	= 2	second–order for shear flow boundary condition
ifupw	= 1	first–order upwind with second–order boundary condition using the same process as that in QUICK scheme. Then iskew=0 should be used.
icheck	= 1	first–order upwind with first–order upwind boundary condition. Namely, this corresponds to original COMMIX–1C. But this is only for momentum equation with x–z domain. This option is installed to check whether new program realizes the original COMMIX–1C by going through the same process as that in QUICK scheme. Then iskew=0 should be used.
ifram	= 1	with FRAM technique
	= 0	without FRAM technique
iofmsu	=	not necessary to specify. When iskew = 4, iofmsu = 1 is automatically specified in specic
mybest	= 1	most-recommended combinations among options

istabl	= 1	stability analysis option (usually = 0)

11.4 Input Data

iskew
= 0 QUICK scheme
= 1 first-order upwind
= 2 original FMSUD
= 3 cos θ FMSUD
= 4 optimized FMSUD for energy equation with prescribed uniform flow field.
Further options are specified in encofm:
ilstup = 0 optimized FMSUD
= 1 1st-order upwind
= 2 original FMSUD

alpha
= 1.0 fully implicit with respect to time
= 0.5 Crank-Nicolson scheme
= 0.0 fully explicit with respect to time

11.5 Program File

11.5.1 Source Program

/strld/sakai/clcsud/srcsud/*

11.5.2 Input Data

strld/sakai/clcsud/*

zwangx.data	2-D momentum calculation for forced channel flow (x – z)
zwangy.data	2-D momentum calculation for forced channel flow (y – z)
zwangz.data	2-D momentum calculation for forced channel flow (z – x)
case5.data	2-D energy calculation with prescribed flow field
case6.data	2-D energy calculation with prescribed flow field (skewness of flow field – 45 degrees)
boxz.datas	2-D momentum and energy calculation – natural circulation
boxy.datas	2-D momentum and energy calculation – natural circulation
karmanxz.data	2-D Von Karmann vortex calculation
cavity.data	2-D shear driven cavity flow (ishear = 1)

11.6 KfK Version of COMMIX - COMMIX-2(V)

11.6.1 Source Program

/strld/sakai/c2v/src/mb.v21

11.6.2 Options

ischem	= 1	LECUSSO scheme
	= 2	1st-order upwind
	= 3	QUICK scheme

12 Discussion and Conclusions

Based on the numerical results of the various test problems, the following conclusions are drawn.

To predict complex flow and temperature field, such as vortex shedding, it is necessary to have a high-order scheme such as QUICK and LECUSSO.

Based on the numerical results of various test problems, the high-order schemes, both QUICK and LECUSSO with oscillation dumping techniques such as FRAM, agree well with experimental data. However, the agreement becomes poor without the oscillation dumping technique FRAM.

From a stability point of view for a problem with uniform mesh, high-order schemes LECUSSO and QUICK are stable. However, it appears that LECUSSO is more stable than QUICK. It can be shown that the truncation error of QUICK is smaller than that of LECUSSO. For a nonuniform mesh system, the situation is very different. Both LECUSSO and QUICK are unable to demonstrate stability. With respect to computer running time and storage requirements, the QUICK scheme has a slight advantage over LECUSSO, because the formula for computing extrapolation coefficients in the LECUSSO scheme is more complicated than in QUICK, and thus requires more CPU time, and because the extrapolation coefficients used in the QUICK scheme are a function of mesh sizes only, they can be computed once and need no updating for subsequent use. This is not the case for LECUSSO because the extrapolation coefficients are a function of mesh sizes and mesh Reynolds numbers. Mesh Reynolds numbers must be updated at every iteration. Thus, the QUICK scheme has an inherent advantage over the LECUSSO from a CPU point of view, providing that sufficient large storage space is available.

Acknowledgment

The first author would like to express his sincere acknowledgment to Dr. M. Bottoni of ANL. At the beginning of this work, Dr. Bottoni kindly gave valuable instructions and direction about the implementation of high-order schemes into the COMMIX-1C program. He gave the original source code of COMMIX-1C and input data for some test calculations.

The authors want to thank Ms. L. S. Wang for her implementation of a streakline plotting routine in the COMMIX plotting package. The financial support of this work by the Multiphase Flow Research Institute is acknowledged.

References

1. H. M. Domanus, Y. S. Cha, T. H. Chien, R. Schmitt, and W. T. Sha, *COMMIX-1C: A Three-Dimensional Transient Single-Phase Computer Program for Thermal Hydraulic Analysis of Single and Multicomponent Systems; Vol. I: Equations and Numerics; Vol. II: User's Manual*, NUREG/CR-5649, Argonne National Laboratory Report ANL-90-33 (Nov. 1990).

2. I. Maekawa and T. Muramatsu, *Higher Order Difference Schemes in Fluid Flow Analysis and Their Applications to In-Vessel Thermal-Hydraulics*, Fifth IAHR Liquid Metal Working Group Meeting, Grenoble, France (June 23-27, 1986).

3. D. Weinberg et al., *Investigation into LMFBR Decay Heat Removal by Natural Convection under Nominal and Non-nominal Conditions*, ASME Winter Annual Meeting, Chicago, Illinois (November 1988).

4. T. Kawamura and K. Kuwahara, *Computation of High Reynolds Number Flow Around a Circular Cylinder with Surface Roughness*, AIAA paper 84-0340 (1984).

5. B. P. Leonard, *A Survey of Finite Differences with Upwinding for Numerical Modelling of the Incompressible Convective Diffusion Equation*, in C. Taylor and K. Morgan (eds.), Computational Techniques in Transient and Turbulent Flow, **2**, pp. 1-36, Pineridge Press, Swansea, UK (1981).

6. D. N. de Allen and R. V. Southwell, *Relaxation Methods Applied to Determine the Motion, in Two Dimensions, of a Viscous Fluid Past a Fixed Cylinder*, Quart. J. Mech. Appl. Math., **8**, 129-145(1955).

7. A. A. Samarsky, *Theory of Difference Method*, Leipzig (1984).

8. A. Harten, *High Resolution Schemes for Hyperbolic Conservation Laws*, J. Compu. Phys., **49**, 357-393 (1983).

9. A. Harten, *ENO schemes with Subcell Resolution* J. Compu. Phys., **83**, 148-184 (1989).

10. M. Chapman, *FRAM-Nonlinear Damping Algorithm for the Continuity Equation*, J. Compu. Phys., **44**, 84-103 (1981).

11. J. P. Boris and D. L. Book, *Flux-Corrected Transport 1. SHASTA, A Fluid Transport Algorithm that Works*, J. Compu. Phys., **11**, 38-69 (1973).

12. I. Maekawa, *Numerical Diffusion in Single-Phase Multidimensional Thermal-Hydraulic Analysis*, Nucl. Eng. Des., **120**, 323-339 (1990).

13. C. Güenther, *A Consistent Upwind Method of Second Order for the Convection-Diffusion Equation*, Proc. of 1987 Int. Conf. on Computational Techniques and Applications, Sydney, Australia, CTAC–87, 249 (1987).

14. K. Barret, *Numerical Modelling in Diffusion Convection*, Pentach Press, London, Plymouth (1982).

15. J. Sakai, *Conservative LECUSSO Scheme in Nonuniform Mesh Size Grid: Numerical Experiments and Natural Circultaion Test Analysis*, J. Compu. Fluid Dynamics, **1**, 34-36 (1992).

16. S. V. Patankar and D. B. Spalding, *A Calculation Procedure for Heat, Mass, and Momentum Transfer in Three–Dimensional Parabolic Flows*, Int. J. Heat Mass Trans. **15**, 1787–1806 (1972).

17. S. V. Patankar, *Numerical Heat Transfer and Fluid Flow Hemisphere*, New York (1980).

18. A. A. Amsden and F. H. Harlow, *The SMAC Method: A Numerical Technique for Calculating Incompressible Flow*, Los Alamos Laboratory Report LA–4370 (1970).

19. A. Wambecq, *Rational Runge–Kutta Methods for Solving Systems of Ordinary Differential Equations*, Computing, **20**, 333–342 (1978).

20. R. M. Beam and R. F. Warming, *An Implicit Factored Scheme for Compressible Navier–Stokes Equations*, AIAA J. **16**, 393–402 (1978).

21. P. J. Roache, *Computational Fluid Dynamics*, Hermosa Publishers, Albuquerque, NM (1976).

22. K. Sakai and D. Weinberg, *Investigation on the LECUSSO (Local Exact Consistent Upwind Scheme of Second Order) Scheme – Extension to Nonuniform Mesh Size Grids and Numerical Stability Analysis and Application for Natural Circulation Test Analysis using COMMIX–2(V)*, Int. Conf. in Super Computing in Nuclear Applications (SNA 90), Mito City, Japan (March 12–16, 1990).

23. Y. Shen, M. Bottoni, and W. T. Sha, *Implementation of the Flow–Modulated Skew–Upwind Difference Scheme in the Momentum Equation of the COMMIX–1C Program: A First Assessment*, ANL/MFRI-8 (Feb. 1991).

24. R. D. Richtmyer, *Difference Methods for Initial–Value Problems*, Interscience Publishers, New York. New York (1957).

25. R. S. Varga, *Matrix Iterative Analysis*, Prentice–Hall, Englewood Cliffs, New Jersey (1962).

26. C. A. J. Fletcher, *Computational Techniques for Fluid Dynamics*, **1**, Springer-Verlag, Berlin (1988).

27. K. Sakai, *Numerical Oscillations Analysis on High–Order LECUSSO Scheme Based on Characteristic Polynomial Technique*, J. Atomic Energy Soc. Japan (in Japanese), **34**, 544-564 (1992).

28. A. Tomiyama and R. Takahashi, *Numerical Stability and Numerical Oscillation of High Order Difference Methods for Computational Fluid Dynamics*, J. Atomic Energy Soc. Japan (in Japanese), **32**, 53 (1990).

29. W. T. Sha, B. T. Chao, and S. L. Soo, *Local Volume-Averaged Transport Equations for Multiphase Flow in Regions Containing Distributed Solid Structures*, USA, NUREG/CR-2354, ANL-81-69 (Dec. 1981).

30. Y. A. Hassan, J. G. Rice, and J. H, Kim, *A Stable Mass Flow Weighted Two–Dimensional Skew–Upwind Scheme*, Numer. Heat Transfer, **6**, 395–408 (1983).

31. I. Maekawa, H. Hinokata, M. Bottoni, and T. Muramatsu, *Assessment and Implementation of Second Order Schemes for Advection Terms in General–Purpose 3D Thermo–Hydraulic Computer Codes*, Proceeding Seventh Int. Conf. Numerical Methods Thermal Problems, Stanford U., CA, July 8–12, 1991.

32. R. W. Davis, E. F. Moore, and L. P. Purtell, *A Numerical-Experiment Study of Confined Flow Around Rectangular Cylinders*, Phys. Fluids, **27**, 46-59 (1984).

33. U. Ghia, K. N. Ghia, and C. T. Shin, *High-Re Solutions for Incompressible Flow Using the Navier-Stokes Equations and a Multigrid Method*, J. Compu. Phys, **48**, 387–411 (1982).

34. A. Huser and S. Biringen, *Calculation of Two-Dimensional Shear-Driven Cavity Flows at High Reynolds Numbers*, Int. J. Numer. Methods Fluids, **14**, 1087-1109 (1992).

35. H. L. Langhaar, *Steady Flow in the Transition Length of a Straight Tube*, J. Appl. Mechanics, Trans. ASME, **9**, A–55–58 (1942).

36 W. D. Campbell, and J. C. Slattery, *Flow in the Entrance of a Tube*, J. Basic Eng., Trans. ASME, **85**, 41–46 (1963).

Distribution for ANL/ATHRP-47

External:
USDOE-OSTI (2)
Library ANL-E (2)
Library ANL-W

Internal:
H. Drucker
R. W. Weeks
R. B. Poeppel
R. A. Valentin
M. Bottoni
F. C. Chang
T. H. Chien
H. M. Domanus
M. Hale
K. Sakai (2)
W. T. Sha (5)
J. G. Sun (5)